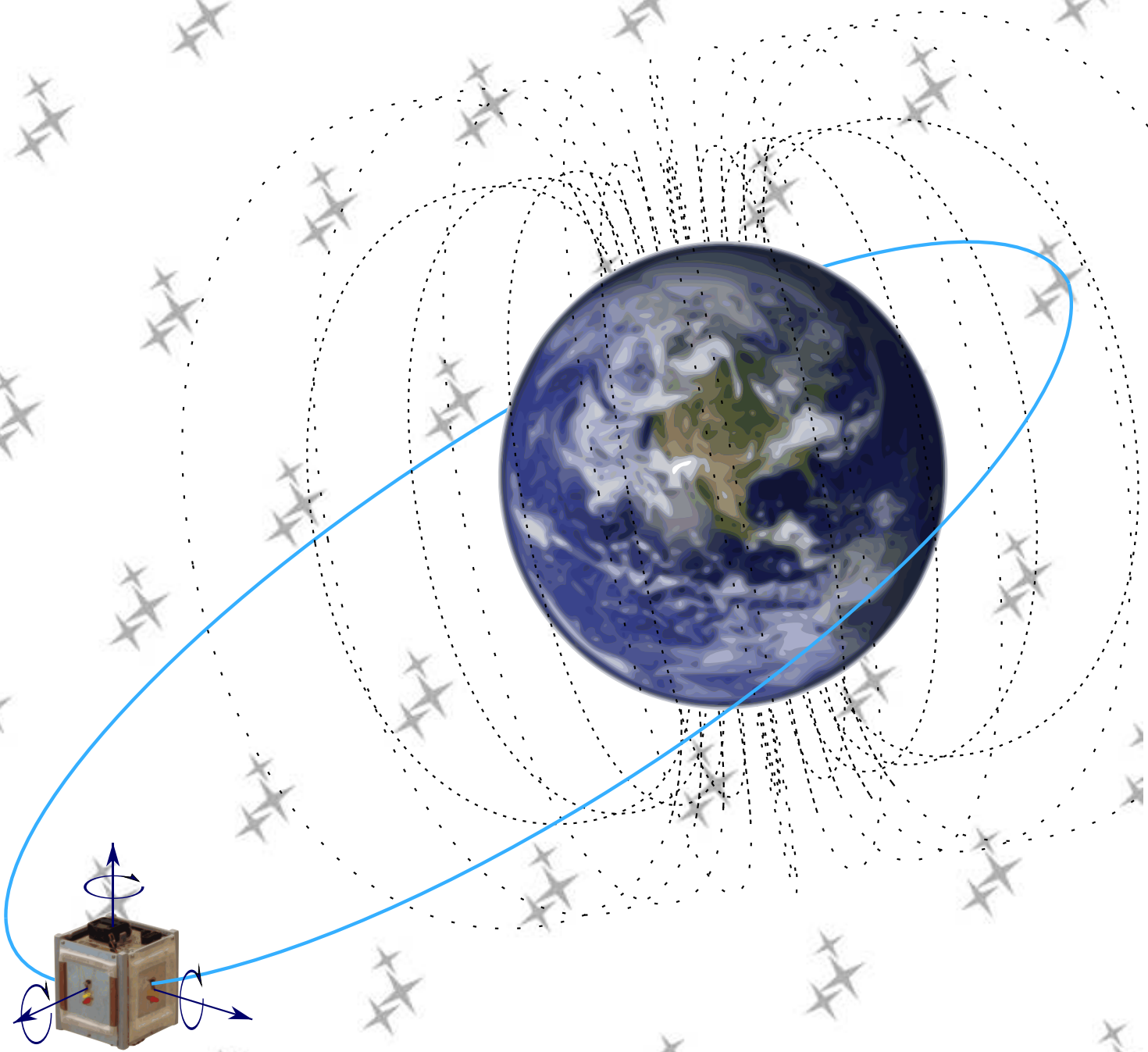




# AAUSAT3

## ADCS

- Attitude Determination and Control System



**Group 633:**

Jesper E. Pedersen / Søren T. Hede / Claus T. B. Pedersen / Henrik Dalsager



AALBORG UNIVERSITET





**Electronic Systems**

**6. Semester**

Fredrik Bajers Vej 7

Telephone 96 35 86 90

<http://control.aau.dk>

**Title:**

AAUSAT3 Attitude and Determination  
Control System

**Theme:**

Feedback Control

**Project Period:**

Spring 2008

**Project Group:**

08gr633

**Group Members:**

Jesper E. Pedersen  
Søren T. Hede  
Claus T. B. Pedersen  
Henrik Dalsager

**Supervisor:**

Palle Andersen

**Print Time:**

Mon Jun 2 23:05:38 CEST 2008

**Publications:** 6

**Pages:** 103

**Number of supporting documents:** 15  
(enclosed on attached CD)

**Finished:** 3. juni 2008

**Synopsis:**

This report concerns the development of the Attitude and Determination Control System for AAUSAT3.

Initially the space environment is analyzed, concerning the ADCS system and how positioning is done in space. It is decided to use magnetorquers to control the attitude, therefore an analysis of different models of the Earth's geomagnetic field and how to generate a magnetic torque is investigated. Different sensors for determining attitude and position in space are analyzed.

An experimental setup for controlling a prototype satellite in one axis is made. For controlling the prototype a PID controller is implemented to prove the functionality of the magnetorquers and the sensors. The controller in the experimental setup is verified and a comparison against the results from the simulation is made to provide an idea of the reliability of the simulations.

The one-axis PID controller is able to control the satellite within the specified requirements.

A state-space model is made of the system, to provide insight into this method for reaching the next step which is to develop a controller in three dimensions. State-space models are ideal for systems with multiple outputs and inputs.

# CHAPTER 1

## Preface

This project concerns the development of the Attitude Determination and Control System Prototype for the AAUSAT3 satellite.

The project is made in the spring 2008 at Aalborg University by 6th semester students of Computer and Electronical Engineering at the Department of Electronic Systems.

References are made using the Harvard method, and a list of sources can be found in the bibliography. The source code for both the report and the implemented software can be found on the enclosed CD, as well as other materials used in the making of the project. The CD content is shown in appendix E on page 103.

The AAUSAT3 mission was initiated last semester, and the basic design for the satellite was laid out. During that phase it was determined which subsystems should be included. Some of the systems, and the interfaces were defined and developed, such as the payload and the internal communications protocol. This semester the subsystems are further developed to a prototype level.

The Attitude Determination and Control System is in this design an autonomous system, which does not rely on anything else than power, and a reference attitude. It has been suggested that it is preferable to avoid mechanical solutions in the design of the actuators. The main goals for this stage of ADCS development is therefore to create a prototype which can be used for further ADCS development, and implement a controller to confirm the feasibility of using only non-mechanical actuators.

The report is build up of chapters concerning different aspects of the project. The introduction chapter provides background knowledge to get a better understanding of the purpose of the ADCS project. It is followed by an analysis chapter that contains some of the analysis which is done to grasp the projects tasks.

After the analysis the requirement specification is presented. The requirements are inherited from the global requirements set in the AAUSAT3 system engineering group, and some are extracted from the analysis. The requirements are summarized in a delimitation, where some of the requirements are postponed to further development, as they are beyond the scope of this project. They should however be considered before the final implementation of an ADCS system.

From the requirements, a test specification is set up, to handle verification of the requirements. The requirements also leads to modelling of the system, where the system is modelled as the experimental setting, and the space setting to aid in evaluating the effect from the suspension. This is used to produce a strategy for controlling the satellite in the 2d environment, and a controller is selected and implemented.

The implementation is described, and a test of the implemented system is compared with the simulated system. After the verification the discussion holds a clarification of how much has been accomplished compared to the goals. The conclusion attempts to clarify how well the system performs at the current level, and if it is acceptable or not. Finally it is commented in the perspectivization how the performance of the implemented systems could have been improved, and ideas are given to the next step in development.

The appendices of the report contains:

- **Appendix A** Helmholtz coil
- **Appendix B** Coil machine
- **Appendix C** Source code
- **Appendix D** Schematics of prototype
- **Appendix E** CD index

## CHAPTER 1. PREFACE

---

Control Engineering, Group 633

Jesper Ellegård Pedersen  
Søren Thorhauge Hede  
Claus Trier B. Pedersen  
Henrik Dalsager Christensen

---



Jesper Ellegård Pedersen

---



Søren Thorhauge Hede

---



Claus Trier B. Pedersen

---



Henrik Dalsager

## Nomenclature

<b>ABBREVIATION</b>	<b>DESCRIPTION</b>
AAU	Aalborg University
ADCS	Attitude Determination and Control System Subsystem responsible for handling the orientation of a satellite
AIS	Automatic Identification System Nautic radiobased system for identifying ships
CAN	Controller Area Network A serial bus intended for use in noisy environments, originally intended for automotive use.
COM	Communications An onboard system for transmitting and receiving data
Cubesat	A satellite with the size 10x10x10 cm and a mass of 1kg.
EPS	Electrical Power System Subsystem responsible for the transfer of power to and from the batteries
ESA	European Space Agency A European pendant to the more famous NASA
FP	Flight Planner An onboard system for executing a scheduled command
GND	Ground Station A system on the Earth's surface consisting of antennas, amplifiers and modems.
IAGA	International Association of Geomagnetism and Aeronomy International group of modellers which maintain and develop the IGRF magnetic field model
LEO	Low Earth Orbit An orbit description of an orbit close to the Earth
MCC	Mission Control Center A software for visualising the data collected by GND

---

## CHAPTER 1. PREFACE

---

ABBREVIATION	DESCRIPTION
MEO	Medium Earth Orbit An orbit where i.e. GPS and some weather satellites are found.
NASA	National Aeronautics and Space Administration An agency funded by the US government to explore and conduct missions in space environment.
NORAD	North American Aerospace Defense Command NORAD tracks all the objects in orbits using a big radar.
P/L	Payload The part of a satellite which sets the mission objectives, usually an external client orders the satellite as they wants some payload to operate in space, and therefore "pays" for it.
PCB	Printed Circuit Board A board consisting usually of glasspolymide or epoxy, with copper lines on the surfaces for connecting the pins on the components.
Picosatellite	Very small satellites with a mass of between 0.1 kg and 1 kg, ie. a Cubesat
PID	Proportional Integral Differential Controller Well known controller, widely used in both industrial applications and in educations.
POD	Picosatellite Orbital Deployer Carries a satellite during launch, an deploys it from the rocket.
PWM	Pulse Width Modulation A scheme for regulating the mean value of a signal by changing a dutycycle between 0 and 100%
RDANH	Royal Danish Administration of Navigation and Hydrography Danish governmental institution for governing the local waters
SPENVIS	Space Environment Information System Space environment simulation software supported by ESA.
SPI	Serial Periphial Interface A defacto standard for interfacing sensor via a serial digital channel.
TLE	Two Line Element A popular keplerian description of an orbit

## Definitions in the Report

$\theta$	is the angle of rotation
$\omega$	is the angular rate
$\alpha$	is the angular acceleration
$\tau$	is a torque
F	is a force
$K_p$	is the Proportional gain of a PID controller
$K_i$	is the Integral gain of a PID controller
$K_d$	is the Differential gain of a PID controller
V	is a velocity
T	is a cycle time
L	is a Length
I	is a current
A	is an area
B	is a magnetic field
t	is the time

## CONTENTS

<b>1 Preface</b>	<b>3</b>
<b>Contents</b>	<b>9</b>
<b>2 Introduction</b>	<b>11</b>
2.1 Mission Purpose . . . . .	11
2.2 AAUSAT3 Subsystems . . . . .	12
2.3 Project Description . . . . .	13
2.4 Overall Goals . . . . .	14
<b>3 Analysis</b>	<b>15</b>
3.1 Satellite Environment . . . . .	15
3.2 Position in Space . . . . .	16
3.3 Expected Orbit for AAUSAT3 . . . . .	18
3.4 Disturbances . . . . .	19
3.5 Models of the Geomagnetic Field . . . . .	22
3.6 Magnetorquers . . . . .	25
3.7 Powering Magnetorquers . . . . .	31
3.8 Actuating Using Magnetorquers . . . . .	33
3.9 Sensors . . . . .	34
3.10 Conclusion . . . . .	37
<b>4 Requirement Specification</b>	<b>38</b>
4.1 Hardware Requirements . . . . .	38
4.2 Functional Requirements . . . . .	39
4.3 Requirements From Other Subsystems . . . . .	39
4.4 Delimitation . . . . .	41
<b>5 Test Specification and Design</b>	<b>42</b>
<b>6 Modelling</b>	<b>43</b>
6.1 Sensor Modelling . . . . .	43
6.2 Satellite Modelling . . . . .	46
6.3 Experimental Model . . . . .	48

<b>7 Controller Strategies</b>	<b>51</b>
7.1 Strategy for Using Magnetorquers as Actuators . . . . .	52
7.2 The Classic Approach, a PID Controller . . . . .	55
7.3 Tuning the PID Controller . . . . .	59
7.4 System Model in State-space . . . . .	64
7.5 State-space controller design . . . . .	65
<b>8 Implementation</b>	<b>69</b>
8.1 Prototype ADCS satellite . . . . .	69
8.2 Debug Interface . . . . .	71
8.3 PID implementation . . . . .	73
<b>9 Verification</b>	<b>75</b>
<b>10 Discussion</b>	<b>79</b>
<b>11 Conclusion</b>	<b>80</b>
<b>12 Perspectives</b>	<b>83</b>
12.1 Geomagnetic Field Strength . . . . .	83
12.2 Magnetorquer Coil Design . . . . .	83
12.3 Three-dimensional Orientation . . . . .	83
<b>13 ICD internal communication</b>	<b>85</b>
13.1 ADCS . . . . .	85
<b>Bibliography</b>	<b>87</b>
<b>Appendix</b>	<b>88</b>
<b>A Helmholtz coil</b>	<b>88</b>
<b>B Coil Machine</b>	<b>90</b>
<b>C Source code</b>	<b>92</b>
C.1 PI controller . . . . .	92
C.2 Main loop . . . . .	93
<b>D Schematics</b>	<b>97</b>
<b>E CD index</b>	<b>103</b>

# CHAPTER 2

## Introduction

For a still increasing number of years Aalborg University has had an educational student space program. The latest satellite project AAUSAT-II which followed AAU CUBESAT, has during the writing of this report been launched into orbit. The subject of this project is the ADCS (Attitude Determination and Control System) on the next AAU satellite, AAUSAT3.

Most satellites are required to be able to control their own direction towards earth. Many different schemes have been used to accomplish this, and both active and passive attitude control systems have been invented. On AAUSAT3 an active system is suggested, and it is proposed only to use magnetic torquers to adjust the attitude of the satellite. This concept evolves around using the planetary magnetic field, and a couple of onboard coils to create torques. The main reasons for this choice is that coils does not take up much room and contains no moving mechanical parts.

### 2.1 Mission Purpose

AAUSAT3 is primarily an educational satellite project with the purpose of introducing the students to the process of developing a satellite. A satellite sets up restraints and requirements to a system, which is quite different from many other systems. This is not only due to the microgravity situation, the radiation, the vacuum and other space hazards. It is also related to the fact that a satellite cannot be repaired if anything is broken.

To overcome these problems the satellite development at Aalborg University has been broken into separate subsystems which each have their own missions and development team. This gives each development team the possibility to focus on the specific project, and ensure that their subsystem is ready for the space environment. The interfacing between the systems, the budgets, and the overall satellite design is done by a system-engineering group, with a representative from each subsystem group. This ensures constant critical evaluation of the project as the development of each subsystem progresses.

The AAUSAT3 satellite is a picosatellite based on the CubeSat standard. This limits the size to approximately a cube with sides with a length of 10 cm, and a weight of 1 kg. As a consequence of this limited size not much surface is available for solar cells, and a power budget with less than 1 watt for all systems must be fulfilled.

The system engineering group have defined the two main purposes for the AAUSAT3 project which are to have students develop a working satellite and to have the payload operational in space. [Engineering Group, 2007]

The payload for AAUSAT3 is developed by the students for the RDANH (Royal Danish Administration of Navigation and Hydrography). RDANH has requested a preliminary prototype

of a satellite, which is to test the possibility of observing and tracking international ship traffic around Greenland. Larger ships are required to constantly send out an AIS (Automatic Identification System) signal to other ships, and the objective of the payload on AAUSAT3 is to determine if it is possible to retrieve these informations from satellites, and how reliably it can be done.

The second mission objective is to observe Aurora Borealis activities. This is used to examine how it interferes with the AIS transponder signals.

The third and last mission objective is to mount a camera on the satellite to take pictures of the earth. This is primarily to improve the publicity surrounding the satellite programme on Aalborg University, as pictures taken from space is very presentable in public relations material. The second and third mission objectives are not mandatory, but are taken into consideration during the development of the preliminary design, as these missions otherwise are less feasible to be accomplished. More information can be found at the AAUSAT3 website <sup>1</sup> as the mission progresses.

## 2.2 AAUSAT3 Subsystems

To fulfill the objectives of the mission statement, AAUSAT3 will be consisting of a number of subsystems: Each of these subsystems are developed individually, but as each subsystem may be dependent of other subsystems, the development is coordinated by a group of system engineers, which consists of representatives from each subsystem development group.

**MCC - Mission Control Center** is a software system that will be responsible for presenting and logging the data collected by the ground station.

**GND - Ground Station** is primarily a system which handles the radio and modem units on earth, but they are also responsible for controlling the direction of the ground antennas.

**FP - Flight Planner** is a virtual subsystem responsible for executing commands while the satellite is in flight, and is fully operational. It also handles logging and similar software services which could be accessed from the other systems.

**EPS - Electrical Power System** is one of the core subsystems as it is providing the power distribution for each subsystem as well as charging the batteries with power from the solar panels.

**COM - Communications on UHF** is also a core subsystem as it provides the primary communication link between the groundstation and subsystems onboard of the satellite.

**COM-S - Communications via S-band** is a secondary communications system, it is operating at higher frequencies than COM, and thus can provide a larger bandwidth, but it requires a stable position of the onboard antennas.

**AIS - Automatic Identifications System** is the main payload of AAUSAT3. It will basically consist of a VHF radio receiver receiving AIS signals, and a software to be used with MCC to handle further processing.

**CAM - Camera** is a secondary payload that is able to take pictures of the Earth to be downloaded to the groundstation. If this payload is activated the S-band link will be used when available. The camera also requires a stabilized orientation of the satellite.

---

<sup>1</sup><http://www.aausat3.space.aau.dk>

**ADCS - Attitude Determination and Control System** is the subsystem concerning this project. Its responsibility is to keep the satellite stable and pointing in a specified direction. This is done to get an optimal performance of the radio links and camera.

## 2.3 Project Description

When a cubesat is launched into a LEO (Low Earth Orbit) it is likely that it will start tumbling. This tumbling, which is defined as an angular rate of the satellite, is due to the deployment process which is done by a tensioned spring that is released and pushes the satellite away from the launch vehicle. An example of a cubesat deployment is illustrated on figure 2.1. Any uneven friction with the POD will make the satellite rotate.

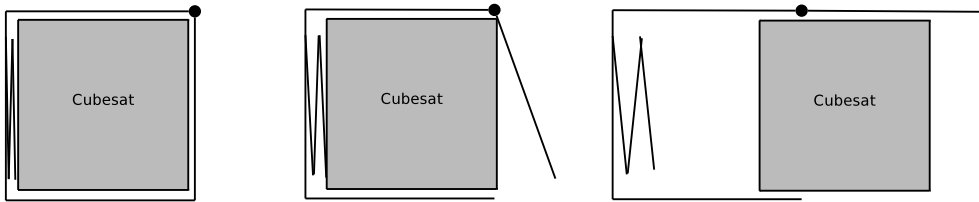


Figure 2.1: Illustration of the deployment of a cubesat. The spring pushes the satellite out of the POD when the door is opened.

Furthermore the satellite will be inflicted to an angular acceleration from the atmosphere, even though it is very thin in LEO, there is still aerodynamic forces affecting the satellite. The attitude determination and control system will consist of sensors determining the attitude and angular rate, as well as actuators to be able to react on the sensor inputs. The actuators could be e.g. thrusters, momentum wheels or powered gyro gimbals. At this stage, however, it has already been decided to use magnetorquers as actuators on AAUSAT3. This provides the operator with some freedom during the operations of the satellite, as it allows for changes in the attitude during the entire mission. However, it also creates a requirement for controlling the actuators, to make sure that the satellite's movements are eventually damped. Thus the project for developing an ADCS system is consisting at least four tasks.

- Selecting a set of sensors.
- Shaping the magnetorquers.
- Develop a controller to handle the satellite's rotations which can be implemented on the satellite.
- Handle the interface with the rest of the satellite

Thus goals for the entire ADCS project can be set up.

## 2.4 Overall Goals

The final goal is to design and implement an attitude determination and control system for AAUSAT3.

To be able to fullfil this goal a roadmap is made of several tasks:

1. Choosing a set of sensors to provide the necessary informations concerning the attitude
2. Modelling the chosen sensors
3. Design and manufacture actuators which are powerful enough to be used for controlling the attitude
4. Modelling the manufactured actuators
5. Modelling the satellite
6. Creating a prototype for testing the actuators and sensors
7. Setting up a 1 plane experiment for testing a the prototypes behavoir in a magnetic field.
8. Designing a 1 plane controller and implement it on the prototype
9. Making a physical experiment with the implemented controller, in 1 plane, to verify the models and the designs.
10. Designing a 3D controller, for use in space
11. Modelling the disturbances from the 3D environment in space
12. Creating a simulation tool for testing the controller in 3D
13. Setting up a 3D experiment if funding allows for it
14. Real life testing in space, verifications can be done with the onboard camera.

In this project the steps 1 to 9 are handled, leaving the task to transfer the 1 plane model to a 3D environment to be done after this project.

To be able to choose sensors and design actuators it is necessary to analyze the environment in which the the system is operating in. This is done in the next chapter which contains the analysis.

# CHAPTER 3

## Analysis

In the analysis the environment in space is described and the influence it has on the project is considered. The chapter continues with a description of some of the models for the orbit, the geomagnetic field and the known disturbances. These models are investigated, as the magnetorquers are dependent on the strength and direction of the external magnetic field relative to the satellite. Thus a description of the geomagnetic field can be used together with an orbit description to predict how the external field is oriented at a given time. The disturbances can provide information on the minimum torque which the magnetorquers must supply.

Finally the existing actuators for AAUSAT-II are evaluated to determine if the existing design is sufficient for the ADCS on AAUSAT3.

### 3.1 Satellite Environment

The working conditions for a satellite are quite different from the electronic systems on the Earth's surface. The most obvious difference is that the satellite is placed in near vacuum. The challenges derived from these conditions are primarily [Wertz and Larson, 1999]

- Vacuum
- Less thermal coupling with the environment than on the surface
- Less shielding from radiation due to less atmosphere

Operating in vacuum conditions can give rise to significant problems for a satellite. In vacuum most organic materials will outgas, which concerns many surface materials of the electronics like plastic. The problem is in its worst case that an electronic circuit can be separated or short-circuited if the isolation of wires outgasses.

This can cause permanent failures in the satellite and should therefore be avoided. Smaller amounts of outgassing should also be avoided. If outgassed particles hits optical surfaces, it could degrade the performance of electro-optical instrumentation such as cameras and solar cells. Therefore all materials used on a satellite must be tested in vacuum before launch.

The second problem a satellite suffers from due to its placement in vacuum is the problem of getting rid of heat. On the Earth's surface any electronic component can transfer heat to the air surrounding it and is thus cooled. In outer space there is no air to transfer heat. The only ways to transfer heat are through infrared radiation and through thermal coupling with the mechanic frame, which then radiates heat.

Besides these problem with heat transfer, a satellites surface temperature changes dramatically by its position in orbit. If it is in the unilluminated side of the Earth the temperature drops to below -25 °Celsius, and in the sun light it easily gets as high as 85 °Celsius.

## 3.2 Position in Space

Orbital elements are parameters to specify an orbit in space, given a model of two point masses obeying the Newtonian laws of motion and the inverse-square law of gravitational attraction. There are multiple ways of parameterising a motion, depending on which set of variables chosen to measure, there are several different ways of defining sets of orbital elements, each of which will specify the same orbit.

### 3.2.1 Keplerian Elements

One such set of orbital elements is the Keplerian elements. This set is part of the NORAD developed TLE (Two-Line Element). Keplerian elements include the following six parameters:

- Semi-major axis ( $a$ )
- Eccentricity ( $e$ )
- Inclination ( $i$ )
- Right ascension of the ascending node ( $\Omega$ )
- Argument of perigee ( $\omega$ )
- Mean anomaly ( $M_0$ )

These describe the shape and orientation of the orbit and the position of the object moving in the orbit.

### 3.2.2 Orbital Shape

The two Keplerian elements describing the shape are the semi-major axis and the eccentricity. The semi-major axis is defined as half the distance between apogee and perigee. The distance between apogee and perigee is the greatest distance between two points on the orbit. This defines the size of the orbit.

Eccentricity describes the deviation of shape from a circle. An eccentricity of zero means the orbit is circular. Elliptic orbits have an eccentricity between 0 and 1. As the eccentricity approached 1 the orbit becomes more elliptic. An eccentricity of 1 results in a parabolic trajectory, and one greater than 1 results in a hyperbolic trajectory. This means an eccentricity of 1 and greater causes the satellite to escape the gravitation Earth. The influence of different values of eccentricity is shown on figure 3.1.

### 3.2.3 Orbital Orientation

It is not adequate to know only the shape of the orbit to determine the position of the satellite at a given time. The shape of the orbit does not take in to account that the Earth is rotating. To find a satellite's position relative to a location on the Earth's surface, it is required to describe the orientation of the orbit at a given time. Firstly it is required to define the axes. With the center of the mass being origo, these are the north pole and the vernal equinox. Figure 3.2 illustrates this. The vernal equinox is the point where the relative movement of the Sun crosses the equator from south to north.

The orientation of the orbit is described by three angles: the inclination, the right ascension of the ascending node and the argument of perigee. The inclination is the angle between the north

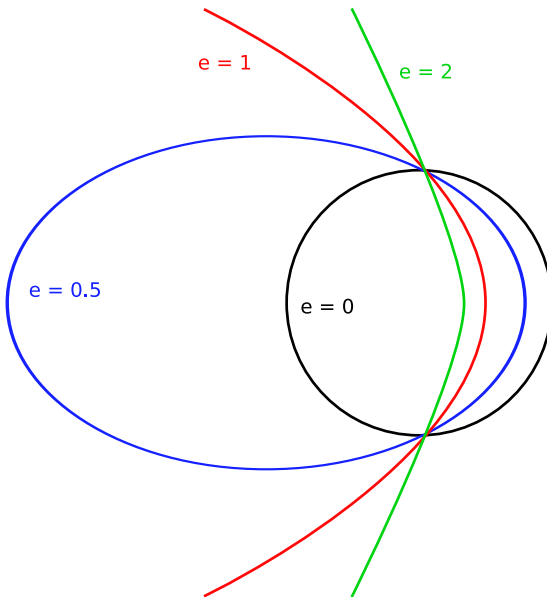


Figure 3.1: Examples of eccentricity and the resulting orbit shapes

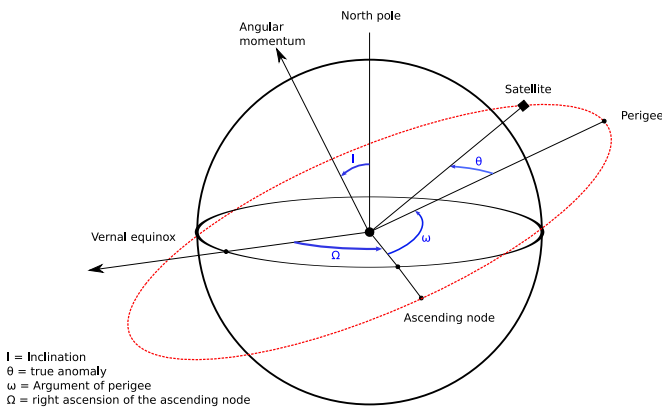


Figure 3.2: Keplerian elements.

pole and the angular momentum of the orbit. The ascending node is the point where the orbit crosses the equator of the orbited mass south to north. The right ascension of the ascending node is the eastward angle between the vernal equinox and the ascending node. The argument of perigee is the angle between the perigee and the ascending node in the direction of satellite movement.

The position of the satellite is given by the true anomaly which is the angle from the perigee to the position of the satellite at a given epoch. However the Keplerian elements include the mean anomaly. This is the position of the satellite if it had had a circular orbit.

The speed of the satellite is not constant when moving in an elliptic orbit. It actually moves slower the further away the satellite is from the center of gravity. By using the mean anomaly it is easier to calculate the position of the satellite at a future epoch.

### 3.2.4 Positioning in Space by NORAD

NORAD (North American Aerospace Defense Command) is a joint organization of Canada and the United States that provides information about satellite positions in space. The specific

information about a position of a satellite is provided by TLE (Two-Line elements), which is the most commonly used format.

All space objects are classified by NORAD as near-Earth if the orbit period is less than 225 minutes or deep-space if the orbit period is greater than or equal to 225 minutes.

Orbits classified as near-Earth uses the SGP4 (Simplified General Perturbations Satellite Orbit model 4)<sup>1</sup> for specifying the position of the object, and SDP4 model is used for deep-space orbits.

Depending on a satellite's orbit, the orbit information must be updated periodically, because the data derived can become unreliable as a result of changes in drag and other disturbances. Furthermore the two-line elements contain information about epoch, i.e. time of observation and the assumed drag.

The two-line elements given by NORAD can be used to determine a position in orbit at an accuracy of 0.1 degree longitude and 0.1 degree latitude.

By using the SGP4 or SDP4 models it is possible to predict where to search for the satellite in the sky with a ground antenna, additionally by giving the satellite its TLE and time, it is also possible to make the satellite to act on the position in space.

### 3.3 Expected Orbit for AAUSAT3

At the time of writing this report, AAUSAT3 is supposed to be launched with the ESA Vega launcher. According to ESA's Call for CubeSat Proposals, [ESA Education Office, 2008], the satellites will be launched into an orbit with a perigee of 350 km and an apogee of 1200 km with an inclination of 71 degree. However, according to the information from ESA, it is being investigated if it is possible to change the orbit to 350 x 350 km instead of 350 x 1200 km. As the disturbances in terms of gravity gradient and atmospheric drag are higher in a 350 x 350 km orbit than 350 x 1200 km, the parameters for a 350 x 350 km are used for making worst-case calculations throughout this project.

The orbital period is defined as:

$$T_{orbit} = 2\pi \sqrt{\frac{r^3}{\mu}} \quad (3.1)$$

where:

$r$  is the length of the semimajor axis, or radius if orbit is circular in km  
 $\mu$  is the standard gravitational parameter which is  $398,600.5 \text{ km}^3 \cdot \text{s}^{-2}$

For an orbit of 350 x 350 km the orbital period is:

$$T_{350x350km} = 2\pi \sqrt{\frac{6,728^3}{398,600.5}} = 5,492 \text{ s} = 91.5 \text{ min} \quad (3.2)$$

Then the orbital velocity can be found by using the value of the orbital period:

$$V_{orbit} = \frac{2\pi \cdot r}{T_{orbit}} = \frac{2\pi \cdot 6,728,000}{5,492} = 7,697 \text{ m/s} \quad (3.3)$$

where:

$V_{orbit}$  is the velocity in m/s

$r$  is the length of the semi-major axis

$T_{orbit}$  is the period of one orbit in seconds

---

<sup>1</sup><http://en.wikipedia.org/wiki/SGP4>

## 3.4 Disturbances

The disturbances influencing the attitude of the satellite is the following:

- Atmospheric drag
- Magnetic residual
- Gravitation
- Radiation

All formulas and parameters in this section are based on [Wertz and Larson, 1999] unless otherwise specified.

### 3.4.1 Atmospheric Drag Disturbance

A satellite in LEO is affected by the friction between the satellite and the thin atmosphere in the orbit altitude. The force is acting in the opposite direction of the velocity vector of the satellite.

$$F_{drag} = -\frac{1}{2}\rho C_D A V^2 \quad (3.4)$$

where:

$\rho$  is the atmospheric density.

$C_D$  is the atmospheric drag coefficient.

$A$  is the surface area.

$V$  is the velocity.

The atmospheric density is, by table lookup in [Wertz and Larson, 1999], set to  $\rho_{350km} = 1.66 \cdot 10^{-11} \text{ kg} \cdot \text{m}^{-3}$ .  $C_D$  is set to 2.2 which is also used for AAUSAT-II which has the same shape as AAUSAT3. The area, which is also derived from the CubeSat specification, is  $A = \sqrt{3}(0.01) \text{ m}^2$ . These parameters are inserted in formula 3.4:

$$F_{drag} = \frac{1}{2} (1.66 \cdot 10^{-11} \text{ kg} \cdot \text{m}^{-3}) (2.2) (\sqrt{3} \cdot 0.01 \text{ m}^2) (7.697 \text{ m/s})^2 = 18.7 \cdot 10^{-6} \text{ N} \quad (3.5)$$

The torque exerted on the satellite by atmospheric drag is expressed by:

$$\tau_{drag} = F_{drag} \cdot L \quad (3.6)$$

where  $L$  is offset of center of mass in relation to geometric center. This offset must, according to the CubeSat specification, [California Polytechnic State University, 2007], be less than 2 cm. This results in a worst-case torque caused by atmospheric drag:

$$\tau_{drag} = 18.7 \cdot 10^{-6} \cdot (0.02) \text{ Nm} = 374 \cdot 10^{-9} \text{ Nm} \quad (3.7)$$

On figure 3.3 the torque caused by atmospheric drag is plotted for other altitudes.

### 3.4.2 Gravitational Disturbances

Gravitational disturbances affecting the satellite attitude consists of:

- Earth's zonal harmonics
- Gravity gradient

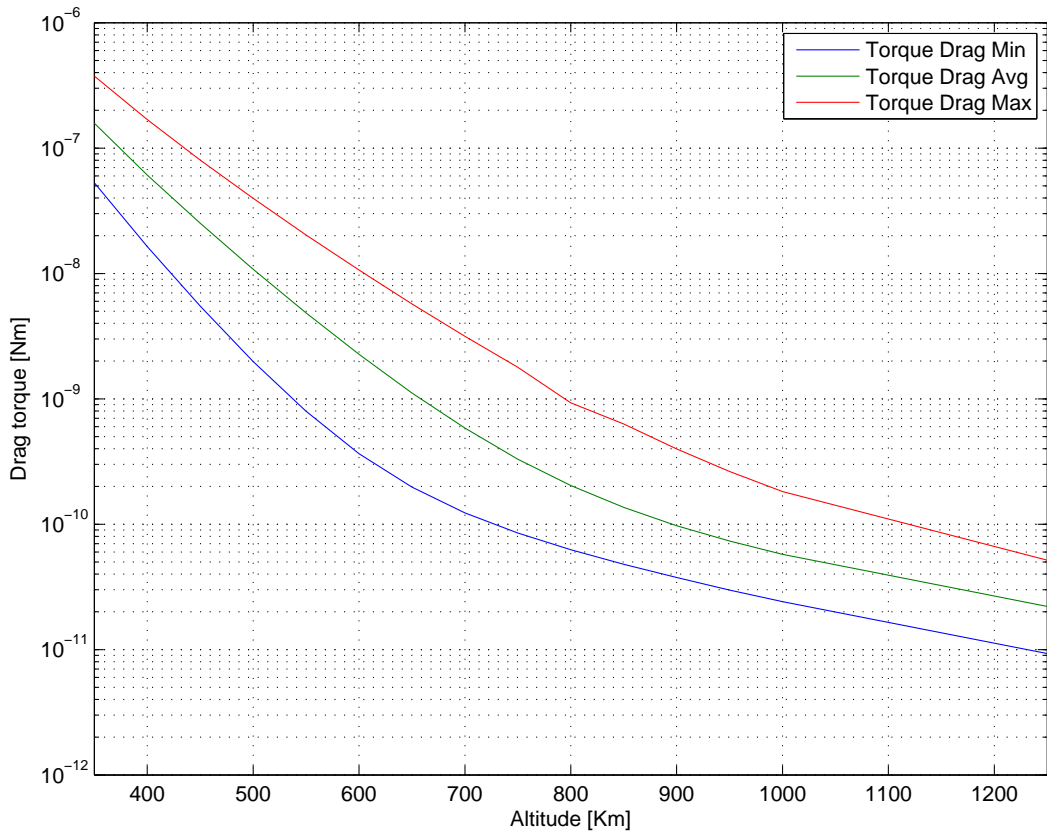


Figure 3.3: The atmospheric drag in the altitude range of 300 km and 1250 km. The graph is based on tabular values from [Wertz and Larson, 1999].

- Gravitational forces from the Sun and the Moon

The orbit of the satellite is affected by the Earth's zonal harmonics, since the Earth is not a perfect sphere. This is due to the fact that the radius is larger at the equator than at the poles and the composition of the Earth is not perfectly uniform.

The satellite will also be affected by the gravitational forces of the Sun and the Moon.

Furthermore the satellite will experience a gravitational torque around its center of mass as it is non-spherical and the mass distribution is non-uniform.

The gravitational disturbance is very small compared to the other possible disturbances. The estimate of the worst-case gravitational disturbance  $\tau_g$  is based on the calculations from AAUSAT-II [Pedersen et al., 2004], since the requirements for mass-distribution are the same.

$$\tau_{gravity} = 802.41 \cdot 10^{-11} \text{ Nm} \quad (3.8)$$

### 3.4.3 Magnetic Residual Disturbance

As the satellite consists of a number of electric circuits it will act as a magnetic dipole. This causes a torque around the center of mass of the satellite. The force of this disturbance is unknown at the writing of this report, since the PCB layouts for the satellite are still to be determined and the strength is also dependent of the placement of wires during the satellite integration phase.

However an estimate is made using a dipole magnet approximation with a field strength of  $0.1 \text{ mA} \cdot \text{m}^2$ .

This disturbance is calculated by the formula:

$$\tau_{magnetic} = D \cdot BB = \frac{2M}{R^3} \quad (3.9)$$

where:

$M = 7.96 \cdot 10^{15} \text{ tesla} \cdot \text{m}^3$  is the magnetic moment of the Earth  
 $R$  is the radius of the orbit

The values are inserted in the formula:

$$\tau_{magnetic} = (0.1 \cdot 10^{-3} A \cdot m^2) \left( \frac{2 \cdot 7.96 \cdot 10^{15} \text{ tesla} \cdot \text{m}^3}{6,728,000m} \right) \text{ Nm} = 5.2 \cdot 10^{-9} \text{ Nm} \quad (3.10)$$

#### 3.4.4 Radiation Disturbance

The satellite will be affected by radiation hitting the surface. This will cause a torque around its center of mass.

The major radiation sources in a LEO is direct solar radiation and solar radiation reflected by the Earth and its atmosphere.

The worst-case torque caused by solar radiation is:

$$\tau_{solar} = F(c_{ps} - cg) = F \cdot L \quad (3.11)$$

$$F = \frac{F_s}{c} A_s (1 + q) \cos i \quad (3.12)$$

where:

$L$  is the difference between center-of-mass and center-of-pressure.

$F_s$  the solar constant  $1,367 \text{ W/m}^2$ .

$A_s$  is the surface area.

$c$  is the speed of light,  $10 \cdot 10^8 \text{ m/s}$ .

The reflectance factor  $q$  is ranging from 1 to 2, depending on the absorbance and reflection of the surface of the satellite.  $i$  is the angle of incidence of the Sun.

The parameters are substituted by the actual values to calculate the worst-case disturbance caused by solar radiation:

$$\tau_{solar} = \frac{(1,367 \text{ W} \cdot \text{m}^{-2}) (\sqrt{3} \cdot 0.01 \text{ m}^2) (2)}{3 \cdot 10^8 \text{ m/s}} (0.02 \text{ m}) = 3.16 \cdot 10^{-9} \text{ Nm} \quad (3.13)$$

#### 3.4.5 Total Disturbance Torque

The worst-case disturbance torque is found by adding the disturbance torques from gravity gradient, radiation, magnetic residual and aerodynamic drag together. By doing so, it is assumed that all these forces act in the same direction. However, this is not very realistic, but the resulting value is very useful for the design of the actuators. The total disturbance torque is:

$$\tau_{disturbance} = \tau_{drag} + \tau_{magnetic} + \tau_{solar} + \tau_{gravity} = 39 \cdot 10^{-6} \text{ Nm} \quad (3.14)$$

### 3.5 Models of the Geomagnetic Field

Several strategies for modelling the geomagnetic field have been used by different scientists and updated by space agencies and geologists. It is assumed preferable, when using magnetorquers as actuators, to utilize a model of the geomagnetic field in the control system, to be able to predict the torque created by the coils for a certain current at a certain place in orbit.

The Earth's geomagnetic field is popularly described and modelled as a simple dipole field. The force from this field excites a compass needle and makes it point approximately towards the geographic north pole. Some confusion can arise when defining the actual pole names of the magnetic field, as the magnetic dipole of the compass needle is also labelled north and south. When the magnetic fields of the needle and the earth react on each other, the end result will be that the magnetic north pole of the needle points approximately towards the geographic north pole. However, this actually defines that the internal dipole magnet of the Earth, has its magnetic south pole placed at the geographic north pole.

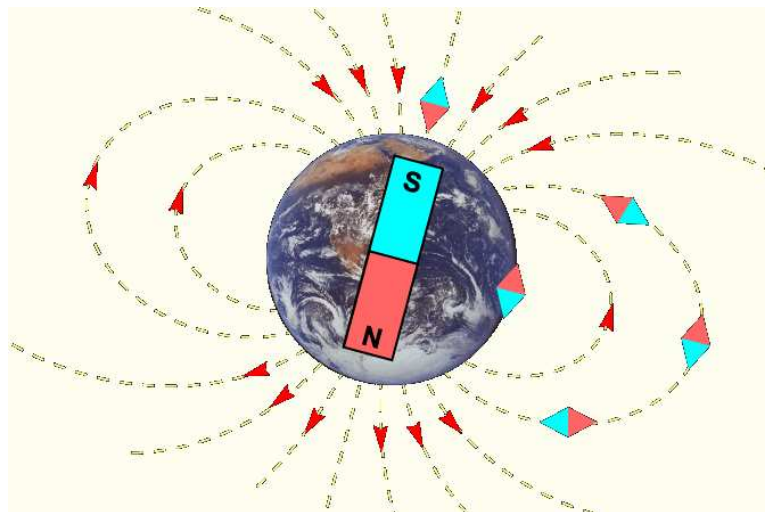


Figure 3.4: Earth magnetic field

Also relating to this definition it should be noted that the geomagnetic poles are not perfectly aligned with the geographic poles, but is currently moving slowly away from the rotational axis of the earth.

Measured on the Earth's surface the field varies from being horizontally oriented (south - north) with a magnitude about 30 000 nT, to being vertically oriented and with a magnitude of about 60,000 nT near the poles; the rms magnitude of the magnetic field vector over the surface is about 45,000 nT. Imagining that a bar magnet could be placed inside the Earth, inclined approximately 11° to the earth's rotational axis and offsetted about 550 km from the Earth's centre, almost 90% of the observed magnetic field could be accounted for. The remaining 10% could be accounted for by placing smaller bar magnets at strategic locations around the primary magnet.

#### 3.5.1 Magnetohydrodynamic Geomagnetic Model

So far the magnetohydrodynamic model type is assumed to be the physically most accurate model. According to [Philips, 2003] a model which deals with magnetohydrodynamics can be based on the assumption that the earth is built up in basically 4 layers. The layers being the crust, the mantle, the liquid outer core, and the solid inner core. The inner core spins at a slightly faster rate than the earth's surface, and due to the rotation of the inner core, it twirls and stirs the outer liquid core. Not allowing it to settle in the center. The outer liquid core, is thus

behaving as an ocean of liquified iron, which through its motions generates the magnetic fields, according to a phenomenon named the dynamo effect. This has been successfully simulated under the title "Geodynamo Computations" at the Pittsburgh Supercomputing Center. The resulting magnetic field is limited by the properties of the mantle, and finally at the crust which hold magnetically reactant materials in the Tectonic Plates. However as could intuitively be comprehended, this model is a quite complex, as it for the dynamo description takes into account the hydrodynamics of an iron ocean, and also deals with the temperature of the cores. Even though this model has the advantage that it can be used for predicting the magnetic poles alignment with the geographic poles, and that it is capable of simulating the reversal of the magnetic field, it has so far not been announced as implemented in anything less than a supercomputer.

### 3.5.2 International Geomagnetic Reference Field (IGRF)

This model of the earth's magnetic field, is released and maintained by the International Association of Geomagnetism and Aeronomy (IAGA). It is developed in collaboration between the magnetic field modellers, and is based on the data collected from a variety of satellites, airplanes, and ground stations. IGRF is a mathematical description of the Earth's main field and its annual rate of change [DSRI and NASA, 2007].

The IGRF model is defined as a series of mathematical models, where each model comprises a set of harmonic (or Gauss) coefficients. It is named so due to the fact that this model type was introduced by Gauss in 1839 and is represented by a spherical harmonic series, where the first term is known as the dipole term.

Each group of functions in the Gauss spherical harmonic series describes a particular field pattern:

- the first three terms describe the field of a dipole;
- the next 5 terms describe a quadrapole field;
- the following 7 terms describe an octopole field.

By adjusting the relative size of each of these component parts the shape of the actual field can be closely approximated.

However in Gauss version no consideration has been taken to changes over time. In IGRF the main field coefficients are described as functions of time and the change is assumed to be linear over five-year intervals.

As this model is based on this mathematical description it is not describing the actual physical magnetic field generator. To compensate for this linearisation it is frequently updated and is in this moment in time at its 10. generation. (Revised 2005).

When a series expansion of the geomagnetic potential is set up, the coefficients can be dubbed at time  $t$ ,  $g_n^m$  and  $h_n^m$ , which gives us:

$$V(r, \theta, \lambda, t) = R \sum_{n=1}^N \left( \frac{R}{r} \right)^{n+1} \sum_{m=0}^n (g_n^m \cos(m\lambda) + h_n^m \sin(m\lambda)) P_n^m(\cos(\theta)) \quad (3.15)$$

where:

$r$  is the radial distance from the centre of the Earth

$R$  is a reference to the mean radius of the Earth (6371.2 km)

$\theta$  is the geocentric colatitude ( $90^\circ$  - latitude)

$\gamma$  is longitude eastward from Greenwich

$P_n^m$  is the Schmidt semi-normalised associated Legendre functions of degree  $n$  and order  $m$ .

The magnetic field components can be calculated through the following derivatives:

$$X = \frac{1}{r} \frac{\delta V}{\delta \theta} \quad (3.16)$$

$$Y = \frac{1}{r \cdot \sin \theta} \frac{\delta V}{\delta \phi} \quad (3.17)$$

$$Z = \frac{\delta V}{\delta r} \quad (3.18)$$

The IGRF model has the advantage of having its coefficients frequently updated, without changing the mathematical algorithm. Thus it is also implemented in the SPENVIS satellite simulation software.

It should be noted however that there are three known issues with this model. These are titled Error of Commission, Errors of Omission, and Not Modelled Effects.

### Error of Commission

Numerically limited coefficients and coefficients based on less than global coverage of measurements, will lead to errors in the model. The coefficients are therefore most reliable for the timeframe of 1979-1980 where MAGSAT measured the magnetic field globally, and again from 1999 and forward, where the CHAMP and Ørsted satellites provide global coverage. IAGA predicts an RMS error value of 20 nT/year due to errors in the coefficients.

### Error of Omission

Due to the number of the coefficients, an upper limitation in the frequency of the field component exists. Because of the large distance of the Earth's surface to the core, the observed core field is predominantly of long wavelength. But a significant contribution comes from the magnetized rocks of the Earth's crust; this contribution is however of much shorter wavelengths, and amounts typically to 200-300 nT RMS.<sup>2</sup>

Although the crustal field is mostly of much shorter length scale than the core field, there is almost certainly a finite (essentially constant) contribution from the crust present in the IGRF models (i.e. in harmonics at and below degree n=10). This contribution is not separably measurable, but it is suggested by IAGA that its magnitude is about 5-10 nT global vector RMS.

Conversely, because the shortest (equatorial) wavelength which can be represented in an IGRF model truncated to n=10 is about 4000 km, any shorter-wavelength field, including that from the core, is ignored by the model. Again, this core-field contribution is not separable from the crustal field, but it is estimated that about 10 nT RMS of short-wavelength core field is being ignored.

### Not Modelled Effects

The IGRF model is not trying to model effects due to manmade objects, magnetic storms, or other external forces.

#### 3.5.3 World Magnetic Model (WMM)

Just as the IGRF model, the WMM is built up around a series of coefficients in a geodetic system, here using the World Geodetic System 1984 (WGS 84) for coordinate references. When comparing WMM to IGRF it should be noted that it basically is the same dataset and algorithms which are used for modelling the Earth's magnetic field. Thus the two models have somewhat the same limitations and advantages. However the WMM modellers provide Fortran and C code, for easy and correct implementation of the WMM model.

---

<sup>2</sup>see <http://www.ngdc.noaa.gov/IAGA/vmod/igrfhw.html>

## CHAPTER 3. ANALYSIS

---

Just as the IGRF model the lifespan of the WMM model is approximately 5 years, and the last edition of the WMM was also released in 2005.<sup>3</sup>

The total magnetic field is usually divided into several components:

- Declination (D) indicates the difference, in degrees, between the headings of true north and magnetic north.
- Inclination (I) is the angle, in degrees, of the magnetic field above or below horizontal.
- Horizontal Intensity (H) defines the horizontal component of the total field intensity.
- Vertical Intensity (Z) defines the vertical component of the total field intensity.
- Total Intensity (F) is the strength of the magnetic field, not divided into its component parts.

The WMM software computes seven components, where the most common components exists but a nordic and eastern component is added:

- D (DEC) - Geomagnetic Declination (Magnetic Variation)
- I (DIP) - Geomagnetic Inclination
- H - Horizontal Intensity of the geomagnetic field
- Z - Vertical Component of the geomagnetic field
- F - Total Intensity of the geomagnetic field
- X - North Component of the geomagnetic field
- Y - East Component of the geomagnetic field

The WMM modellers also provides an easy to find, clear documentation of how the measured data from both satellite and ground stations was used.

## 3.6 Magnetorquers

This chapter is based on the knowledge given by the magnetorquer designers from AAUSAT-II. The magnetorquers on AAUSAT-II are designed with the idea of making the coil area as big as possible to react on the Earth's magnetic field. The coils on AAUSAT-II are therefore designed as a square coil with a length of 71 mm, and the wire thickness have been chosen to be 0.1mm. The magnetorquer designers for AAUSAT-II have noted that the coils made for AAUSAT-II have some unsolved issues.

At the calculated workable current the wire overheats in the corners of the square coil, and as a result, the maximum current through the coil has been chosen to be 8.2 mA, which is equivalent to running at a dutycycle of 50%.

Thus it is investigated how to overcome this problem, and determine the efficiency of the coil. The following areas are of interest:

- Avoiding superheating of the wire at a dutycycle of 100%
- Investigate the efficiency of the coil
- Investigate the temperature influence on the coil

---

<sup>3</sup>[http://www.ngdc.noaa.gov/geomag/WMM/data/TRWMM\\_2005.pdf](http://www.ngdc.noaa.gov/geomag/WMM/data/TRWMM_2005.pdf)

### 3.6.1 Avoiding Superheating

One of the suggestions from the magnetorquer designers on AAUSAT-II is to increase the thickness of the wire used on the coil. This increases the weight of the coil, but also reduces the resistance in the wire, which means less energy consumed and transformed into heat.

Figure 3.5 shows the calculation of the weight, power and voltage over the wire to get the same current of different wire thickness at the same length as used on AAUSAT-II.

By using a 0.14 mm wire the cross area is almost twice of the wire used on the AAUSAT-II. And instead of consuming 20 mW the coil only consumes 10 mW for a current of 8.2 mA.

A thicker wire also gives the opportunity to increase the current without damaging the wire, and the saved consuming energy can therefore be used to increase the strength of the magnetic field generated.

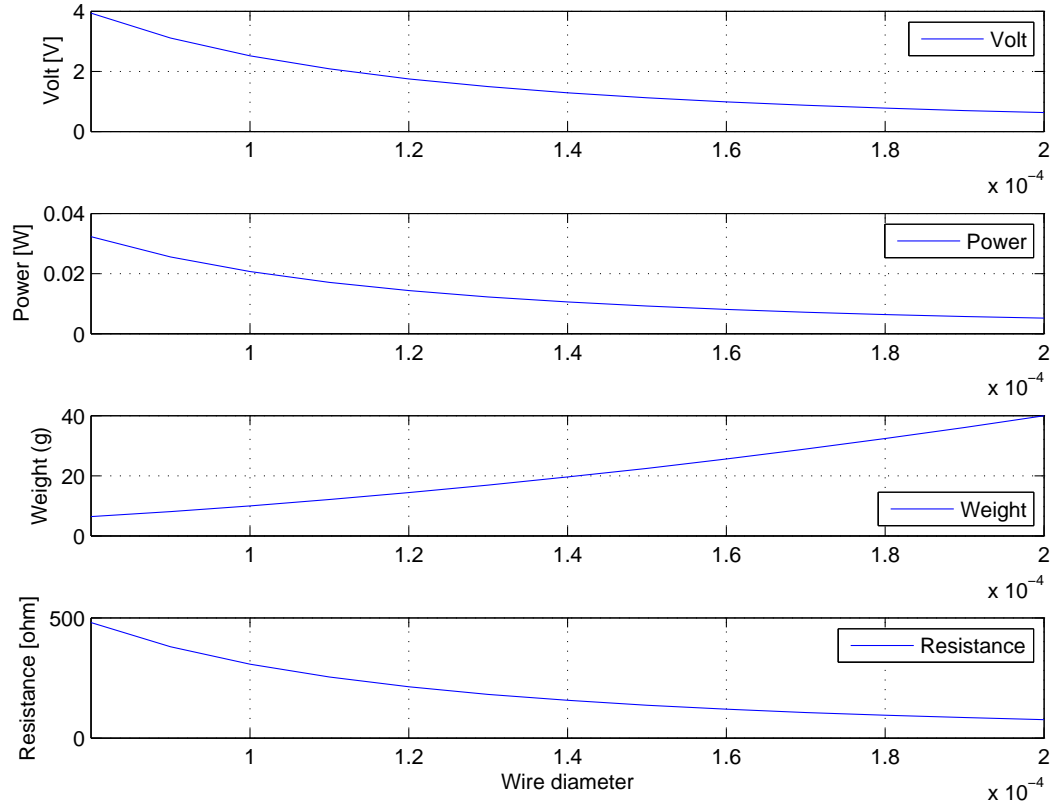


Figure 3.5: The properties of the coil in relation to different wire diameters.

Another opportunity to reduce superheating is to choose a coil shape that does not stretch the wire in the corners as rectangular coil do, eventually this can be improved by using a circular coil form.

### 3.6.2 Coil Efficiency

The design for AAUSAT-II is a square coil with 500 windings of 0.1 mm copper wire, designed as an air coil.

The coil efficiency is for this purpose the torque it produces in relation to the power consumption. The formula for the torque which a coil produces is shown at 3.19.

$$\tau_{coil} = n \cdot I \cdot A \cdot B \cdot \sin(\theta) \quad (3.19)$$

where:

$\tau$  is the torque the coil produces in Nm

n is the number of windings (500 windings)

I is the current in the coil in A

A is the area enclosed by the coil in  $m^2$

B is the homogenous magnetic field surrounding the coil in tesla

$\theta$  = The angle between the coil and the magnetic field

As described above the coil used on AAUSAT-II is a square coil. The formula can be simplified by using a specific amount of wire, as the the number of turns is  $n = \frac{W}{L}$  and the area the coil enclose  $A = L^2$ . By using this definition for the square coil the formula can be rewritten to 3.20.

$$\tau = \frac{W \cdot I \cdot L \cdot B}{4} \cdot \sin(\theta) \quad (3.20)$$

where:

L is the side length in a square coil in m

W is the total length of wire used in m

As described previously a circular coil is also a possibility. By using the same formula 3.19 the number of windings can be calculated by  $n = \frac{W}{2\pi \cdot R}$  and the area the coil encloses  $A = \pi R^2$ . The formula can then be rewritten to formula 3.21

$$\tau = \frac{W \cdot I \cdot R \cdot B}{2} \cdot \sin(\theta) \quad (3.21)$$

where:

R is the radius of a circular coil in m

Evaluating the two coil formulas the relation between them is  $R = \frac{L}{2}$ , this means that using equal side length and diameter, both coils produce the same amount of torque.

### Coil Inductance

Another important part of the coil is the inductance of the coil. The coil self-inductance represents the magnetic flux to the current in the coil and is measured in Henry. This can be interpreted as an amount of the current stored in a coil after power has been turned off. This mean that a coil does not go to steady-state immediately but discharges over time. It is basicly the inverse component to a capacitor.

The magnetic field the coil produces is therefore consequently also reduced over time, after the power is removed. A part of this project is to detect the satelite direction on Earth's magnetic field. Since some sensors are required to detect the magnetic field direction of Earth, a discharging coil, will probably measure incorrect data. Therefore the coil discharging time must be calculated to be able to know when the coils are discharged enough to be sure that the sensor will measure the correct data.

To do this the magnetic field of the coils first must be known. The formula for calculating the magnetic field of a square coil is 3.22 and for a circular coil the formula is 3.23

$$B_{square} = \mu_0 \frac{2\sqrt{2}nI}{\pi l} = 7967.4I \cdot 10^{-6} \quad (3.22)$$

$$B_{circular} = \frac{\mu_0 n I R^2}{2(R^2)^{3/2}} = 11579I \cdot 10^{-6} \quad (3.23)$$

where:

$B$  is magnetic field generated by the coil in  $\frac{tesla}{m^2}$

$\mu_0$  is magnetic permeability for vacuum ( $4\pi \cdot 10^{-7}$ )

$n$  is number of windings (500)

$I$  is the current in the coil in A

R is Coil radius, in meters (35.5 mm)

$l$  is side of the equivalent square coil (71 mm)

To calculate the coil flux the B field must be calculated on the area the coil encloses. The formula 3.24 is used to calculate the flux through the coil.

$$\Phi = BA \quad (3.24)$$

The resulting flux for the square coil is:

$$\Phi = B_{square} A_{square} = 4016I \cdot 10^{-8} \quad (3.25)$$

And the flux for the circular coil is:

$$\Phi = B_{circular} A_{circular} = 4456I \cdot 10^{-8} \quad (3.26)$$

By evaluating the results from the square and the circular coils, it is shown that the circular coil gives a higher flux than the rectangular coil.

The equation to calculate the self-inductance of a coil is done by using formula 3.27

$$L = \frac{\Phi}{I} \quad (3.27)$$

where:

L is the self-inductance in Henry

The coil can be seen as a circuit with the coil and the resistance in series. The figure 3.6 gives an illustration of the circuit.

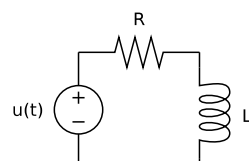


Figure 3.6: Model of the coil, including an inner resistance.

To calculate the coils time response, the circuit is defined as:

$$L \frac{di}{dt} + R \cdot i = v \quad (3.28)$$

where:

v is the voltage in V

$i$  is the current in A

Laplace transform of the circuit with unit step:

$$LsI(s) + RI(s) = \frac{1}{s}I(s)(Ls + R) = \frac{1}{s}I(s) = \frac{v}{Ls^2 + Rs}$$

By applying inverse Laplace transform, the formula for how the circuit current in the coil behaves in the time domain:

$$i(t) = \frac{v}{R}(1 - e^{-R*t/L}) \quad (3.29)$$

The formula for the discharging of the coil, where  $I_0$  is the current charged in the coil, at time  $t_0$ .

$$I_0 e^{-\frac{R(t-t_0)}{L}} \quad (3.30)$$

Using these formulas and the definition of a coil with a wire diameter of 0.14 mm it is possible to calculate the charging/discharging time of the coils. A graph of the charging/discharging of the coil is shown at figure 3.7.

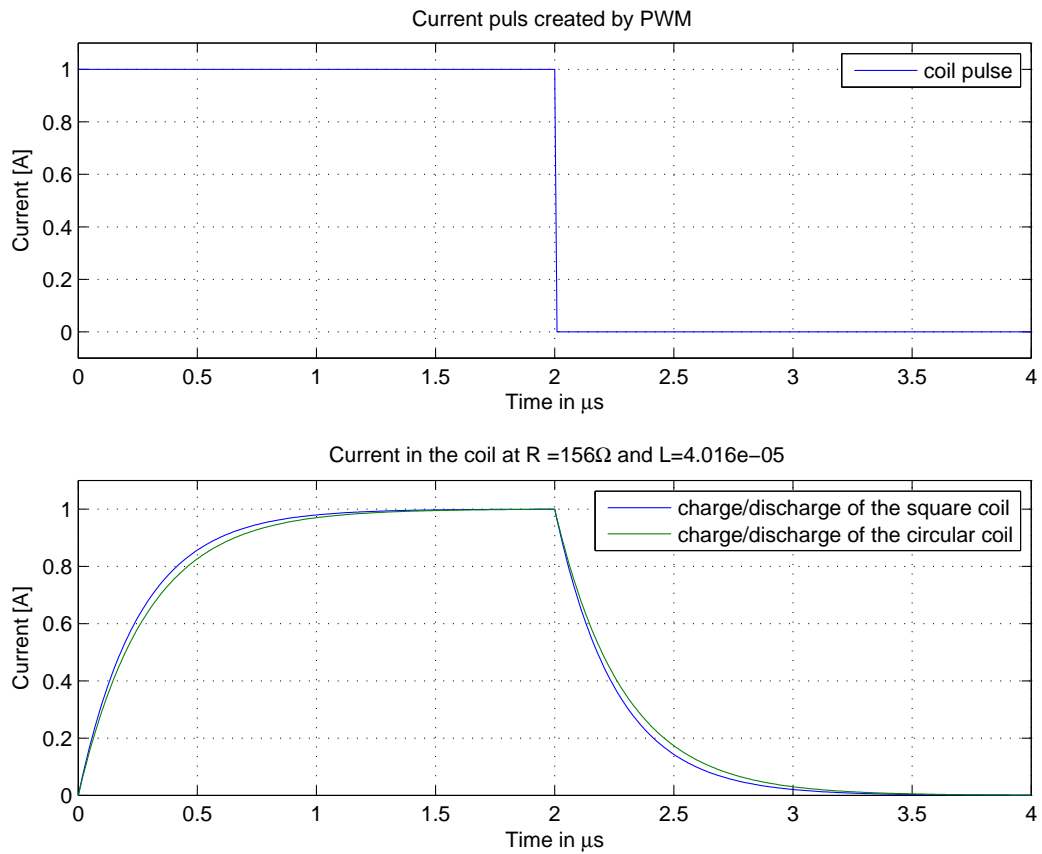


Figure 3.7: The current drawn from the PWM source, compared to the current charged due to self-inductance in the coil

By observing the graph, it can be identified that discharging the coil takes  $1.5\mu s$ . After the power has been shut off, this time must pass, otherwise the magnetic sensors will give incorrect data.

### 3.6.3 Temperature Influence on the Coils

The temperature of the satellite is varying during an orbit. This is mainly caused by the position of the satellite in relation to the Earth and the Sun. When the Earth is in the line of sight to the Sun, the satellite temperature drops as low as  $-25^{\circ}$  Celsius. When the satellite is exposed to sunlight the temperature reaches  $85^{\circ}$  Celsius.

The temperature influence on the coil is visible as the resistance is changing. In the table 3.6.3 it is shown how much the wire resistance changes at different temperatures.

$$R = R_0[1 + a(T - T_0)] \quad (3.31)$$

where:

$a$  is temperature coefficient  $3.9 \cdot 10^{-3}$  from [Physics for Scientists and Engineers, 2004]

$p$  is resistivity ( $\Omega \cdot m$ )  $1.7 \cdot 10^{-8}$

$A_{cross}$  is the cross area of  $0.14mm$  wire gives  $\pi(0.7 \cdot 10^{-4}m)^2 = 15394 \cdot 10^{-12}m^2$

$\frac{R_0}{m}$  is  $\frac{p}{A_{cross}} = 1.1 \frac{\Omega}{m}$  at  $20^{\circ} C$

$R_0$  is  $\frac{R_0}{m} \cdot 142m$  wire =  $156.8\Omega$

$T_0$  is the temperature of  $R_0 = 293.15K$  ( $20^{\circ} C$ )

Temperature	$\Omega$	Current at 5 Volt
$75^{\circ}C$	190.4 $\Omega$	26.3 mA
$50^{\circ}C$	175.2 $\Omega$	28.5 mA
$25^{\circ}C$	159.9 $\Omega$	31.3 mA
$20^{\circ}C$	156.8 $\Omega$	31.9 mA
$0^{\circ}C$	144.6 $\Omega$	34.6 mA
$-25^{\circ}C$	129.3 $\Omega$	38.7 mA

Table 3.1: Wire resistance at different temperature.

### 3.6.4 Magnetorquer Disturbance

When the magnetorquers are active they produce a magnetic field around them. Electronics could be effected by them and become unreliable, if this field is strong enough. A magnetorquer creates a magnetic field where the magnetic field direction is shaped as a torus. The magnetic field will be strongest in the middle of the magnetorquer, and fade out as the distance to the coil increases. The magnetic field can be calculated using the formula 3.32 where  $x$  is the distance to the coil, perpendicular to the area spanned by the coil. On figure 3.8 a calculation of the strength of the field produced by the magnetorquer at maximum setting is shown. The green line is the average strength of earth magnetic field.

As the satellite is  $10 \times 10 \times 10$  cm the equipment placed farthest away from the magnetorquers should be almost undisturbed.

$$B_{circular} = \frac{\mu_0 n I R^2}{2(R^2 + x^2)^{3/2}} \quad (3.32)$$

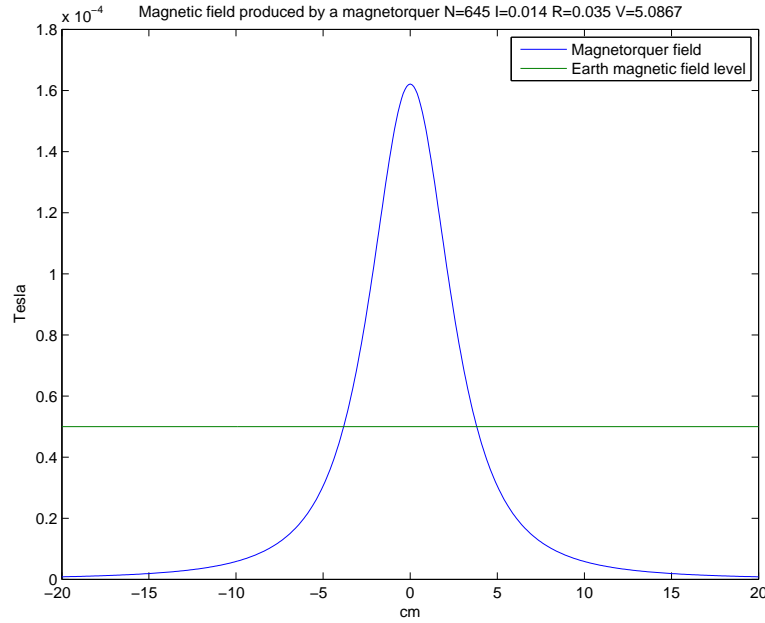


Figure 3.8: The field strength of the magnetorquers compared to that of the Earth.  
The field produced drops rapidly with the distance

### 3.7 Powering Magnetorquers

For controlling the magnetorquers it must be possible to regulate the current in the coils, not just in means of direction but also the level of current.

A common way to control the output is to use pulse-width modulation. Pulse-width modulation creates a square wave signal where the resulting average value is the integral over the waveform. As shown on figure 3.9 the value  $T$  represents the length of each cycle, and  $D$  represents the dutycycle. The area enclosed by the dutycycle is also the area of the average of the whole cycle enclosed by that period.

By adjusting the dutycycle time from zero to maximum time  $T$  it is possible to control the amount of current average between  $Y_{min}$  and  $Y_{max}$

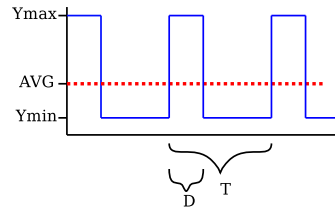


Figure 3.9: A PWM signal, marked the cycle time  $T$  and the dutycycle  $D$

By using pulse-width modulation, the current pulsed on the coil is not directly the average. It will give a torque which is equivalent to the average current. However, the coil will get pulsed as shown on figure 3.9, and the coil is an inductor and therefore the coil current will charge/dischARGE in the coil as seen at figure 3.7 on page 29.

The torque is proportional to the current in the coil wire, but the power used to apply the current is

$$P = R \cdot I^2 \quad (3.33)$$

The power consumed is proportional to the square of the current. A short pulse with a high amplitude consumes more power than a longer pulse with a lower amplitude assuming they cover the same area. The power used to make a three times higher pulsed current in one second is not the same as using the current in three seconds.

This is shown in figure 3.10.

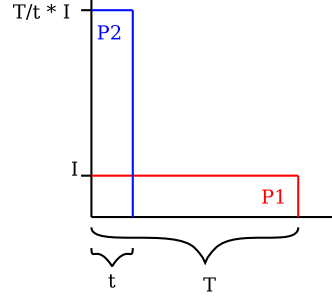


Figure 3.10: The area covered by P2 is equal to the area covered by P1. The power consumption of P2 is higher than that of P1.

Inserting the cycle time  $T$  over the complete period into formula 3.33 the result is:

$$P1 = T \cdot R \cdot I^2 \quad (3.34)$$

However by using  $\frac{T}{t} \cdot I$  of current in only the  $t$  time the result is:

$$P2 = t \cdot R \left( \frac{T}{t} \cdot I \right)^2 = \frac{1}{t} \cdot T^2 \cdot I^2 \cdot R \quad (3.35)$$

From this it can be observed that a pulsed current is more expensive in terms of power usage by  $\frac{T}{t} \cdot P1$ .

As it happens, it will be most effective to be able to control the current constantly so that it always is the average of the current. Knowing the coil charge/discharge time it is possible to select a cycle time that allows to smoothen the current, and thus minimize the loss in efficiency. On the figure 3.11 a calculation has been done with a cycle time of  $0.1 \mu s$ . This gives a small amount of ripple, but it smoothens the current. The cycle time at  $0.1 \mu s$  means that the switching frequency must be 10 MHz. To be able to control the dutycycle the frequency of the controller must be even higher. If it is desired to control the level  $y_{min}$  and  $y_{max}$  by 100 different levels. The dutycycle control frequency must be even 100 times greater, not including the higher frequency harmonics that allows for creating a squared signal. In this particular case the dutycycle control frequency should be 1 GHz, which is much higher than the limit of most microprocessors. As diodes of some sort, usually a H-Bridge is used for amplifying the PWM signal, and power is lost when switching the diode state, the frequency should not be chosen too high either.

As the frequency cannot be set high enough to smoothen out the curve, it becomes less important to select a very high PWM frequency, in relation to the efficiency.

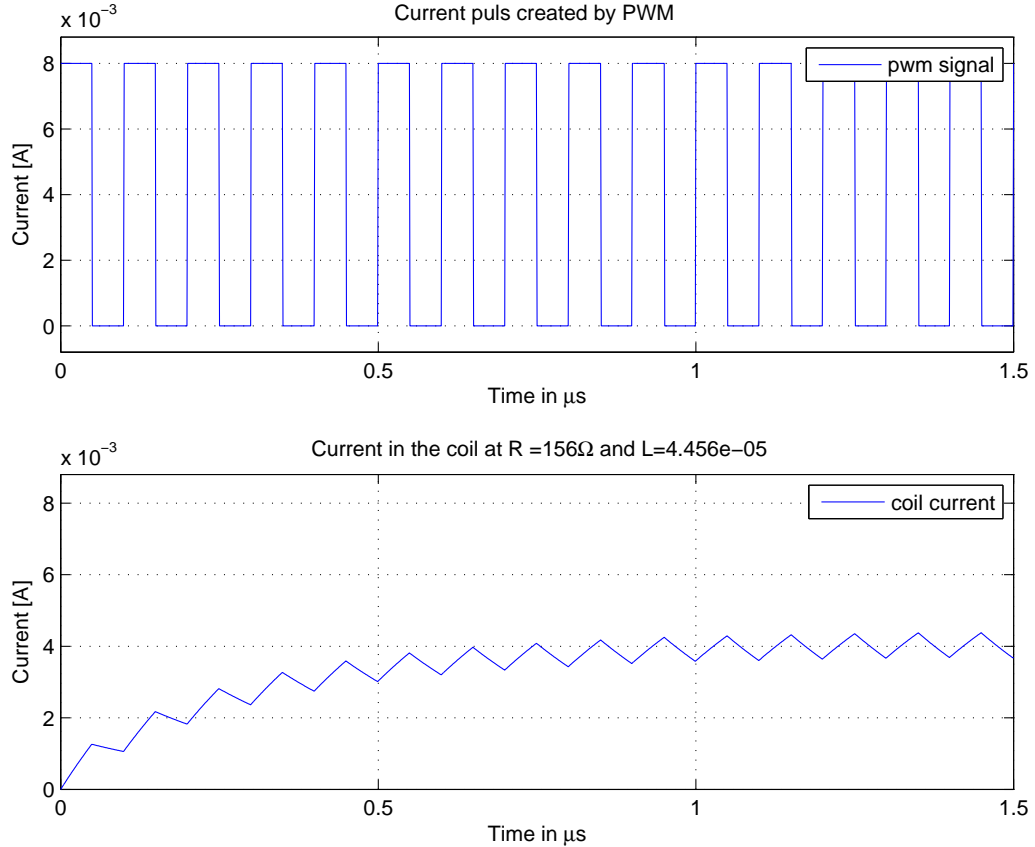


Figure 3.11: A smoother curve with a small ripple, unfortunately the frequency is very high

### 3.8 Actuating Using Magnetorquers

Magnetorquers introduce some challenges when controlling a satellite in space because magnetorquers only provide a torque at an angle in direction to the B-field, and not around it. The torque produced by magnetorquers works by producing a magnetic field, where the field direction will try to obtain the same direction as the B-field.

Figure 3.12 illustrates the direction the satellite can be controlled in. At figure B it is shown that in case the B-field is the same direction as the Z-axis on the satellite it is only possible to generate torque towards the Z axis. This means that it is not possible to control the rotation around the Z axis.

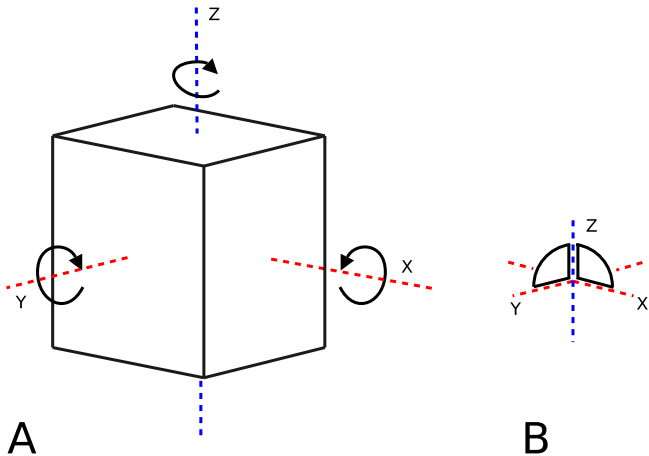


Figure 3.12: The dashed blue line represents the B-field. Figure A shows the alignment of the axes. Rotations are only possible around the red axes. On figure B the orientation of the torques

### 3.9 Sensors

This section contains an analysis of the different types of sensors able to measure movement and attitude in space. Most of the sensors in this analysis have already been used in satellites before. The AAUSAT-II satellite uses gyroscopes to detect the rotational velocity, and magnetometers to detect Earth magnetic field direction at the position of the satellite. AAUSAT-II also uses sunlight sensors to detect the Sun. The Ørsted satellite, of which the mission purpose was to map the geomagnetic field, used a star camera produced by Terma to get very precise information about the satellites attitude.

#### 3.9.1 Gyroscopes

Using a gyroscope is a way to utilize angular momentum to determine an angular rate. Angular rate is also known as angular velocity and corresponds to linear velocity, but is to distinguish between rotations and other motions, named angular rate.

Gyros have been implemented in a multitude of ways. Optical gyros permit the reflection of a laser ray many times within an enclosure. If the enclosure rotates, the duration between the moment of laser emittance and eventual reception differs. With ring laser gyros (RLF), the laser reflection is achieved with mirrors inside the enclosure. With fiber optic gyros (FOG), the laser reflection is achieved with a coil of optical fiber.

Spinning mass gyros use a steadily-moving mass with a free-moving axis (gimbal). These are classical mechanical gyros, and requires electrical motors to overcome friction and continue operations. A mechanical gyro with applied force, could be used as an actuator, but takes up a lot of room.

Vibrating gyros use microelectromechanical system (MEMS) technology and a vibrating, quartz tuning-fork to measure Coriolis force. When rotated, a vibrating element (vibrating resonator) is subjected to the Coriolis Effect, causing secondary vibration orthogonal to the original vibrating direction. By sensing the secondary vibration, the gyro can detect the rate of turning. At AAUSAT-II analog gyroscopes from Analog Devices were used, but a new family of gyroscopes with digital interface is available.

### 3.9.2 Magnetometers

Magnetometers can be made in many ways, basically the magnetorquer coils can be used for this as a fluxgate meter. The fluxgate sensors are basically coils, which are magnetically shielded, in such a way that they only can measure components in a single axis. In this way a compass can be made out of two fluxgates.

A completely different approach for measuring the magnetic field vector, is using magnetoresistors which are magnetically sensitive ohmic devices. Some of the available components have built-in shielding to ensure that they only react in one axis, others have special coating to make them reactive in a given direction.

Magnetometers can be used for validating / calibrating the magnetic field model as a way to measure the direction and field strength. However, they require the actuators to be shut off and discharged before measuring if placed too close to the torquers, otherwise the magnetorquers field is measured.

The magnetometers can be used for navigation, if a three-dimensional compass is utilized. This will provide information on how the magnetic field is oriented in all axes. Thus if the position of the satellite is known, the orientation can be estimated from a comparison between 3D compass readings and a 3D geomagnetic map.

However knowing the direction of the B-field does not mean that the attitude is known. The rotation around the B-field is not detectable using magnetometers, because all the measured vectors will be the same for all angles.

An example of this can be seen in figure 3.13 A and B.

In figure 3.13 A the Z axis is the parallel with the B-field direction. In this case a rotation on the Z axis will be undetectable. This happens because the magnetometers on the Y and X axis will be measuring orthogonally on the B-field and therefore measure a zero field. The magnetometer in the Z axis will give a constant response as it is always oriented directly on the magnetic field, and therefore it is not possible to detect this rotation.

In figure 3.13 B the Z axis is not directly parallel on the B field, but if there is a rotation directly on the B field, the Z axis will be rotated in the circumference of a cone around the B field. The response given by the magnetometers in the Z axis will still be constant around the B-field. The same effect will also happen for the X and Y axis, and thus the rotation around the B-field is undetectable.

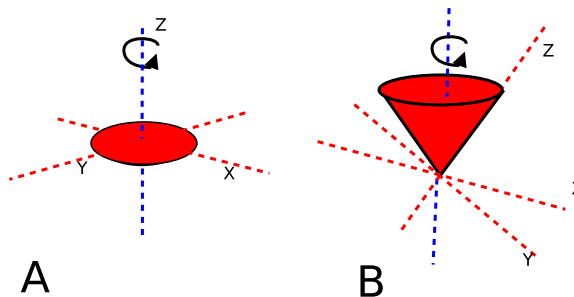


Figure 3.13: Rotating a system with magnetometers on the B-field.

### 3.9.3 Sunlight Angle Measurement

This is commonly used on satellites. On all surfaces a small hole is made, and beneath it in a known distance, an array of light sensitive diodes are placed. This could be image sensors but are often just photodiode arrays as known from scanners.

When the sunlight hits the surface of the satellite, some of the light radiates through the hole, as a single ray of light. The place where the ray hits is measured with the diodes, and this

allows for determining the angle from where it came. The strongest light source seen from orbit is the sun, thus the satellite can determine where the sun is. A calculation of where the satellite is in orbit allows it to determine its attitude relative to the Earth's surface.

### 3.9.4 Star Camera

A star camera provides a very good estimate of the attitude. It functions by capturing an image of the stars within the field of view. These stars are located with software and are finally compared with a star map, usually containing constellations for pattern recognition. When a constellation is found in the database, the informations about the satellites rotation on all three axes can be extracted, due to the location of and rotation of the constellation within the image captured.

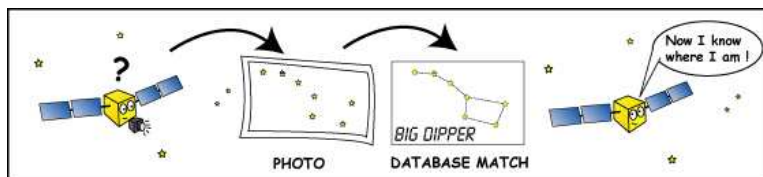


Figure 3.14: Borrowed from [www.NASA.gov](http://www.NASA.gov)

The star camera requires an onboard camera, which is already proposed on AAUSAT3, a lot of memory for the star maps, and a powerful processor for doing the software comparison. The proposed camera, which is already constructed, has enough memory, and the ARM7 processor on the camera would take some time to do this image-processing, but it is not impossible to get data validation on old data from this hardware. However, the camera has no shielding against direct sunlight in its current form, and therefore it would only be able to recognize stars at some angles.

### 3.9.5 NAVSTAR Global Position System (GPS)

The GPS satellites travels in MEO, and AAUSAT3 travels in LEO. This altitude difference allows for a GPS receiver to calculate its current location. Multiple antennas with enough spacing, could even provide the attitude, but this would in known configurations require more space than is found on a picosatellite.

The location of the satellite is intended to be used for determining the magnetic field strength and orientation. Other applications could be found for a GPS receiver. During the first weeks after launching AAUSAT-II, the orbital elements was unknown, which made it difficult to track it from the ground station. This happened because other satellites was launched from the same rocket, so NORAD had multiple new elements to track at once. NORAD can easily do this, but the output is an orbital element for all of the new satellites. This leaves the groundstation operators to choose which one they believe to be the correct satellite. As beacons was recorded fairly early, even at poor tracking, data in a beacon provided by a GPS receiver could have helped in determining which new element was AAUSAT-II.

The GPS satellites orbits at an altitude of 20,200 kilometers. They are contrary to popular belief not geostationary. This is also the reason why it can vary over time how many satellites you can see from a point on the surface. 4 satellites are often used to determine the location, if the altitude is known 3 can be used, but at all times 4 or more are preferable. For a satellite in orbit much more than 4 satellites would be in view. However if the AAUSAT tumbles, or if the GPS antennas on it are not omnidirectional, the result could easily be that no GPS satellites are tracked successfully, and thus the system would not provide anything.

The GPS receivers requires antennas which takes up surface area which allows for less solarpanels. Some of the commercial GPS receivers have been tested in LEO before, and has been known

to operate for approximately a year. A GPS receiver in general uses 100 mA or more at 3.3 V while tracking. So even though it is feasible and convenient to mount a GPS receiver on the satellite, problems could arise in the power budget.

Other subsystems like AIS holds an interest in getting the coordinates of the satellite, and very accurate timestamp when recording an AIS signal and a GPS signal can provide both. At the time of writing the report, no final decision has yet been made about carrying a GPS module or not.

### 3.10 Conclusion

The space environment was analyzed, and it is determined that the hazards of primary interest are vacuum and temperature fluctuations. The influence from vacuum can be somewhat overcome by treating the components with a special coating, but the temperature sets up limitations for the choice of hardware, as they must be able to operate while in orbit.

The disturbance torques influencing the attitude of the satellite has been calculated. The sum of disturbances is the minimum torque that the magnetorquers must be able to provide in order to keep the satellite detumbled.

The TLE orbit description created by NORAD provides a standardized way to describe the orbit, and it is suggested that this is used to determine the position of the satellite. Should GPS be available this will provide even better position estimates, and should of course be harnessed when possible. The position can be combined with the WMM geomagnetic field model to determine the orientation of the magnetic field for the position. Using the magnetorquers to determine the geomagnetic field this will give an estimate of the attitude.

However this will not be enough as rotations around the field vector are undetectable, so the entire orbit must be used to extrapolate the attitude. To help determine this, gyroscopes will provide information about the angular rate, and can also be used to estimate the attitude for a shorter period of time.

A controller that can measure the magnetic field, and the angular rate at all axes, will be able to determine its attitude after half an orbit.

# CHAPTER 4

## Requirement Specification

The following requirements are for the final ADCS subsystem on AAUSAT3 and must be fulfilled before flight.

### 4.1 Hardware Requirements

The hardware must be able to operate as a subsystem in AAUSAT3 to ensure this a list of requirements are set to the hardware.

**The ADCS hardware must be build from components that have an estimated lifespan of at least half a year**

This requirement is inherited from the expected minimum lifespan of the subsystems on AAUSAT-II, as the minimum lifespan is not yet set for AAUSAT3

**The ADCS hardware must not rely on moving parts.**

This requirement is set by the system engineering group

**The system must be able to withstand the vibrations during launch**

The specific pattern is currently set by ESA Vega Maiden Flight Campaign  
Fulfilled by vibration testing the system with the values described in the Vega Users Manual [ARIANESPACE, 2006].

**The assembly of ADCS must be done with class 3 soldering quality**

This is a standard requirement for all subsystems.

**The hardware must provide the entire platform for the autonomous ADCS controller**

Due to the design of AAUSAT3, the ADCS subsystem is not included in the basic system, and must therefore provide the necessary hardware for the controllers.

**The system has to use either 5 V or 3.3 V, or both for supply.**

The AAUSAT3 system has voltage levels of 5 and 3.3 V available. It is however possible to gain direct access to the batteries for powering the magnetorquer coils.

**The power budget must be complied with.**

Currently the powerbudget has not been defined. Before the system is finished the powerbudget including a powerslot for ADCS must be accepted.

**A CAN transceiver must exist**

For transmitting and receiving commands a protocol has been developed to run on the CAN. This is due to its high noise tolerance, and experiences from AAUSAT-II.

**The operating temperature range for the system must be at least -40 to +80 °Celsius**

This requirement is set by the system engineering group.

This requirement is fulfilled by testing the system in a controlled test environment within the given range.

**The system must be able to operate in near vacuum, more specific at a pressure of 66.7mPa**

This requirement is set by the system engineering group.

**The operating radiation resistance is 10 krad**

This requirement is set by the system engineering group.

## 4.2 Functional Requirements

To perform as ADCS, some requirements are set to the performance of the system.

**Magnetorquers must supply more torque than  $39 \cdot 10^{-6}$  Nm**

The magnetorquers must be able to provide more power than the worst case disturbance force, to keep the satellite stabilized at all times.

**Overshoot must be avoided**

As the satellite will be in space it is difficult to test if the satellite will do as predicted when in orbit. Thus it is preferred that the controller design is made with a minimum of aggression, as the risk of starting a rotation that cannot be stopped is then minimized.

**Heartbeat, housekeeping and commands via CsP**

The system must be able to reply on a heartbeat ping and transmit housekeeping data and raw sensor data over the CANspace Protocol. This is a standard requirement for all subsystems.

## 4.3 Requirements From Other Subsystems

The subsystems found on AAUSAT3 sets some requirements to the ADCS system. As ADCS requires a lot of power to create torque, it is one of the last systems to be switched on. Thus the high priority systems as EPS and COM are designed to be operational even when the satellite is tumbling. The lower priority systems, such as payloads have set up requirements for the ADCS system.

- UHF communication(COM).

- Automatic Identification System (AIS)
- S-Band Radio (COM-S)
- Camera (CAM)

The requirements are listed and described for each subsystem below.

## COM

The COM system uses a dual dipole antenna which is almost omnidirectional as it has a radiation pattern the shape of a double torus and therefore does not have any requirements to the direction of the antenna.

- **Requirement:**

- none

## AIS

The AIS system mainly uses dipole antennas which must be tangential to the surface of the Earth in the area it is tracking. The reason for this is that the AIS antenna on ships are also dipole antennas, which give very little or no signal upwards. An illustration of this is shown on figure 4.1. The antenna on the satellite is given a margin of  $\pm 45$  degrees. Furthermore the satellite must be stable and information about the orientation of it must be available.

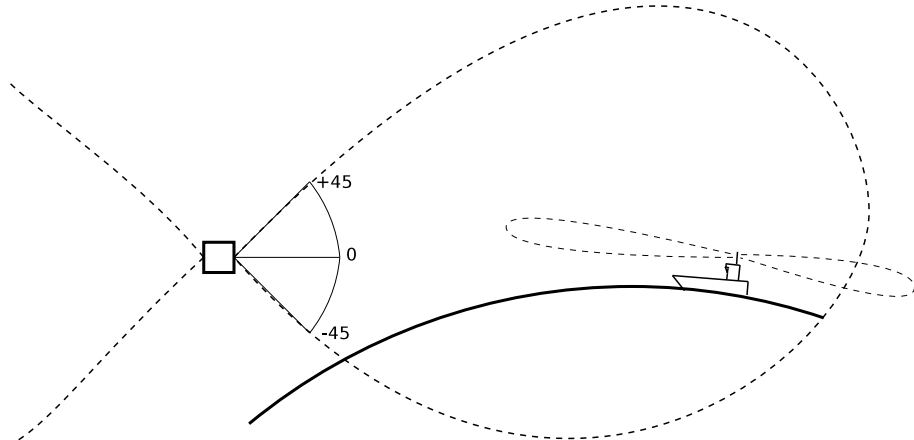


Figure 4.1: The directivity of the AIS antennas on AAUSAT3 and an arbitrary ship.

- **Requirements:**

- Detumbled to less than  $2 \frac{\text{deg}}{\text{sec}}$ .
- Point  $\pm 45$  degree for tangential line on Earth.
- Measured angle accuracy of  $\pm 5$  degree

## COM-S

The S-band radio system is designed to use directional antenna on all side, thus functioning as an omni-directional antenna. Therefore the orientation of the satellite does not matter. This subsystem requires to be detumbled to avoid doppler effect.

- Requirements:

- Detumbled to less than  $5 \frac{\text{deg}}{\text{sec}}$

## CAM

The camera subsystem requires that the attitude of the satellite is controllable so that the lens can be pointed in a desired direction. Under operation the satellite must be detumbled to avoid blurred and skewed images.

The shutter time can be set from the ground station, and the default setting is low, as the Earth is a strong light source. If an image is however to be taken of the moon, a much longer shutter time is required to get good contrast in the image.

- Requirements:

- Detumbled to less than  $5 \frac{\text{deg}}{\text{sec}}$
- Point  $\pm 10$  degree on the desired photo object.

## 4.4 Delimitation

This project is limited by the available testing facilities. It is not currently possible to test the system in a zero gravity, depressurized and frictionless environment. Creating a test environment that accommodates all these parameters are out of the scope of this project.

The focus of the project is to control the satellite in one axis, in a homogenous magnetic field, to test the usability of the magnetorquers. This means that the control strategy is adapted towards this.

However this does not mean the requirements cannot be met. The requirements for accuracy, rotational speed, and orientation are still obtainable, but in an approximated environment with less freedom of movement for the satellite.

The requirements for the hardware should be considered as well. The choice of the sensors and the design of the magnetorquers should be adapted, but it is of less importance for the rest of the prototype as it could be replaced with space graded equipment without changing the performance of the controller.

The usage of the Csp protocol is also left for later implementation.

The following requirements are set up for the 1-dimensional prototype system:

**Magnetorquers must supply more torque than  $39 \cdot 10^{-6}$  Nm**

**Overshoot must be avoided**

**Detumbled to less than  $2 \frac{\text{deg}}{\text{sec}}$ .**

**Measured angle accuracy of  $\pm 5$  degree**

**Point  $\pm 10$  degree on the desired photo object.**

## CHAPTER 5

### Test Specification and Design

The delimitation provides the inherited requirements that must be dealt with in the test specification.

The test cases are as follows:

#### **Magnetorquers must supply more torque than $39 \cdot 10^{-6}$ Nm**

Mount the magnetorquer on a strain gauge and place it perpendicular to the spanned area of the helmholtz coils. Apply maximum voltage and measure the strain gauge. Calculate the gearing of the helmholtz coils.

#### **Overshoot must be avoided**

Apply a step to the controller for half a rotation and sample the angle of the satellite. Evaluate the samples.

#### **Detumbled to less than $2 \frac{deg}{sec}$ .**

Make the satellite tumble by applying an external force when the controller is enabled. Verify the gyroscope readings.

#### **Measured angle accuracy of $\pm 5$ degree**

Mount a camera above the satellite test-setup pointing towards the satellite. Verify the the angle using image processing software and the measured angle from the magnetometers.

#### **Point $\pm 10$ degree on the desired object.**

Mount a camera above the satellite test-setup pointing towards the satellite. Use a controller to point the satellite in the chosen direction. Verify the the angle using image processing software.

# CHAPTER 6

## Modelling

In this chapter modelling of the different parts of the system is done. The chosen sensors are described to give insight to their behaviour as their models are provided by datasheets. The satellite behaviour is modelled and the test setups influence likewise. Actuators are not modelled as they are already contained in the analysis.

### 6.1 Sensor Modelling

The sensors are modelled to define how the sensors response on different movements and inputs to the system. The sensors frequency response is later used in the model of the overall experiment to verify how the system acts.

#### 6.1.1 Gyroscopes

The gyroscope chosen (ADIS16100), has been selected due to its ability to handle high g-forces and operate in the temperature range from -40 to +80 °Celsius. Another reason for selecting this gyroscope is that it has two external ADC input channels and an internal temperature sensor. This allows connecting all the sensors through a single digital SPI connection. This configuration sets the least restrictions for the microprocessor hardware, and allows for almost any microcontroller to be used for processing the data, as there are no requirements set for an ADC.

The gyroscope features a  $V_{drive}$  and a  $V_{cc}$  connection. The  $V_{cc}$  requires a 5 V source to operate the gyroscope, but the  $V_{drive}$  allows for any voltage between 2.7 V and 5.25 V, and drives the logic gates only. This also increases the possible choices of microcontrollers, as both 3.3 V and 5 V supplies are possible for the logic connections.

The gyroscope is made of two separate vibrating polysilicon sensing structures, that senses Coriolis motion with capacitive pickup. The dual-sensor design rejects external g-forces and vibration, and there is a single-pole, low-pass filter included on-chip that is used to limit high frequency artifacts before final amplification. The frequency response is dominated by the second low-pass filter, which from the factory has a 3 dB bandwidth at 40 Hz. Thus this filter is used for modelling the continuous part of the sensor.

The built in ADCs operate in the same sample scheme as the gyro, but is not coupled through the filter. It is an iterative comparator, and takes 14 iterations to complete its sample. The iteration speed is driven by the SPI master clock (SCLK).

The gyroscope is able to sense speeds up to 300 deg / s, which is less than a completed rotation per second, but assumed fast enough for determining the satellites actual tumbling speed. After

analog to digital conversion a digital representation of the measurements is outputted on the SPI interface. The sampling speed of the ADC that samples the lowpass filtered signal, is set by the SPI interface, and defined from the SPI's master clock (SCLK), and is given as 16 cycles of SCLK, with a maximum SCLK at 20 Mhz. This enables the gyroscope to sample at all most 1.25 MHz when driven at maximum speed, (not including wait states) which is disproportionately a high frequency when compared to the 40 Hz 3 dB bandwidth of the built-in lowpass filter.

The advantage however is that a microcontroller can be handed a new measurement of the angular rate very often, which is noise filtered analogous, so that a software filter is not necessary, and processing power is thus saved for other purposes.

To verify the accuracy of the gyroscope a stability test have been made to verify the gyroscope value in a stable position. The test have been made by placing the gyroscope on a box, and recode the sensors value. At figure 6.1 the gyroscope value is shown, for the stable test of the gyroscope.

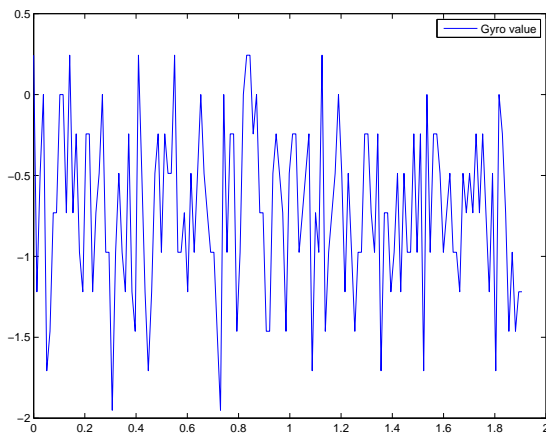


Figure 6.1: Test of the gyroscope precision when it is stable.

### 6.1.2 Magnetometers

Honeywell has a family of magnetoresistors which can deal with the temperature range that is required. A double axis magnetoresistor from the same family is found in AAUSAT-II.

The chosen magnetometers are basically magnetoresistors and silicium based resistors coupled in a Wheatstone bridge. A Wheatstone bridge operates by utilizing Kirchovs laws, and was originally created to measure resistors. In the Wheatstone bridge one of the four resistors is the one being measured, and voltmeter is placed over the outputs. In this way the resistor will cause a voltage difference on the outputs, and thus making it possible to estimate the resistors value. The magnetometer chosen is made so that two resistors are sensitive to the magnetic field, in a given direction, and thus the output is doubled.

The sensitivity is accomplished by a small film of an NiFe alloy, this is a magnetic alloy, which conducts current. The result is a resistor which varies according to a magnetic fields component in the direction of the films magnetized axis. This sensitive direction can be set or reset, which implies driving a current through straps within the component that realigns the films magnetization. A reset current will turn it one way and a set current will drive it the opposite way.

To keep the magnetometer as sensitive as possible, a pulse is recommended to be given regularly. This pulse is according to the datasheet required to have an amplitude of 0.5 to 1 A. Usually such high powers should be avoided in space applications, but as the duration of the pulse does not need to be very long ( $2 \mu\text{s}$ ), it merely requires some capacitive elements to build up

the required current over some time, instead of spiking the batteries. It is suggested in the data-sheet to do this set / reset every 10 minutes.

The bandwidth of the sensor is dependent on the reaction speed of the films, and is thus guaranteed to 10 Hz 3 dB bandwidth only. This is however plenty, as the intended use for the magnetometer is to determine the attitude when the satellite is no longer tumbling.

The sensor can be modelled much like the gyroscope, however instead of measuring angular rate, the magnetic fields angles are measured.

If the gyroscope ADC is used for sampling as proposed, the sampling speed of the magnetometer is like the gyroscope readings determined by the SPI interface. But unlike the gyroscope readings, the actual reading will be influenced by the usage of the actuators, as they will generate magnetic field, and thus measurements require the magnetorquers to be shut off, and discharged when measuring. As a result measurements should be done as seldom as possible.

For measuring the angle of the satellite on the B-field two magnetometers are used, placed orthogonal to each other. Each sensor gives a value plus/minus the offset as it points on the B-field. Using only one sensor the value on each side will be mirrored on both sides of the B-field. This means that it is not possible to determine the difference between 45° left or right on the B-field. Using the two sensors, the second sensor will tell which side the satellite is. An example of each sensor's response on the B-field can be seen at figure 6.2. The left figure represent the satellite in the middle, the arrow in the picture is the satellites attitude, when the satellite points as shown on the picture the blue ellipse will represent sensitivity of sensor 1, which is placed straight on the B-field and will give a full response. At the same attitude the red ellipse represents sensor 2 orthogonal on the other sensor, which will give the value zero. Turning the satellite the sensors will change as they are effected by the B-field.

Figure 6.2 B shows the response of the sensors from 0 to  $2\pi$  radians. The position of the satellite is given using arctan on both values:  $\arctan(\frac{Sensor1}{Sensor2})$ .

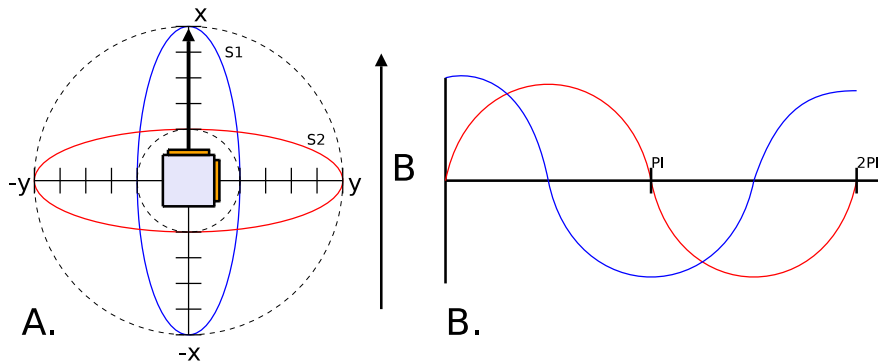


Figure 6.2: Magnetometer response at different positions.

## 6.2 Satellite Modelling

The satellite is modeled first without any disturbances. As the controller is a one-axis system the disturbance forces are not included in the model, however the nylon wire is modeled and added. This is to determine if the wire can be neglected when designing the controller.

### 6.2.1 Physical Environment

The satellite can be seen as an ordinary DC motor except that it does not have any friction forces involved. By using a free-body diagram as shown on 6.3 the physical environment for the satellite can be modelled. The free-body diagram shows the satellite in the middle with the definition of the direction of the torque and  $\omega$  the angular rate.

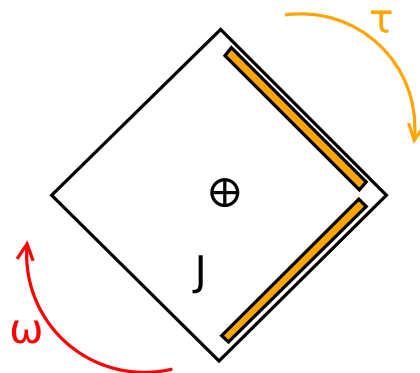


Figure 6.3: Free-body diagram of the satellite.

To calculate the moment of the inertia of the satellite some definitions are made. For a rotating body, there is a relation between torque and angular acceleration. This is expressed as

$$J\dot{\omega}(t) = \tau(t)$$

where:

$J$  is the moment of inertia in  $kg \cdot m^2$

$\dot{\omega}$  is the angular acceleration

Assuming that the satellite has a uniform mass, the moment of inertia,  $J$ , is expressed as:

$$J = \frac{1}{12} \cdot m \cdot (a^2 + b^2) = 1,667 \cdot 10^{-6} kg \cdot m^2 \quad (6.1)$$

where:

$a$  is the width of the satellite in  $m$

$b$  is the length of the satellite in  $m$

$m$  is the mass of the satellite in  $kg$

The formula is from the Wikipedia entry for solid cuboid moments of inertia<sup>1</sup>.

By applying Laplace transform to the model:  $J\omega(s) = \tau(s)$

---

<sup>1</sup>[http://en.wikipedia.org/wiki/List\\_of\\_moments\\_of\\_inertia](http://en.wikipedia.org/wiki/List_of_moments_of_inertia)

The transfer function for the model is

$$\frac{\omega(s)}{\tau(s)} = \frac{1}{Js}$$

This is the result of a satellite with one degree of freedom and no included disturbances. In outer space the satellite will have this result in all three dimensions.

### Verification of the Inertia

The assumption that the mass is distributed uniformly should be evaluated for the final satellite. For the prototype the moment of inertia is evaluated by applying the maximum torque which can be provided and is calculated to be  $1.0532 \cdot 10^{-5} \text{ Nm}$ . The angle and angular rates are plotted and an approximation is done to both curves by adjusting the moment of inertia in the simple model. The result of the fit can be seen on figure 6.4, this sets the moment of inertia to

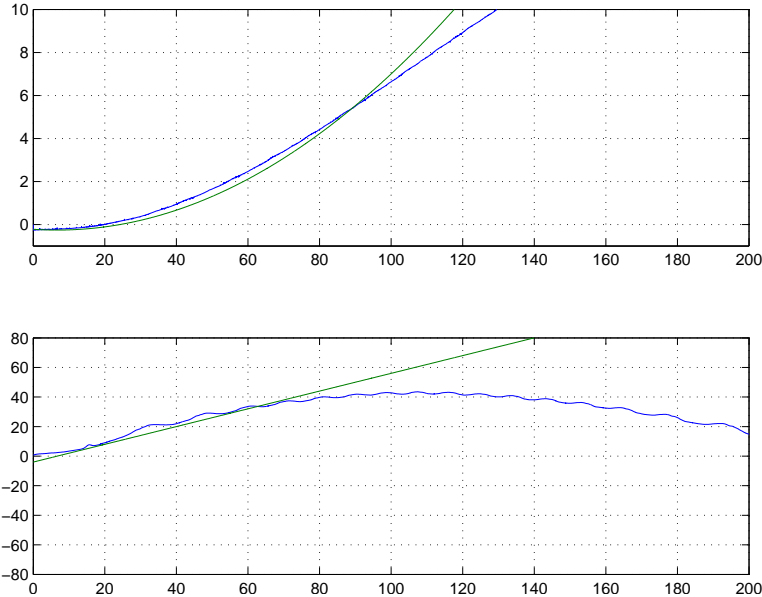


Figure 6.4: Calculation of the inertia

$$J = J_{calculated} * 1.3 \quad (6.2)$$

### 6.3 Experimental Model

The experimental test setup is a satellite attached to a wire in the ceiling. The wire is used to simulate microgravity and a zero friction environment. However, when the satellite rotates in one direction the wire will get twisted and the result will be a torque in the opposite direction. Furthermore there are dampening factors from the environment, such as friction from the wire and the air surrounding the satellite. This was also apparent in figure 6.4, where the speed slowly decreases after some time.

The free-body diagram for this is shown in figure 6.5.

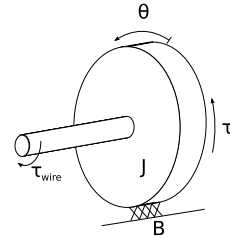


Figure 6.5: Free-body for the experimental test setup.

To determine the size of the dampening constant  $b$ , and the spring constant  $K$  of the wire an experiment has been done. The experiment has been conducted by simply rotating the satellite and thereby twisting the wire a number of times and measure and store the output of the gyro and magnetometers until the satellite is in steady-state. The measurements are shown in figure 6.6 and 6.7.

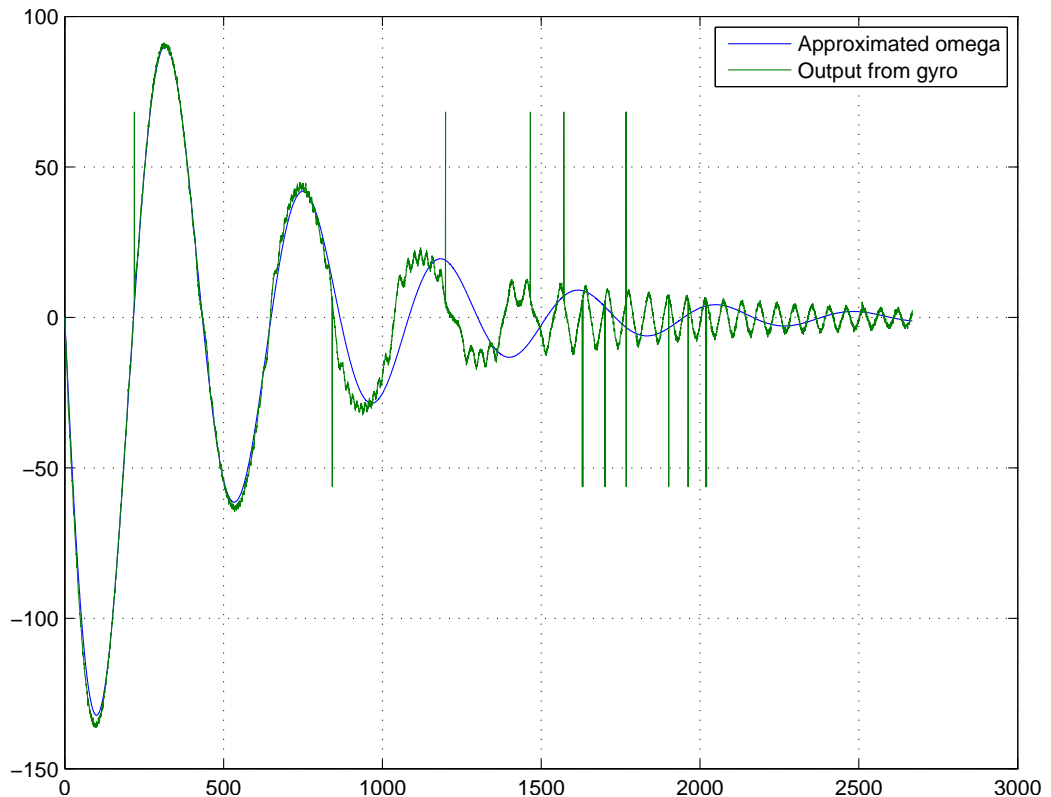


Figure 6.6: Estimation of dampening constant  $b$  by approximation of  $\omega$ .

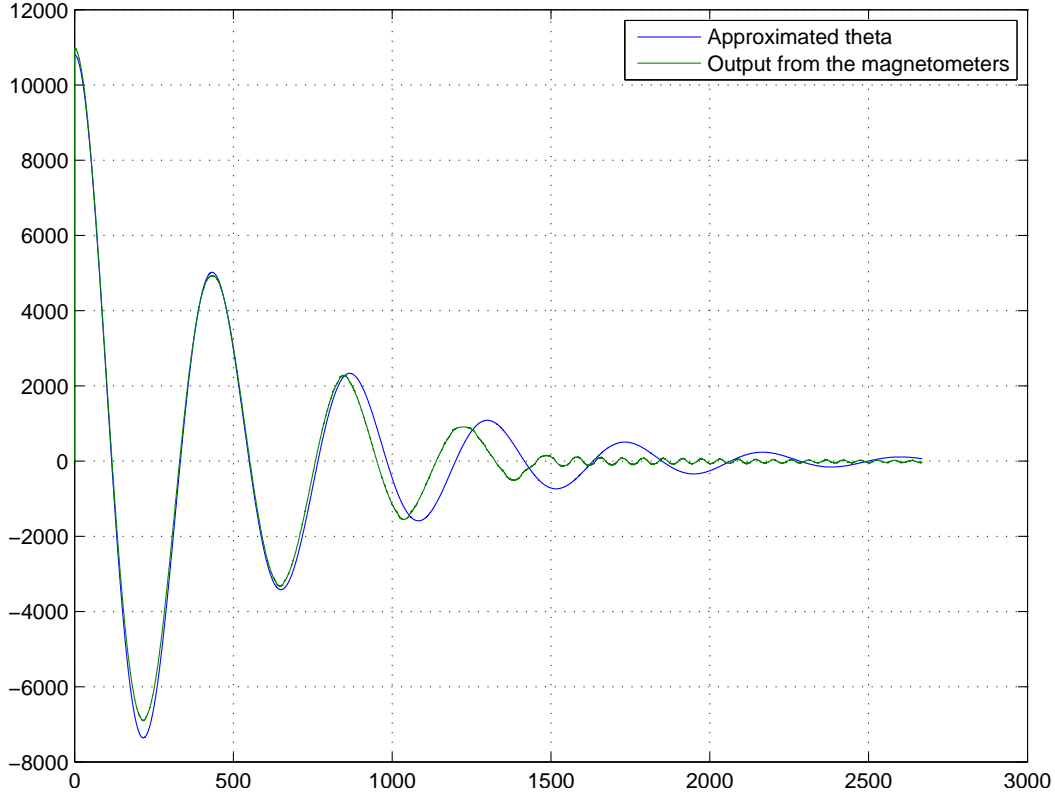


Figure 6.7: Estimation of dampening constant  $b$  by approximation of  $\theta$ .

In order to find one of the constants, the transfer function for the system is found and the frequency from the measurements is inserted. From the free-body diagram:

$$J\ddot{\theta}(t) = \tau(t) - \tau_{wire}(t) - B(t) \quad (6.3)$$

where:

$$\tau_{wire} = K\theta(t)$$

$$B(t) = b\dot{\theta}(t)$$

$J$  is the moment of inertia

$$J\ddot{\theta}(t) = \tau(t) - K\theta(t) - b\dot{\theta}(t) \quad (6.4)$$

By Laplace transforming the model:

$$J(s^2\theta(s) - s\theta_0 - \omega_0) = \tau(s) - K\theta(s) - b(s\theta(s) - \theta_0)$$

The transfer function for the model is:

$$\theta(s) = \frac{\tau}{Js^2 + bs + K} + \frac{Js\theta_0 - b\theta_0}{Js^2 + bs + K} = \frac{\tau}{s^2 + \frac{b}{J}s + \frac{K}{J}} + \frac{s\theta_0 - \frac{b}{J}\theta_0}{s^2 + \frac{b}{J}s + \frac{K}{J}}$$

For a standard second-order closed loop system it is known that:

$$\omega_n^2 = \frac{K}{J} \Rightarrow K = \omega_n^2 J$$

The first cycles of the measurements indicates a cycletime  $T$  of 430 seconds. Inserting  $\omega = \frac{1}{T}$  and the moment of inertia  $J$  yields:  $K = \left(\frac{1}{430}\right)^2 \cdot 0.001 = 2.1351 \cdot 10^{-7}$

The dampening constant  $b$  is found through interpolation. From equation 6.4:

$$\dot{\omega} = -\frac{K}{J} - \frac{b}{J}$$

it is easily deducible that:

$$\dot{\theta} = \omega$$

It is desired to create a matrix such that:

$$\dot{x} = Ax + B\tau$$

where:

$$x = \begin{bmatrix} \theta \\ \omega \end{bmatrix}$$

This yields:

$$\dot{x} = \begin{bmatrix} \dot{\theta} \\ \dot{\omega} \end{bmatrix} = \begin{bmatrix} 0 & 1 \\ -\frac{K}{J} & -\frac{b}{J} \end{bmatrix} \begin{bmatrix} \theta \\ \omega \end{bmatrix} + B\tau$$

In the experiment no torque was applied,  $\tau = 0$

The solution for such a system is:

$$x = e^{At} \begin{bmatrix} \theta_0 \\ \omega_0 \end{bmatrix} \quad (6.5)$$

The dampening constant  $b$  is found to be  $4.6 \cdot 10^{-6}$  and the spring constant  $K$  was found to be  $2.7757 \cdot 10^{-7}$ . The resulting open-loop responses are shown on figure 6.6 and figure 6.7.

These values apply well to the first four changes in direction, however there is a sudden change in frequency as the amplitude gets lower. This indicates an interference which is negligible as long as the amplitude does not cross  $\approx 25$  deg/s as the frequency seems constant both before and after this mark. This might also indicate that  $K$  is not a constant but somehow dependent on the amplitude. The readings are sampled with the gyroscope which is not located in the center of rotation. Furthermore the suspended satellite could be acting as a pendulum which might also appear in the gyroscope data.

## CHAPTER 7

### Controller Strategies

The attitude control system of an element is linked with the chosen method of describing the attitude error. To clarify this statement consider a situation where the attitude is described in a cartesian coordinate system. If origo is chosen as the centre of mass of the satellite, the description of the attitude can in two dimensions be determined by a vector. It will contain an x and a y component, and thus the attitude is described with 2 inputs.

A different description could be a polar description. the same vector here contains an angle and a length component. The length is indicating the magnetic field strength, this should be varying very slowly and is therefore of less importance. Should the variance give a considerable change in the magnetorquers performance, it could be fed back separately in an inner loop. This description can therefore be reduced to the angle. So actually only 1 variable is needed, for creating the controller.

The choice of strategy for controlling the attitude is thus closely linked with how the problem is described. If the cartesian coordinates are used, the system is described in a vectorized system where the inputs should be handled individually. Thus it seems to be an advantage to keep this description in a matrix/vector form, and treat this problem as a multiple input, multiple output problem (MIMO). For this a state-space based controller seems to be the controller type which in its formatting is suited best for MIMO systems.

On the other hand, it can be claimed that if the polar system is used, the angle can be transferred directly as a feedback branch to the reference and thus produce an error. This will simplify the entire system to a Single Input, Single Output controller (SISO).

Furthermore the length which describe the field strength, is in the test setup a homogenic field, with known strength, so it is not necessary to handle this. This claim is investigated in the following, and controllers are designed to control the applied torque level, based on the angular error.

## 7.1 Strategy for Using Magnetorquers as Actuators

The magnetorquers are basically coils that act on the geomagnetic field when a current is applied, and thus causes a torque to arise. The torque that arises will cause the satellite to rotate, and the Earth to react with the same amount of force, but as the Earth which creates the geomagnetic field is vastly larger than the satellite, this influence is immensely small.

It is assumed that the geomagnetic field at a given point in orbit can be simplified to a homogenous field, with an orientation and a strength. Thus the basic formula for the torque that arises from a current loop in a homogenous magnetic field can be applied [Physics for Scientists and Engineers, 2004]. Here it has been modified with a multiplier to allow for easy insertion of the number of windings.

$$\tau = nIA \times B \quad (7.1)$$

where:

$\tau$  is the torque in  $N \cdot m$

$n$  is the number of coil windings

$I$  is the current in the wire in  $A$

$A$  is a vector perpendicular to, and with the length of, the area spanned by the current loop

$B$  is the homogenous magnetic field in *tesla*

which can be translated into the formula 3.19 on page 27, shown here for convenience.

$$|\tau| = nIAB \cdot \sin(\theta)$$

where:

$\theta$  is the angle between the  $B$  field and the  $A$  vector

This is illustrated in figure 7.1.

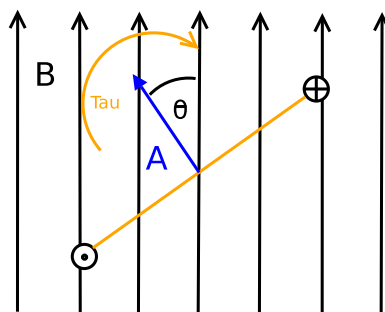


Figure 7.1: A current loop in a homogenous magnetic field  $B$ .

One thing that becomes apparent is that the direction of the current will define the direction of the torque. This is a highly desirable feature, as both the direction, and amount of torque can be controlled from a single control signal. Another thing that also becomes apparent from this equation and from the figure is that it is assumed that the coil is placed perpendicular to the magnetic field in the axis which is being rotated around.

This is unfortunately not always the case in space, as the satellite rotates freely on all three axes. However, if more than one coil is put on the satellite, the fields generated by each coil can be summed, and the resulting magnetic field can be calculated. The direction and power of the summed field will be defined by each coils individual current. Such a summed magnetic field will then react on the  $B$  field in the same manner as just shown when a single coil was oriented such that it created a similar field.

In other words, a virtual coil can be created, by controlling the currents.

In an environment where only rotations on one axis is possible, the system could be described by placing the y-axis of a (x,y) coordinate system in the same direction as the B field and place the satellite so that its center is placed in origo. Then it becomes clear that the axis of rotation will be perpendicular to the x-y plane. A torque will therefore occur around this axis whenever a magnetic field is created by the satellite, assuming that the created field is not parallel with the B-field. The maximum torque that can be applied at all times will occur when the magnetic field is perpendicular to the y-axis.

To handle this alignment an abstraction layer can be created, which solves a set of geometric equations, and thus always applies the appropriate currents to orient a created magnetic field on the x-axis. This can be done simply by cancelling out the y-axis components. Selecting the two currents as output, the only input which is then not defined by the geometry, is the desired amount of field in the x-axis. Thus a linkage is created through this abstraction layer, between the desired torque, and the size of the created field, as it will at all times be parallel to the x-axis.

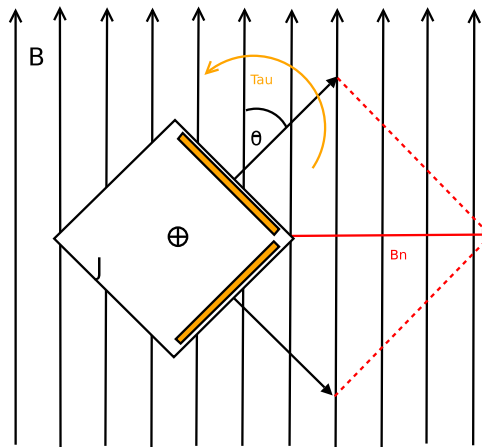


Figure 7.2: Diagram of the satellite placed in a homogenous B field.

The geometric equations can be seen below for a single-axis system:

$$\begin{aligned}\theta_2 &= \text{theta}_1 + 90 \\ y_1 &= \cos(\theta_1) \\ x_1 &= \sin(\theta_1) \\ y_2 &= \cos(\theta_2) \\ x_2 &= \sin(\theta_2)\end{aligned}$$

$$(x, y) = I_1 \cdot K_1 + I_2 \cdot K_2$$

$$\begin{aligned}0 &= I_1 \cdot y_1 + I_2 \cdot y_2 \\ |B_n| &= I_1 \cdot x_1 + I_2 \cdot x_2\end{aligned}$$

where:

$K_x$  is a gain which is defined from the capabilities of the individual coils  
 $B_n$  is the resulting magnetic field strength

This allows for calculating the distribution of currents on both coils. The coils are connected to the microprocessor through an H-bridge. Thus the signals required for control is between 0 and

$V_{cc}$ . This is regulated with a PWM signal and cannot handle negative currents. Therefore one more abstraction layer is placed in the design that converts a  $\pm$ PWM setting to two separate PWM signals, one for each direction of current in the coil.

As at least one of these separate PWM signals are always zero. The system can be seen as a block diagram at figure 7.3.

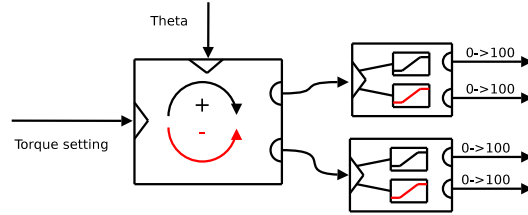


Figure 7.3: Block diagram of the abstraction layer

This provides a torque which is constant at all angles for a setting between  $\pm 100\%$  dutycycle. If this setting is 100% a minimum detumbling time can be found.

$$\alpha = \frac{\tau}{J} \quad (7.2)$$

where:

$\alpha$  is the angular acceleration

Minimum detumbling time assuming the ADCS system can provide a constant torque.

$$T_{detumbling} = \frac{\omega}{\alpha} \quad (7.3)$$

This is however of less importance as a requirement for this time is not yet determined by the system engineering group.

It should also be defined how the satellite is oriented. An example of an orientation is seen in figure 7.4

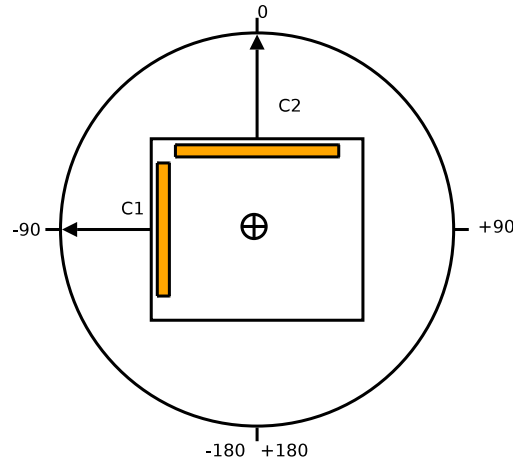


Figure 7.4: The attitude of the satellite is here chosen to be the angle of  $C_2$ , the attitude angle is shown in degrees.

## 7.2 The Classic Approach, a PID Controller

With the abstraction layer ready to transfer a calculated torque to an actual torque with the proper orientation, the controller is reduced to a SISO (Single Input Single Output) system. For such type of systems the PID (Proportional/Integral/Derivative) controller has been used with success for a very long time. It has all the properties that are required for controlling the attitude, namely feedback, and adjustable aggression towards the error.

In the PID controller, the feedback branch is a measured value of the output, and is subtracted from a reference point to find the current error. A gain is applied to the error to ensure that a larger error gives a larger correction. This gain is directly transferable to the proportional part of the controller. The integral part integrates the error over time, and then applies a gain. Thus a small error will over time be added up to a larger error, and this gives a control signal that also increases in time. Finally the differential part of the controller gives an output that is determined by a gain applied to the rate of change of the error. In a system where the attitude is controlled, it is chosen that the pointing angle is provided in the feedback. Thus the differential part would be a gain applied on the angular speed error. This gives a system as figure 7.5.

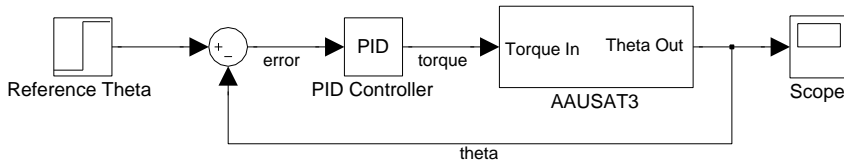


Figure 7.5: A very simple PID setup

However, an implemented differentiation can give rise to some challenges. The first one being that you do not have the future sample, so you cannot actually differentiate for the latest sample. Then of course you can guess at the next sample, based on earlier samples, or simply live with that the differentiation is delayed. In this case however, where the system is rotating, the gyroscope already measures the differentiated signal of the angle (angular speed).

Thus the differentiation part of the controller can be reduced to taking the gyroscope output and applying a gain to it, which corresponds to using a proportional controller on the speed. This is shown on figure 7.6.

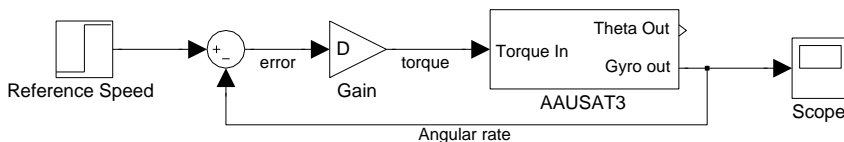


Figure 7.6: Proportional gain control on the speed

The controller, regulating theta, is reduced to a PI controller, as the D part is already handled in this configuration by the inner loop. The two systems can now be merged together, and to make sure that the D-gain only applies to the angular speed, it is placed in the feedback instead of the feedforward. The system levels are now set up making the differentiated branch the inner loop. This is illustrated on figure 7.7.

The derived design allows for tweaking the controller. The integrator should have an anti-windup feature, before it is brought into the tuned system. This is though not concerned,

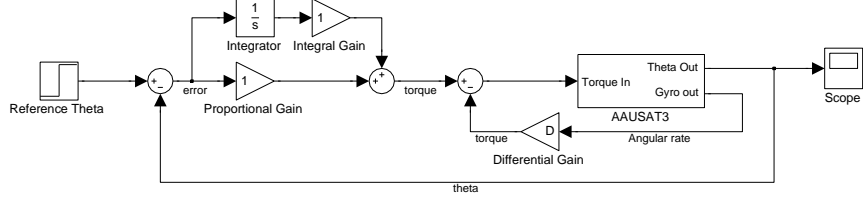


Figure 7.7: A PID controller implemented as two feedback controllers, the Differentiation is done by a sensor

because the integral part is not used, as a steady-state error should not exist, as no outer constant forces are applied.

The PID controller is however best suited to control a system that progresses continuously or at least close to it. A rotational system does not progress continuously. Consider the very abrupt change that arises in the measured theta, when the pointing angle goes from  $+179^\circ$  to  $-179^\circ$ . Even though it is in reality a small change of 2 degrees, the controller will interpret it as a huge difference. The controller will react on it, as it should on an error equivalent to  $358^\circ$ . As can be easily understood when considering a circle, the actual error is very small, and a well designed controller should respond to it accordingly. This can be dealt with in many ways, however as this system should be designed to have a no overshoot, the solution does not require to be very advanced.

The controller will actually respond as wanted if it is never set to handle an angle very close to  $\pm 180$  degrees, so an area of safe operation can be defined with a relative small margin to the  $180^\circ$ . Letting the safe area cover only a semicircle, it is easy to see that a full quadrant is chosen as safe margin. However this limits the reference angle to be set only in the semicircle chosen as safe area. This is shown in figure 7.8.

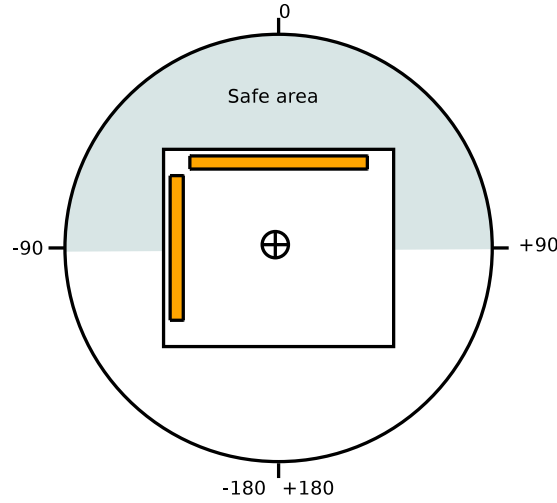


Figure 7.8: The satellite with a defined safe area.

To overcome this, the area can be inverted to cover the other part of the circle. Rotating both the reference angle and the measured angle, corresponds to rotate the area of the circle, thus this can provide the coverage, without inverting the sign of the rotation.

Another problem occurs due to the fact that it is rotations which is being controlled. If the

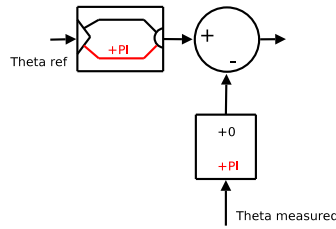


Figure 7.9: Rotating reference and measurements when the reference is set outside the safe area.

satellite is tumbling at such a high speed that the controller cannot stop it before it has turned more than a semicircle, the result will be that when it passes the opposite side of the circle (seen from  $\theta_{ref}$ ) it will be accelerated again to reach the chosen  $\theta_{ref}$ . This will create a oscillating speed change, with a constant amplitude, and the satellite will never be stopped. To avoid this situation, a detumbling scheme has been put into the design.

The measured angular rate is compared to a maximum speed, and if it is turning at a higher rate than allowed, the inner controller is given a speed reference that is zero. This will force the inner control loop to slow down the satellite, not matter what the current angle is. This is illustrated as a switch with a comparator in figure 7.10.

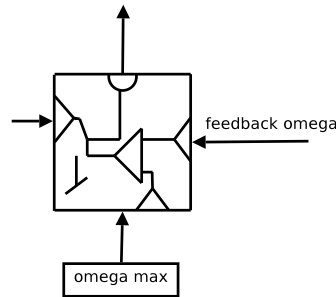


Figure 7.10: Detumbling mode is enabled when the feedback omega is greater than a maximum value.

This speed is chosen to be below, but very close to, the speed where the controller cannot stop the system. The reason for this choice is that the controller is operating as a linear system when below this speed, and is therefore easier to tune if the area of linear operation is as large as possible.

It is now clear that the only necessary features is two proportional controllers, one for the angular rate, and one for the angle. However as measurement errors can occur, a gain on this error will result in a torque. This will give a steady state error, that in the end should be eliminated.

Thus it is chosen to implement the two controllers as PI controllers in the software, leaving the option open to tune an integral gain, if the error due to measurement errors are large or constant external forces exists. To implement the controller, it is noted that a discrete-time and a continuous-time controller is approximately the same, if the sampling frequency is high enough. Thus by looking at the Laplace form of a PI controller:

$$D(s) = K_p + \frac{K_i}{s} \quad (7.4)$$

Then Tustin is applied for transforming from continuous-time to discrete-time.

$$s = \frac{2(z - 1)}{T(z + 1)} \quad (7.5)$$

where:

T is the sampling time

By substituting directly:

$$D(z) = K_p + \frac{K_i}{\frac{2(z-1)}{T(z+1)}} \quad (7.6)$$

rewriting to get it in standard form:

$$\begin{aligned} D(z) &= K_p + \frac{T(z+1)K_i}{2(z-1)} \\ D(z) &= K_p + \frac{Tz+TK_i}{2(z-1)} \\ D(z) &= \frac{2(z-1)K_p}{2(z-1)} + \frac{TzK_i+TK_i}{2(z-1)} \\ D(z) &= \frac{\frac{1}{2}(2zK_p-2K_p+TzK_i+TK_i)}{z-1} \\ D(z) &= \frac{\frac{1}{2}z^{-1}(2zK_p-2K_p+TzK_i+TK_i)}{1-z^{-1}} \\ D(z) &= \frac{\frac{1}{2}(2K_p-2z^{-1}K_p+TK_i+z^{-1}TK_i)}{1-z^{-1}} \\ D(z) &= \frac{K_p-z^{-1}K_p+\frac{1}{2}TK_i+\frac{1}{2}z^{-1}TK_i}{1-z^{-1}} \end{aligned}$$

Now it can be written with the input X and the output Y, and it is almost ready for the inverse Z-transformation, which will provide a discrete equation which can be implemented.

$$D(z) = \frac{U(z)}{X(z)}$$

$$Y(z)(1-z^{-1}) = (K_p - z^{-1}K_p + \frac{1}{2}TK_i + \frac{1}{2}z^{-1}TK_i)X(z)$$

$$Y(z) - Y(z)z^{-1} = (K_p + \frac{1}{2}TK_i)X(z) + (\frac{1}{2}TK_i - K_p)z^{-1}X(z)$$

The inverse Z-transform is applied:

$$y[n] = y[n-1] + (K_p + \frac{1}{2}TK_i)x[n] + (\frac{1}{2}TK_i - K_p)x[n-1] \quad (7.7)$$

It is also intuitively obvious that this is a PI controller.

The design is later implemented in the prototype satellite, and if it is drawn together with the abstraction layer a complete drawing of the system can be shown as on figure 7.11.

The implemented PI controller software code can be found in appendix C.1 on page 92.

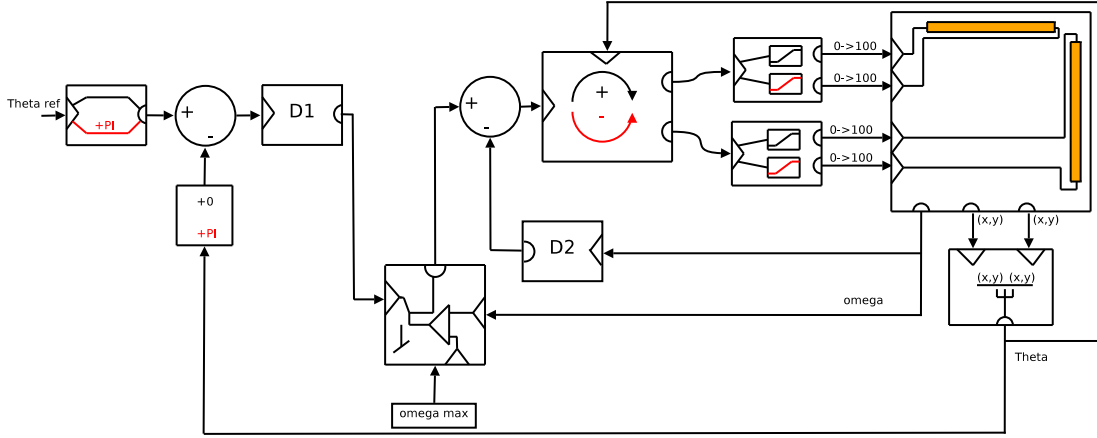


Figure 7.11: The system with the abstraction layer, the detumble system and a PID controller.

### 7.3 Tuning the PID Controller

When dealing with a satellite, the model of the plant is somewhat simple. If all disturbances are excluded, it can be described simply by the moment of inertia. The PWM signal and the magnetorquers provide a linear actuator between the saturation limits that act as a well defined cut-off. Thus the optimal control signal for rotating is a signal that to gain a speed provides an initial burst of torque, which in duration can be up to half the time of a rotation, and then a signal which is the inverse, to slow it down again.

The design of the system appears as an inner loop and an outer loop. If the controller is to provide the torque level as a dutycycle, the system will be saturated in  $\pm 100\%$ . The entire magnetorquer layer, including the coils can simply be modelled as a scalar on the PWM signal, dubbed  $\tau_{max}$ . The produced torque is divided by the moment of inertia to calculate the resulting angular acceleration. This can be integrated to provide the angular rate, and if integrated again the angle is found. Both the angle and the angular rate are measured by sensors which are modelled as lowpass filters, thus they are placed in the feedback branches.

The plant is also affected by the suspension modelled here as a spring and damper, which are just feedbacks with gains applied from theta and the angular rate. On the figure 7.12 the model described is illustrated.

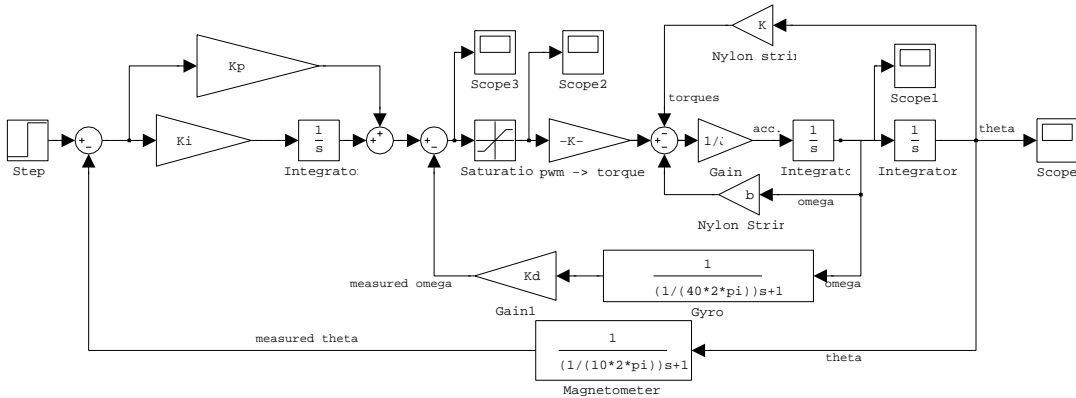


Figure 7.12: The model describing the system used in the test setup.

To be able to tune the controller quickly, some assumptions are made.

- The bandwidth of the sensors filters are located at such high frequencies that they do not influence the systems behavoir
- The nylon wire spring and damper coeffecients are so low that they can be neglected
- The saturations has little influence and can be ignored while tuning
- The integral part of the controller is not necessary and is therefore not applied

After these assumptions are applied the system will appear as shown on figure 7.13 which only includes 2 integrators, and is somewhat similar to a standard second order system. Thus it

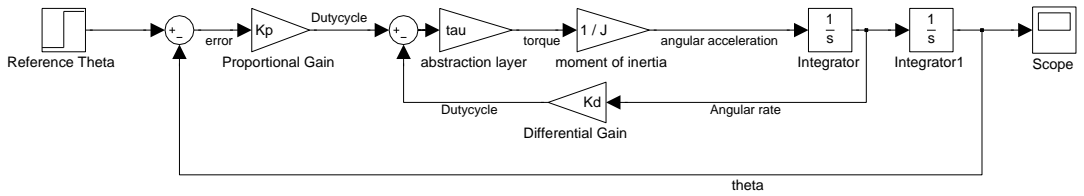


Figure 7.13: A simplified PD controller.

should be possible to determine reasonable values for the two gains directly from the rise time and the damping factor. This requires that the closed loop transfer function is set on standard form.

$$\frac{y}{u} = \frac{\omega_n^2}{s^2 + 2\zeta\omega_n s + \omega_n^2} \quad (7.8)$$

The rise time defines  $\omega_n$  as (from [Feedback control of dynamic systems, 2006]):

$$\omega_n = \frac{1.8}{t_{rise}} \quad (7.9)$$

The inner loop is described in closed loop as:

$$\begin{aligned} \frac{U(k_p)}{\text{angular rate}} &= \frac{\tau \omega \frac{1}{J} \frac{1}{s}}{1 + \tau \omega \frac{1}{J} \frac{1}{s} K_d} \\ \frac{U(k_p)}{\text{angular rate}} &= \frac{\frac{1}{K_d}}{\frac{1}{K_d} \frac{J}{\tau \omega} s + 1} \end{aligned}$$

Now the closed loop of the outer loop can be determined:

$$\begin{aligned} \frac{\theta}{\theta_{ref}} &= \frac{\frac{1}{s} K_p \left( \frac{\frac{1}{K_d}}{\frac{1}{K_d} \frac{J}{\tau \omega} s + 1} \right)}{1 + K_p \left( \frac{\frac{1}{K_d}}{\frac{1}{K_d} \frac{J}{\tau \omega} s + 1} \right) \frac{1}{s}} \\ \frac{\theta}{\theta_{ref}} &= \frac{1}{1 + s \frac{1}{K_p} \left( \frac{\frac{1}{K_d} \frac{J}{\tau \omega} s + 1}{\frac{1}{K_d}} \right)} \\ \frac{\theta}{\theta_{ref}} &= \frac{1}{\frac{\tau \omega s^2}{K_p} + \frac{K_d}{K_p} s + 1} \\ \frac{\theta}{\theta_{ref}} &= \frac{\frac{\tau \omega}{J} K_p}{s^2 + \frac{\tau \omega}{J} K_d s + \frac{\tau \omega}{J} K_p} \end{aligned}$$

Now it is comparable to the elements in the standard form, and it is obvious that:

$$\omega_n^2 = \frac{\tau u}{J} K_p$$

and  $K_p$  can be found as:

$$K_p = \frac{\omega_n^2}{\frac{\tau u}{J}}$$

The damping factor is then expressed as

$$\zeta = \frac{\frac{1}{2} \frac{\tau u}{J} K_d}{\omega_n}$$

and  $K_d$  can be expressed as

$$K_d = \frac{2J\zeta\omega_n}{\tau u}$$

The damping factor can be found viewing at figure 7.14, the figure is calculated by the formula shown underneath. To accommodate the requirement for no overshoot the graph shows that  $\zeta$  must be 0.9.

$$\text{Overshoot } M_p = e^{\frac{-\pi\zeta}{\sqrt{1-\zeta^2}}}$$

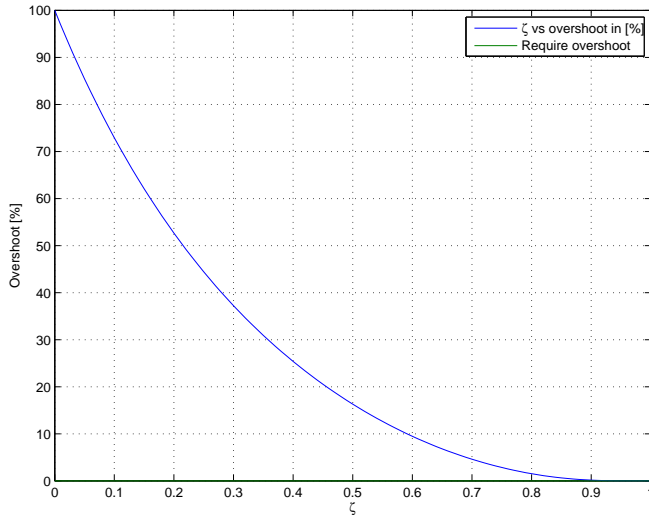


Figure 7.14: Overshoot as a function of the damping factor  $\zeta$ .

Running this algorithm with a damping factor of 0.9,  $K_p$  and  $K_d$  are found, and a step response for a PD regulator with the used  $K_p$  and  $K_d$  in the modelled system is shown in figure 7.15.

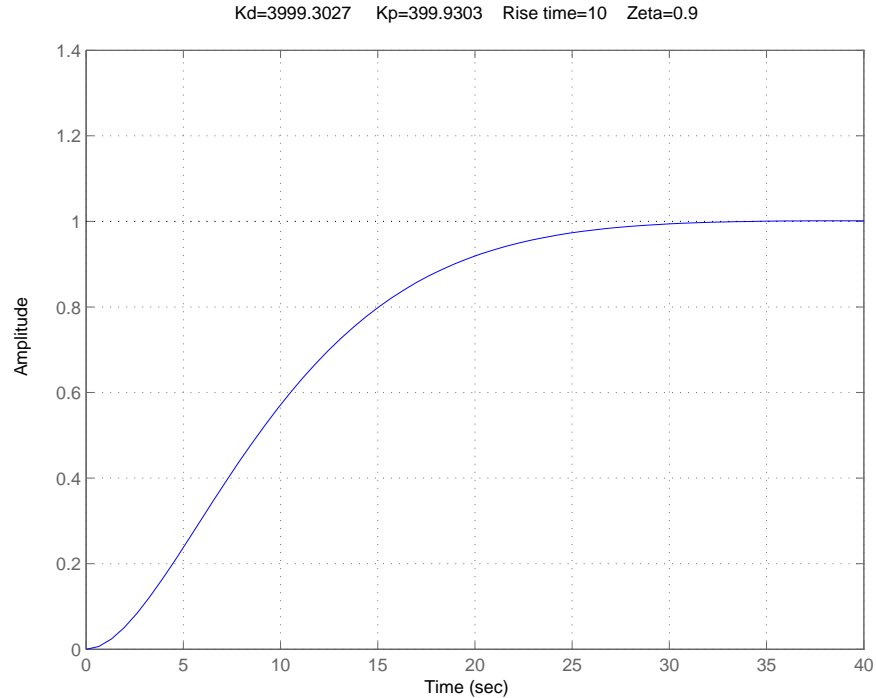


Figure 7.15:  $K_p$ ,  $K_d$  and the step response it provides.

### Transferring the Controller to Discrete-Time

The single most important impact of implementing a controller digitally is the delay associated with the sample and hold circuits. Usually at least 20 times the bandwidth is required to apply the continuous-time design for a digital controller [Feedback control of dynamic systems, 2006]. The level of oversampling is inversely proportional with the error due to sample and hold. An example bodeplot of a first-order system is illustrated in figure 7.16. The bandwidth frequency is clearly marked.

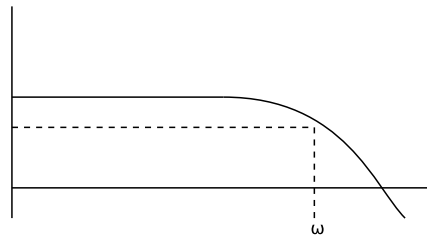


Figure 7.16: Finding the  $T$  value when going from continuous-time to discrete-time. The value  $T$  must be 20 times smaller than  $\frac{1}{\omega}$ .

A quick analysis of the actual bodeplots for the system using the MATLAB function margin, provides the bandwidth, as illustrated in figure 7.17. It is determined as 0.1 rad/s which corresponds to approximately 0.016 Hz. This is then multiplied by 20 and provides a sample time  $T$  at  $\pi$  seconds.

The system is currently run at a sample rate of 50 Hz, ( $T = \frac{1}{50}$  seconds) which is greatly oversampling. No compensation is thus made to the tuned constants before implementation.

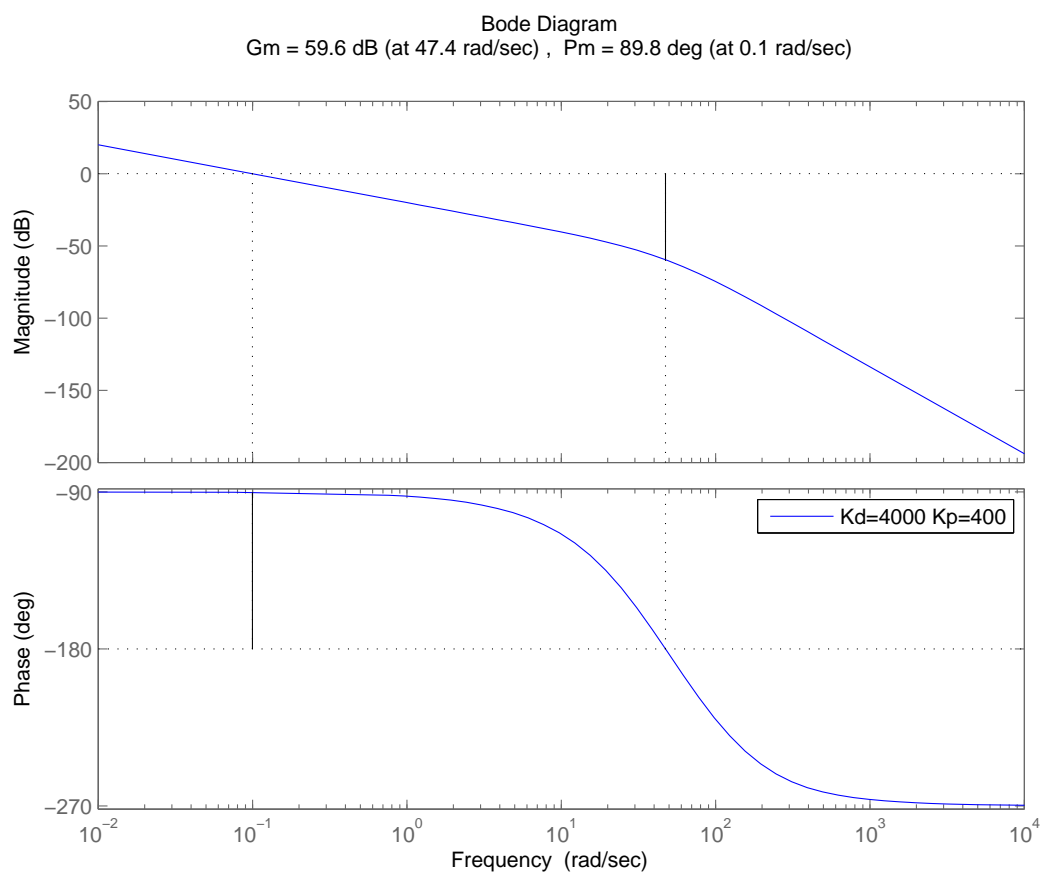


Figure 7.17: The phase margin reveals the bandwidth. This provides the sample time  $T$  which must be 20 times smaller than  $\frac{1}{\omega}$ .

## 7.4 System Model in State-space

The system can be described using a state-space model. States are the variables and their derivatives that are to be regulated. This means that every integration added to the system adds another state. In the example of a satellite in orbit, the states are the orientation and its derivatives, i.e. the angular velocity and the angular acceleration.

A standard state-space model would appear as follows:

$$\begin{aligned}\dot{\vec{x}}(t) &= \bar{A}\vec{x}(t) + \bar{B}\vec{u}(t) \\ y(t) &= \bar{C}\vec{x}(t) + \bar{D}\vec{u}(t)\end{aligned}$$

where:

$\vec{x}(t)$  is a vector containing the states at time t

$\bar{A}$  is a matrix describing the plant behaviour on the current states, without any inputs

$\bar{B}$  is a matrix describing the influence on the plant from the applied inputs

$\vec{u}(t)$  is a vector holding the inputs at the time t

$y(t)$  is the output of the system

$\bar{C}$  is a matrix for selecting which state to output from the state-space system

$\bar{D}$  is a matrix for describing a feedforward of the inputs to the output if any

The system is illustrated in figure 7.18

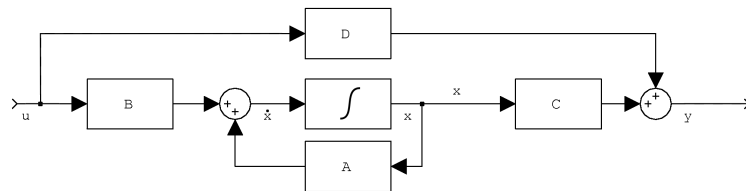


Figure 7.18: General state-space system model.

A rotational system  $\vec{x}(t)$  can be described as a vector with the elements  $\begin{bmatrix} \theta(t) \\ \omega(t) \end{bmatrix}$ . From this follows the matrix  $\bar{A}$  which describes the behaviour of the plant in the angle and angular velocity states. For the satellite system the vector  $\vec{u}(t)$  is the torque applied by the magnetorquers at a given time  $[\tau(t)]$ . Finally the  $y(t)$  is selected as the angular rate.

$$\dot{\omega}(t) = -\frac{K}{J}\theta(t) - \frac{b}{J}\omega(t) + \frac{\tau(t)}{J}$$

It is easily deducible that:

$$\dot{\theta}(t) = \omega(t)$$

The matrices of the system become:

$$\begin{aligned}\bar{A} &= \begin{bmatrix} 0 & 1 \\ -\frac{K}{J} & -\frac{b}{J} \end{bmatrix} \\ \bar{B} &= \begin{bmatrix} 0 \\ \frac{1}{J} \end{bmatrix} \\ \bar{C} &= \begin{bmatrix} 0 & 1 \end{bmatrix} \\ \bar{D} &= [0]\end{aligned}$$

where:

$\bar{A}$  contains a model of the plants behaviour without inputs, and is therefore identical to the nylon string model

$\bar{B}$  applies  $\frac{1}{J}$  on the input torque to determine its effect on the angular velocity

$\bar{C}$  selects the orientation,  $\theta$  as the output of the state-space system

$\bar{D}$  is set to zero, as there is no direct influence from an applied input

$J$  is the moment of inertia calculated in chapter 6.2.1

The constants are as found in chapter 6.2.1 and 6.3:  $\tau_{max} = 1.0532 \cdot 10^{-5}$   $K = 2.7757 \cdot 10^{-7}$

$b = 4.6 \cdot 10^{-6}$   $J = 1.3 \cdot 10^{-3}$

Inserting these into the state-space model yields:

$$A = \begin{bmatrix} 0 & 1 \\ \frac{2.7757 \cdot 10^{-7}}{1.3 \cdot 10^{-3}} & \frac{4.6 \cdot 10^{-6}}{1.3 \cdot 10^{-3}} \end{bmatrix}$$

The input of the B matrix is a PWM signal between -100 and 100. This must be converted to actual torque by multiplying B by the maximum applicable torque and dividing by 100:

$$B = \begin{bmatrix} 0 \\ \frac{\tau_{max}}{J \cdot 100} \end{bmatrix} = \begin{bmatrix} 0 \\ \frac{1.0532 \cdot 10^{-5}}{1.3 \cdot 10^{-3} \cdot 100} \end{bmatrix}$$

## 7.5 State-space controller design

A feedback is added by setting  $u(t) = \bar{F} \cdot x$ , where  $\bar{F}$  is a matrix containing the gains for the controller. A reference is added to the system by adding it to the feedback. The reference is multiplied by af matrix  $\bar{M}$  to apply it to the appropriate state. The system then becomes:

$$\begin{aligned}\dot{x}(t) &= \bar{A}x(t) + \bar{B}\bar{F}(x(t) + \bar{M}ref) \\ y(t) &= \bar{C}x(t) + \bar{D}u(t)\end{aligned}$$

This is illustrated in figure 7.19

Before creating the feedback matrix  $\bar{F}$  it is determined whether the system is controllable or not. Hence the controllability matrix is created:

$$\begin{aligned}\bar{C}_c &= \begin{bmatrix} \bar{B} & \bar{A}\bar{B} \end{bmatrix} \\ &= \begin{bmatrix} 0 & 8.1 \cdot 10^{-5} \\ 8.1 \cdot 10^{-5} & -2.9 \cdot 10^{-3} \end{bmatrix}\end{aligned}$$

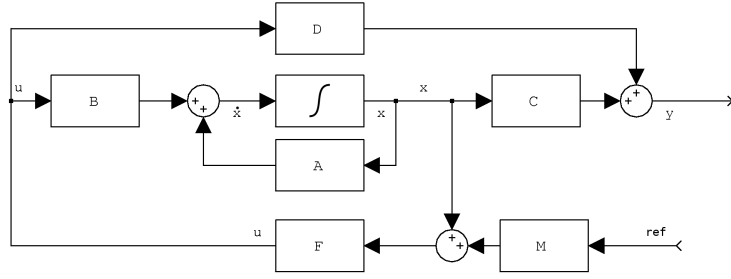


Figure 7.19: General diagram of a state-space controller

If  $\det(\bar{C}_c) \neq 0$  the system is controllable:

$$\det(\bar{C}_c) = -6.56 \cdot 10^{-9} \neq 0$$

The feedback matrix is created by first determining a matrix  $\bar{T}$ , such that:

$$\bar{A}_c \bar{T}^{-1} = \bar{T}^{-1} \bar{A}$$

where  $\bar{T}$  is an  $n \times n$  matrix containing the rows  $\vec{s}_1$  to  $\vec{s}_n$ :

$$\bar{T} = \begin{bmatrix} \vec{s}_1 \\ \vec{s}_2 \end{bmatrix}$$

$\bar{A}_c$  is  $\bar{A}$  in controllable canonical form which has the following appearance:

$$\bar{A}_c = \begin{bmatrix} a_1 & a_2 \\ 1 & 0 \end{bmatrix}$$

where  $a_1$  and  $a_2$  are the constants for the open-loop polynomial  $\lambda^2 + a_1\lambda + a_2$ .  $\bar{T}$  is then found by:

$$\begin{aligned} \vec{s}_2 &= \begin{bmatrix} 0 & 1 \end{bmatrix} \bar{C}_c^{-1} \\ \vec{s}_1 &= \vec{s}_2 \bar{A} \\ \bar{T}^{-1} &= \begin{bmatrix} \vec{s}_1 \\ \vec{s}_2 \end{bmatrix} \end{aligned}$$

$$\begin{aligned} \vec{s}_2 &= \begin{bmatrix} 0 & 1 \end{bmatrix} \begin{bmatrix} 0 & 8.1 \cdot 10^{-5} \\ 8.1 \cdot 10^{-5} & -2.9 \cdot 10^{-3} \end{bmatrix}^{-1} = \begin{bmatrix} 1.2344 & 0 \end{bmatrix} \\ \vec{s}_1 &= \begin{bmatrix} 1.2344 \cdot 10^4 & 0 \end{bmatrix} \begin{bmatrix} 0 & 1 \\ \frac{2.7757 \cdot 10^{-7}}{1.3 \cdot 10^{-3}} & \frac{4.6 \cdot 10^{-6}}{1.3 \cdot 10^{-3}} \end{bmatrix} \begin{bmatrix} 0 \\ 1.2344 \cdot 10^4 \end{bmatrix} \\ \bar{T} &= \begin{bmatrix} \vec{s}_1 \\ \vec{s}_2 \end{bmatrix}^{-1} = \begin{bmatrix} 0 & 8.1 \cdot 10^{-5} \\ 8.1 \cdot 10^{-5} & 0 \end{bmatrix} \end{aligned}$$

$$\begin{aligned}\bar{A}_c &= \bar{T}^{-1} \bar{A} \bar{T} = \begin{bmatrix} 0 & 1.2344 \cdot 10^4 \\ 1.2344 \cdot 10^4 & 0 \end{bmatrix} \begin{bmatrix} 0 & 1 \\ \frac{2.7757 \cdot 10^{-7}}{1.3 \cdot 10^{-3}} & \frac{4.6 \cdot 10^{-6}}{1.3 \cdot 10^{-3}} \end{bmatrix} \begin{bmatrix} 0 & 0.8101 \cdot 10^{-4} \\ 0.8101 \cdot 10^{-4} & 0 \end{bmatrix} \\ &= \begin{bmatrix} -3.5 \cdot 10^{-3} & -2.1351 \cdot 10^{-4} \\ 1 & 0 \end{bmatrix}\end{aligned}$$

The open-loop polynomial is:

$$\lambda^2 + 3.5 \cdot 10^{-3} \lambda + 2.1351 \cdot 10^{-4}$$

The desired closed-loop polynomial is corresponding to that of the PID controller:

$$\lambda^2 + \frac{\tau_{max} \cdot K_d}{100J} \lambda + \frac{\tau_{max} \cdot K_p}{100J}$$

Inserting the constants calculated for the PID controller yields:

$$\lambda^2 + \frac{1.0532 \cdot 10^{-5} \cdot 4000}{100 \cdot 1.3 \cdot 10^{-3}} \lambda + \frac{1.0532 \cdot 10^{-5} \cdot 400}{100 \cdot 1.3 \cdot 10^{-3}} = \lambda^2 + 0.3241\lambda + 0.0324$$

The feedback matrix in controllable canonic form is found by simply subtracting the constants from the desired closed-loop polynomial from the constants of the open-loop polynomial::

$$\begin{aligned}\bar{F}_c &= \begin{bmatrix} 0.0035 - 0.3241 & 0.0002 - 0.0324 \end{bmatrix} = \begin{bmatrix} -0.3205 & -0.0322 \end{bmatrix} \\ \bar{F} &= \bar{F}_c \bar{T}^{-1} = \begin{bmatrix} -0.3205 & -0.0322 \end{bmatrix} \begin{bmatrix} 0 & 1.2344 \cdot 10^4 \\ 1.2344 \cdot 10^4 & 0 \end{bmatrix} \\ &= \begin{bmatrix} -397.4 & -3956.3 \end{bmatrix}\end{aligned}$$

These numbers are not far from the values of  $K_p$  and  $K_d$  which is not a surprise as the  $\bar{F}$  matrix is the controller gain for the errors of  $\theta$  and  $\omega$  corresponding to the gains of the PID controller, i.e.  $K_p$  and  $K_d$ . Since there is no observer in this state-space system the feedback is bound to be very similar to a PID. additionally both the PID and the state-space controller regulate the orientation and the angular velocity.

The step response of the state-space controller is shown in figure 7.20. It is to be noted that the state-space model includes the model for the wire that holds the experimental system setup, and the PID model does not. Even so the step responses are nearly identical. This is not the case with a larger step as the torque applied by the string is proportional to the amount the string has been twisted. With a step from 0 to 1 rad the string is negligible.

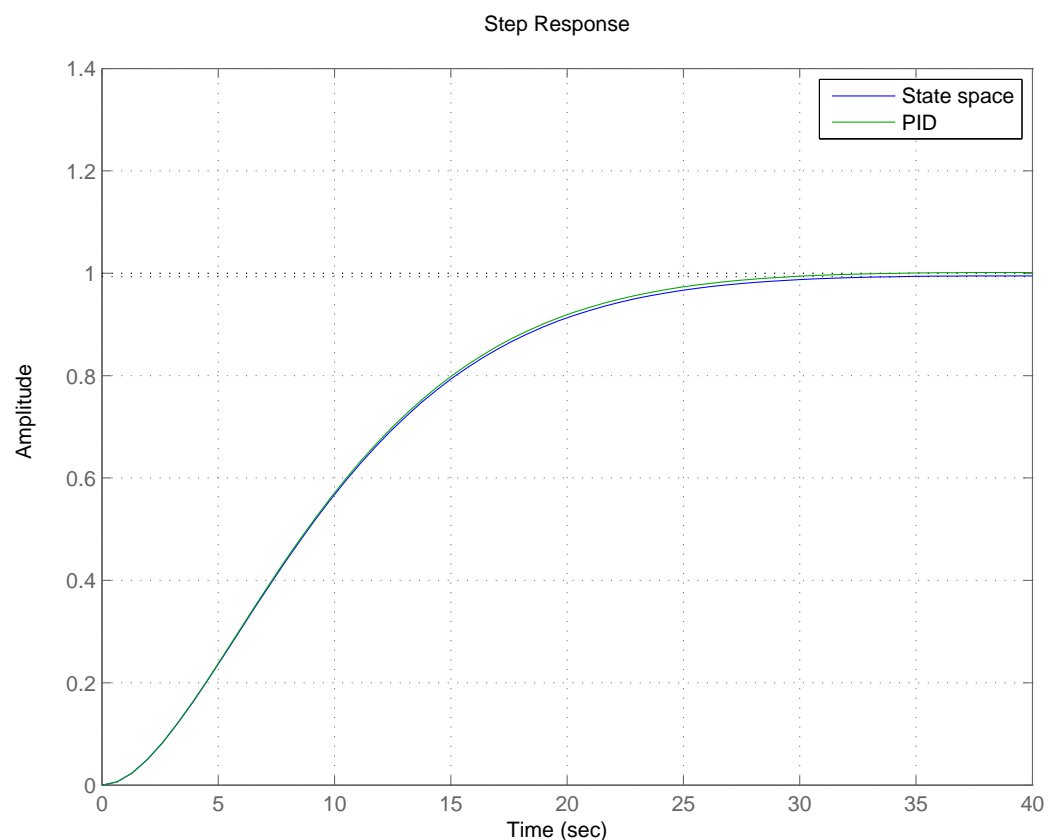


Figure 7.20: Closed-loop Step response of the state-space model compared to that of the PID controller.

# CHAPTER 8

## Implementation

The tuned controllers are implemented in the programming language 'C' using the GNU C compiler, gcc. This chapter contains a short description of how the software is implemented for each controller setup. At first, however, the prototype hardware is described, and a basic structure of the software designed is presented, as it contains a command interface to aid in debugging and running tests.

### 8.1 Prototype ADCS satellite

The prototype ADCS satellite should be build up in the same manner as a CubeSat, to have the same type of dynamics. To be able to conduct the experiments where the prototype is suspended in a nylon string, it is vital that the prototype is able to function in a wireless state. Therefore the prototype must contain a battery to avoid the requirement for power cables. It is also an advantage to have a prototype where communications can be established wireless. Otherwise the prototype would have to be taken out of the experiment to change i.e. the reference angle, and interference with the prototype should be avoided as it can introduce horizontal movements, which makes the suspension model less reliable as well as the gyroscope readings.

To work around these obstacles, a way to bundle the electronics to a battery is required, and an original AAUSAT-II frame is used for the prototype. This frame is assumed to be reused on AAUSAT3, and is therefore the perfect choice for the prototype model. Its basic shape is an outer frame for solar panels, with an inner stack of circuit boards mounted on 4 legs. The prototype electronics therefore consists of a set of circuit boards, all less than 9 cm in width, connected to each other with cables. The functions required of the prototype hardware can be addressed separately, this is considered an advantage as it speeds up the development, and each functionality is placed at its own circuit board.

#### Power

A Lithium-Ion battery is chosen which will provide a long lifespan of the prototype between charging. It also has the advantage that the voltage level of the battery pack is close to the levels that can be expected on the AAUSAT3. And the board placed in the bottom is simply acting as brackets for the battery. A different board holds voltage regulators, which ensures a stable supply of 5 V and 3.3 V. Finally a side panel is made which holds connectors to the battery and the voltage regulators, allowing for external powering and charging without disassembling the prototype.

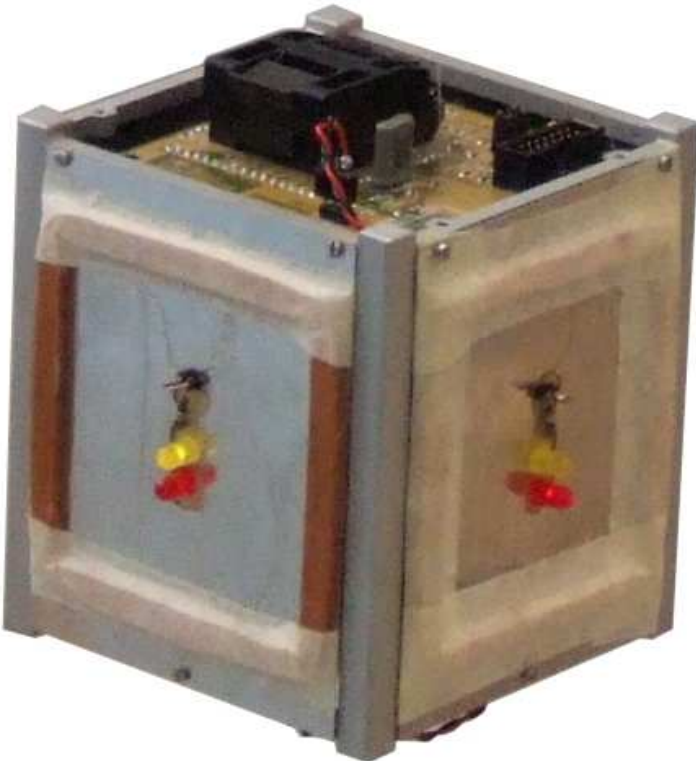


Figure 8.1: Picture taken of the prototype.

### Communications

A Bluetooth module, which interfaces an RS232 to the bluetooth COM port channel is placed in the stack. In this manner wireless communications can be achieved with a RS232 interface, this is a simple solution and is very powerful. The most unfortunate consequence is that it is not using a CAN bus, which is supposed to be used on AAUSAT3 as interface between subsystems.

### Magnetorquers

To be able to control the torque created from the magnetorquers in both a positive and a negative direction, an H-bridge is set up to help switch a PWM signal on the coils. As the prototype only holds 2 magnetorquer coils. A single H-bridge can supply the switching of all the four channels required. The actual coils are taped onto sidepanels which is the position they will have in the finished satellite. The sidepanels for the coils are also equipped with LEDs to visually confirm the direction of the currents in the coil.

### Sensors

The sensors which are selected are magnetometers and gyroscopes. The magnetometers are placed farthest away from the magnetorquer coils, on a circuit board in the stack. As they consist only of a Wheatstone bridge some peripheral amplifier is required to amplify the minute changes on the two output pins. This is done using simple op-amp couplings, and the output from these are inputted to the gyroscopes ADC channels. As the magnetic field which is being measured is 5 times stronger than the geomagnetic field, it is not necessary to amplify very much, and thus the available 3.3 V is used for reference, instead of the optimal 2.5 V. This was

done to avoid adding one more voltage regulator. The gyroscope does output a 2.5 V reference, but when this was attempted as reference voltage, the gyroscope readings became unstable, probably due to the currents drawn by the op-amp.

### Microcontroller

To handle the communication and the PWM signal generation, a microcontroller is used. From this follows the option to implement the controllers in software, which is a feature that is highly preferable, as it allows for rapidly changing the controllers behaviour from the wireless interface. The controller used is an 8 MHz MSP430 development board. This choice differs from the rest of the AAUSAT3 projects, as it is determined in the system engineering group, that only AVR and ARM processors should be used due to their power consumption. However, the SPI interface that the gyroscopes supply, is found on both the ARM and the AVR, and therefore this difference should be of no concern to the future developments. The fact that the MSP430 development board is small enough to fit into the frame, and that no AVR or ARM units were available without the requirement for PCB production and soldering, also aided in this choice.

Schematics for all the systems can be found in appendix D on page 97.

## 8.2 Debug Interface

Before the implementation of the controllers begun, a basic interface software was designed. This was done primarily to test the hardware and to allow for a debug output. But also to have a system that was ready for the controller implementation when the controllers were tuned.

The magnetorquer abstraction layer and the interfacing to the sensors are considered a part of the basic system. This includes the calculation of the current attitude based on the magnetometer readings.

Timer A executes an interrupt that handles the sampling of the sensors, and timer B handles the generation of the PWM outputs. For debugging purposes the system regularly outputs housekeeping data in the main loop. When housekeeping is outputted the screen is cleared, and the command history is printed after the debug data. This allows an operator to continue typing while housekeeping data is printed in the top of the screen.

By default the magnetometer readings, the calculated attitude, the angular rate readings, the temperatures and the battery voltage are outputted in housekeeping.

The command handler has been kept as simple as possible. It is structured as a switch-case performed on the first word in an inputted string. Input strings are analyzed when a return character is received. Switch-case statements in C are only allowed with an integral type, so it is replaced with if-else sentences to allow for a string comparison. This is done to create a set of commands that is readable, and can intercept parameters, both floats and integers can be read from input strings.

The basic flow of the main loop is shown in figure 8.2.

The commands implemented on the basic system is:

**cls**

Clears the output, and flushes the history buffer.

**data**

Turns off housekeeping data, and instead outputs the theta value calculated, and the angular rate measured.

**help**

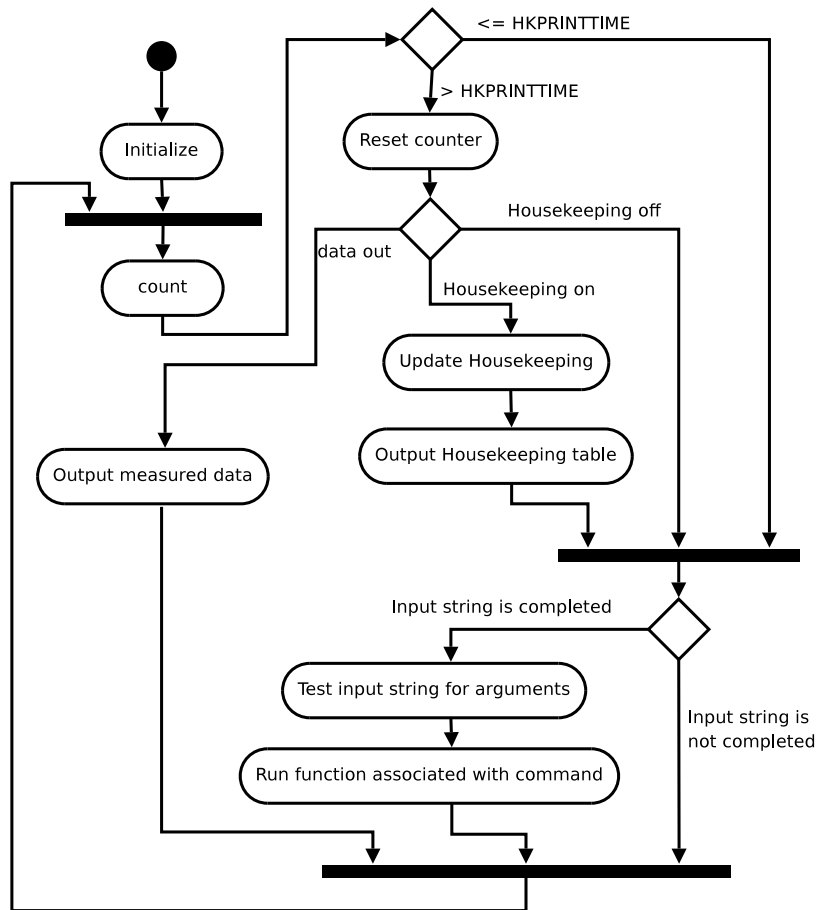


Figure 8.2: Main loop of the basic software.

This command responds with a printout of a list of commands. **hkoff**  
Turn off the processing and printing of the housekeeping data.

**hkon**

Turn on the processing and printing of the housekeeping data.

**pwmset**

Change the pwm setting for a single output. This command allows the operator to specify an output dutycycle for each of the 4 PWM outputs.

**pwmread**

Prints the dutycycle setting for the four output pins.

**tset**

Sets the torque level, this a direct command to the coil abstraction layer.

The source code is included in appendix C.2

### 8.3 PID implementation

Figure 7.11 directly provides the basic flow of the data to the design of the PID controller implementation.

Looking at the basic software that is implemented, a starting point for the design is given. The magnetorquer abstraction layer is designed to have its inputs updated separately to allow for a flexible implementation. The torque level which is to be outputted by the layer is set using a provided function and the outputted currents can be continuously updated by providing a new measurement of the attitude angle theta. This allows for implementing the execution separately from the update, however, it does not require it to be executed separately.

The PID controller is chosen to be implemented together with the sampling of sensor data, resulting in an update frequency of the controller that follows the sample frequency. This way it is possible to use the same interrupt service routine for sampling and updating the PID controller with the latest sample.

In this configuration the block diagram on figure 7.11 shows that the output of the two PID controllers can be updated separately. They have different input branches, and their outputs are simply summed to provide the torque setting. Another argument for updating the two controller outputs separately, is that it allows for a simple implementation of the detumbling mode. When the controllers D1 and D2 have been executed, the outputs can thus be summed and sent to the abstraction layer, which should then be executed afterwards.

An overview of this flow can be seen in figure 8.3.

The source code is included in appendix C.1.

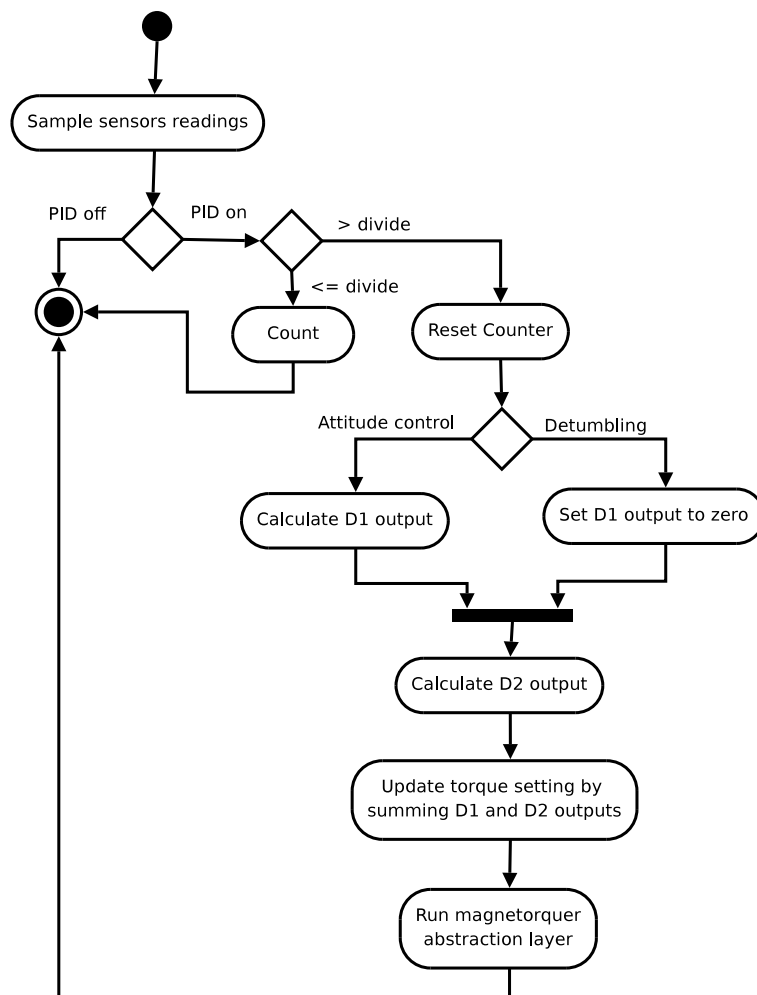


Figure 8.3: Interrupt service routine for running the PID controller

# CHAPTER 9

## Verification

The PID and the state-space controllers are basically the same controller as shown in section 7.4. It is therefore only necessary to verify one of them. It is chosen to verify the PID controller.

### 9.0.1 Verification of the PID Controller

Measurements of the satellites attitude are not done with external meter as proposed in the test specification. This is primarily due to the fact that no such meter was available. The magnetometers measured angles are verified by eyesight only.

The system is set in data output mode, and the data is timestamped at the client side. Three reference steps are given to the PID controlled satellite.

The first figure 9.1 shows a step from 180° to 0°. This step is centered in the safe margin of rotation, and has therefore the largest margin of errors.

The second figure 9.2 shows a step from 90 to -90 degrees. It should turn the other way around, and is performed to ensure that the system functions for both right and left rotations.

The third figure 9.3 shows a step from -90 to 135 degrees. This is an angle set outside the safe margin, to test if the system rotates the coordinate system properly.

From the three applied steps, it follows that a steady-state error occurs. It is between  $\pm 10$  degrees but very close to it. This is a fulfillment of the requirements, but could with very little effort be improved to a larger margin by tuning the integral part of the controller.

It was required that overshoot should be avoided. The three experiments shows that no overshoot is occurring.

The requirement specifying detumbling to less than  $2 \frac{\text{deg}}{\text{sec}}$ , is difficult to verify in the experimental test setup. This is due to the influence of the nylon wire, which acts like a spring.

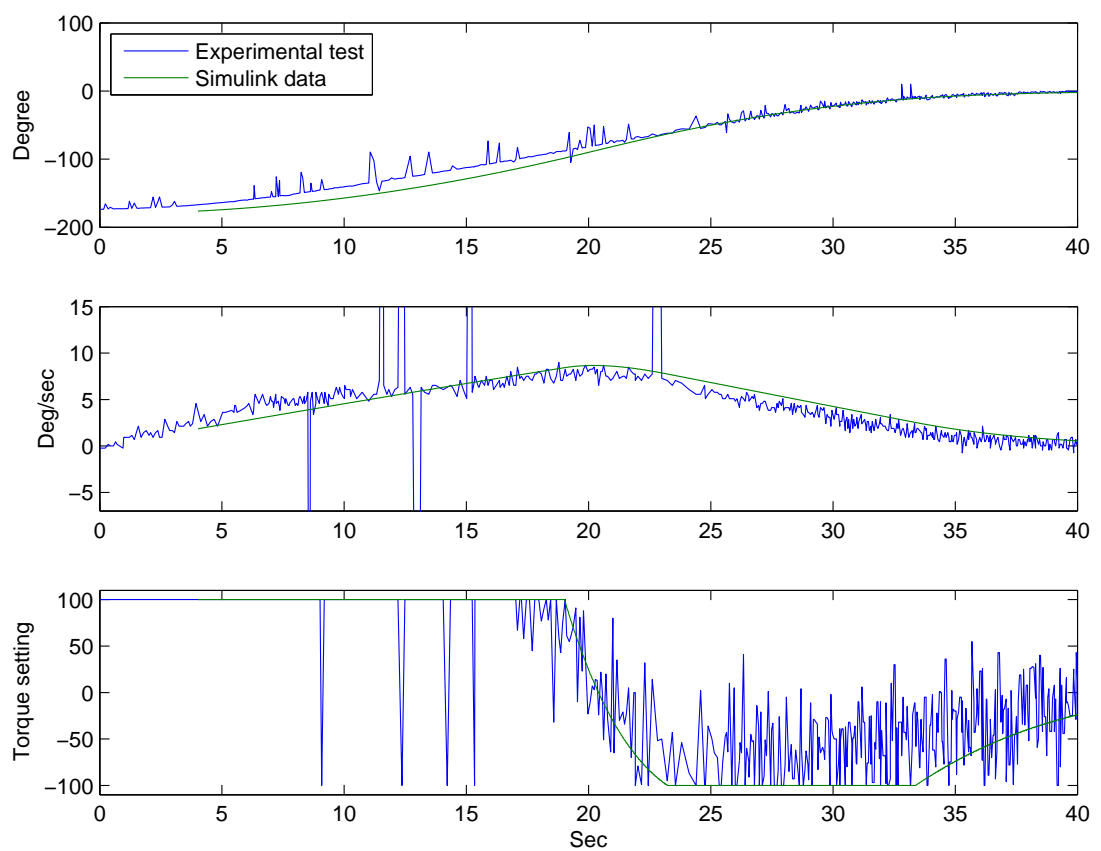


Figure 9.1: The result of the experiment with a step from  $180^\circ$  to  $0^\circ$ .

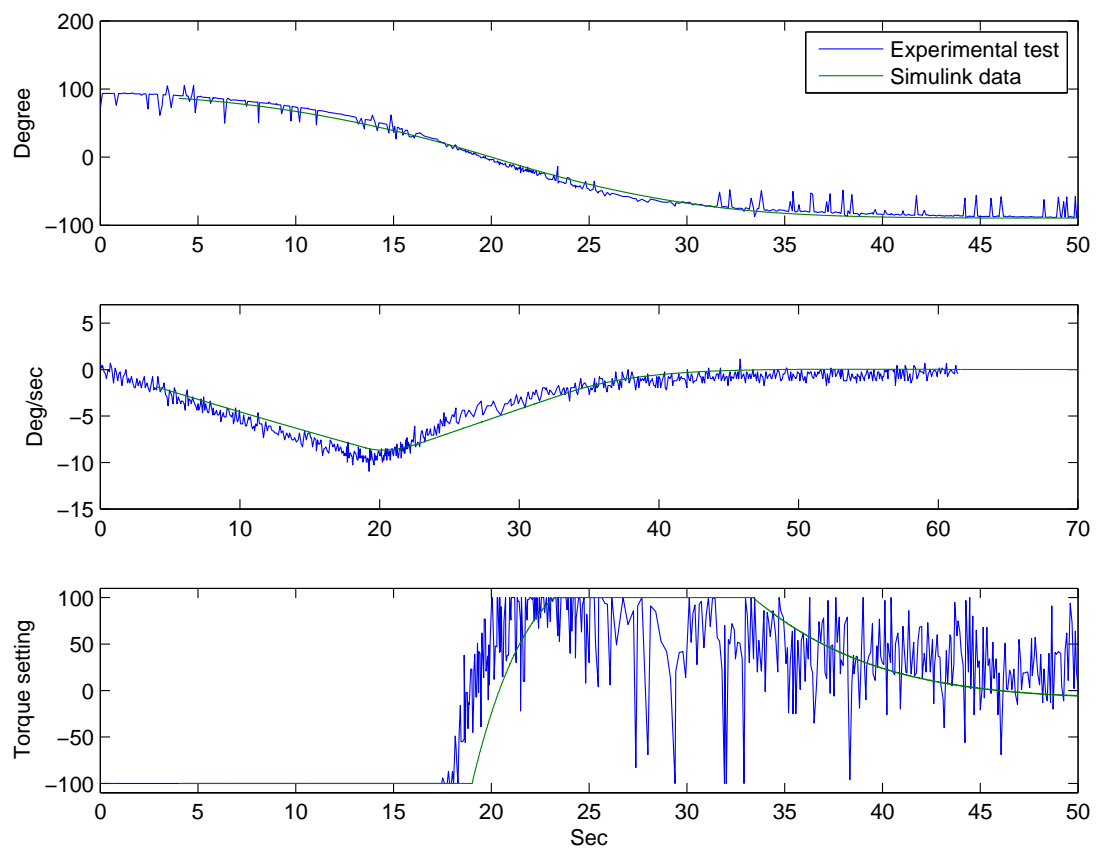


Figure 9.2: The result of the experiment with a step from  $90^\circ$  to  $-90^\circ$ .

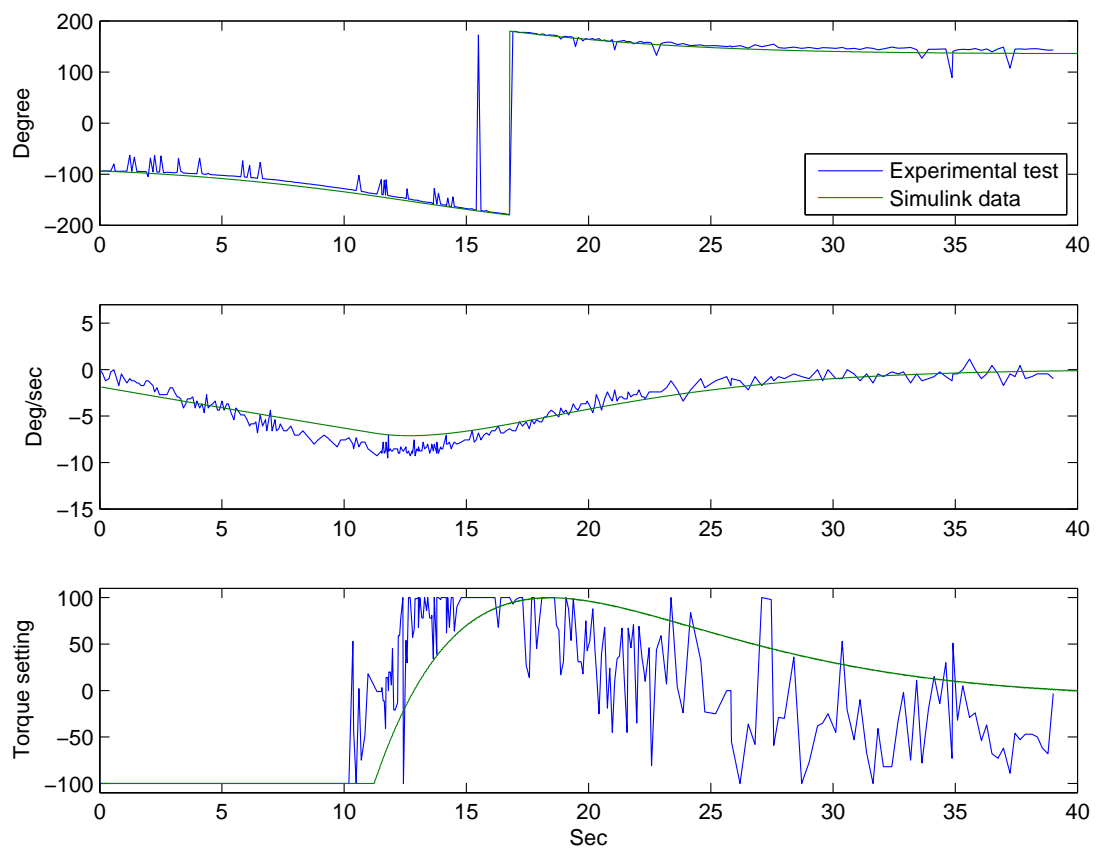


Figure 9.3: The result of the experiment with a step from  $-90^\circ$  to  $0^\circ$ .

# CHAPTER 10

---

## Discussion

The ADCS project is a part of the AAUSAT3 development. A consequence of this is that much of the project dedicated time is used at meetings and coordination with the other AAUSAT projects, to ensure a better overall satellite design. Another consequence is that the project gets access to everything that has been developed in the AAUSAT projects earlier. ADCS is usually developed as a project at 8th semester, and as a consequence the ADCS projects for the previous satellites has been focussed on the control strategies.

As the system enters the three-dimensional environment it faces the issue of becoming a MIMO system, and it is very hard to physically emulate microgravity in three dimensions, as it requires some sort of suspension with little or no friction. This problem has had the consequence that only a single ADCS project from AAU, has before this one, been tested physically. That project focussed on the possibility to control using momentum wheels, and was tested in a parabolic flight campaign.

This set up a requirement to test if the magnetorquer coils were even capable of acting as actuators, before the momentum wheels was removed from the AAUSAT3 design. Thus coils had to be wound, as nobody could find any of the original AAUSAT-II coils. Compared to the intentions of a 6th semester project, a lot of time was used on creating tools for manufacturing the coils. The tools developed are documented in appendix B.

To be able to test the coils, it was necessary to create a setup for simulating microgravity, and some different strategies was discussed. The simplest suggestion was chosen, being to suspend the satellite prototype in a long wire. To ensure that the wire's effect could be neglected, it was suggested to have a homogenous magnetic field which was more powerful than the earths. Thus effort was made to create a set of Helmholtz coils large enough to contain the satellite. However, this also meant that output from the magnetometers onboard the prototype had to fit a stronger magnetic field, otherwise they would saturate. This had the consequence that most of the measurements on the spring and damping constants of the wire was done after the Helmholtz coils was created. Here it was shown that the magnetorquers should be powerful enough to overcome the wire even without the Helmholtz coils. A prototype could have been created which was closer to the final version, if this had been realised earlier.

The forces arising from the disturbances were evaluated to the plausible worst-case orbit, and were used to determine if the coil design is powerful enough. These forces could have been used for setting up a computer simulation of the space environment. However it was the focus of this project to control the prototype model, and thus the controller was only designed for operation in the test setup environment.

# CHAPTER 11

---

## Conclusion

The sensors chosen should enable the ADCS system to determine its attitude, and its angular rate, with a relatively small margin of error. The sensor models are reduced to transfer functions, both reassembling simple lowpass filters. They predict a linear behaviour at DC for the magnetometers, and a resolution of over 4000 steps can be achieved if properly calibrated. To calibrate them to perform well in the less powerful geomagnetic field, the amplifiers should be changed, and would benefit from a reference voltage at 2.5 V instead of the current 3.3 V. The error is however not measured as the sensors were not calibrated due to the lack of a powerful angular measurement device. Therefore it is not confirmed. The only verification that was done was to turn the satellite to angles that could visually be confirmed by eyesight. The measurements of the angle performed by the magnetometers seems to be very close, and could probably be even better if the sensors were calibrated. Even so, the expected redundancy of the sensors in the final implementation should improve the measurement data even further.

A model of the satellite was set up, and it was assumed that the external forces are small enough to be negligible. This assumption allowed a description of the satellites behaviour simply as a function of the moment of inertia. A transfer to the experimental system became therefore a matter of describing suspensions influence, as this was an external force not found in space.

The suspension devised for achieving microgravity simulation was simply a very long nylon wire suspended from the ceiling. This is modelled as a rotational spring and damper system. This model is compared with actual measurements of the prototype satellite as a rotational pendulum, and it is experienced that the model is valid for greater movements. The experiment also reveals that the influence from the wire is very small until the movements are within the area where the model can be applied. Thus it is accepted as a usable model.

The magnetorquer coils from AAUSAT-II was investigated to determine if the design could be improved. It was found that an expansion of the diameter of the wire would lower the resistance, and keep the inductance almost unchanged. This should create a similar torque to a given current, but at a lower voltage level, and therefore the efficiency would be improved. It was also investigated if another shape of the coil could improve the performance, and it was found that a circular coil with the same length of wire would create a greater flux, and a greater inductance, but due to the less area, the torque produced would be unchanged for the same length of wire.

To be able to produce the new magnetorquers a set of custom tools were created. As the original tools for making the AAUSAT-II coils were lost, and nobody could remember how the original AAUSAT-II coils were produced, a method was devised based on a photo of the old

## CHAPTER 11. CONCLUSION

---

coil machine. It did however take some time to get this to work properly, therefore only the square coils were produced within the projects timeframe.

The prototype was assembled and a Helmholtz coil was designed and produced for the test, as it provides a near homogenous field, allowing for the experiments to be reproduced.

A model for the produced torque from the two coil currents in a homogenous field is set up and tested, and the same model is used to measure the angle of the magnetic field. This model allows for the controller to handle the torque as a single output and the angle as a single input, and a PID controller is designed. The P and D parts of the controller are according to the plant model sufficient to control the system efficiently. Unfortunately the gyroscope which provides the angular rate feedback, generates some sensor noise, and even though the errors are not very large, the high gain on the differential part of the controller, creates a steady-state error. The steady-state error could be corrected with a tuned integral part, but this was not finally implemented in the project due to the relatively small steady-state error. The step response reveals that when detumbled the controlled system can turn half a rotation in less than a minute in the test setup. Here the magnetic field is however 5 times larger than the earth's magnetic field. The produced torque should thus drop with a factor of 5, reducing the speed of the system. In figure 11.1 a step response is presented of the existing PID controllers behaviour if placed in an environment without the Helmholtz coils, assuming the magnetometers are recalibrated to measure this weaker field. Here it is shown that the controller set up for the test, will due to the lower torque generated still react reasonable. Its step response will be slower, and an overshoot is introduced, but the system is stable and is at steady-state at an acceptable rate.

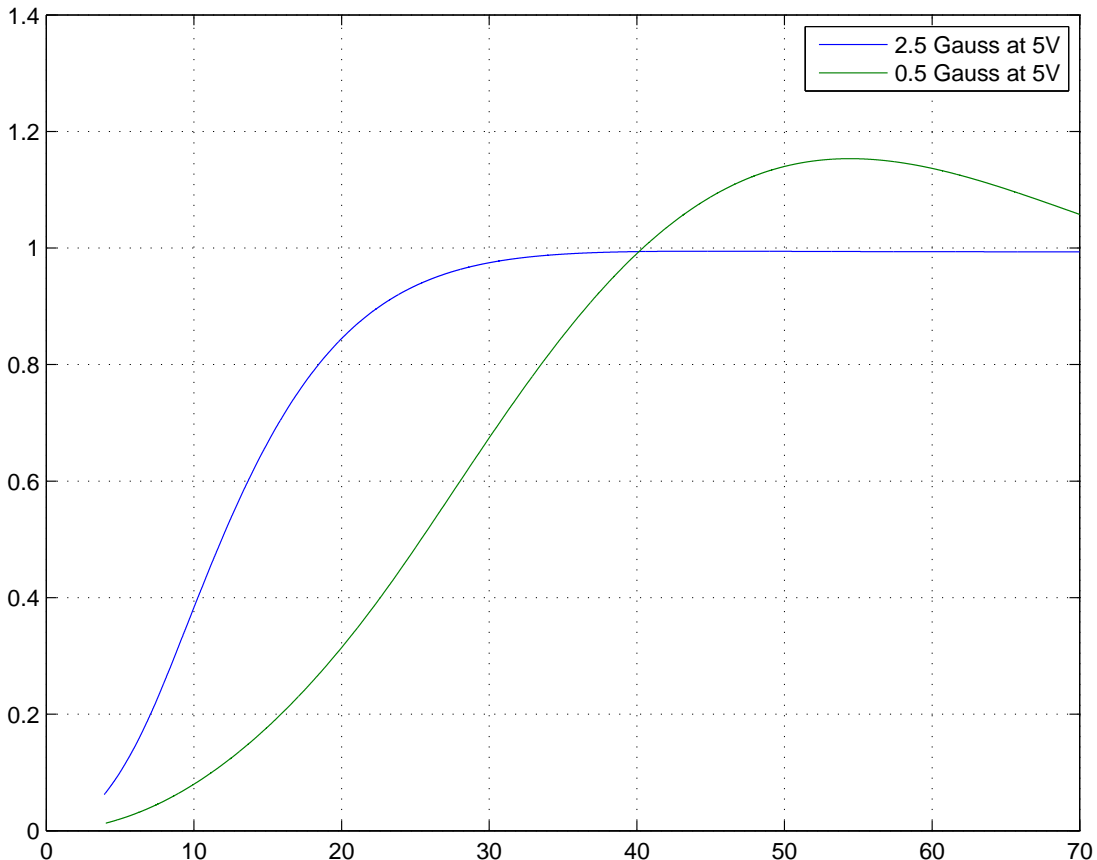


Figure 11.1: PID controller if transferred to a realistic magnetic field strength

A state-space model was also derived, as it is better suited for handling MIMO systems, which the 3D model will eventually be. The model assumes that the test setup is modelled, and the two spring/damper constants should be replaced by the orbit disturbances modelled in the analysis before transferral to a space model.

The prototype ADCS system with one-dimensional controllers is operational, and the test setup is verified as a feasible way to test the controllers performance. It is shown that the attitude can be controlled using only magnetorquers assuming that the magnetic field is not directly aligned with the angle of rotation. For a completed orbit in space the magnetic fields direction seen from the satellite, will change direction, and thus it will be possible to correct the attitude on all dimensions when the entire orbit is used.

# CHAPTER 12

Perspectives

## 12.1 Geomagnetic Field Strength

As the geomagnetic field is 5 times less than the homogenic field produced, it creates significantly less torque. This produces a slower system, and even introduces some overshooting, which should be avoided if possible in the space version. To compensate for this, the strength of the torquers can be doubled by coupling the supply voltage of the coils directly to the batteries instead of the 5 V regulated line. Thus the torque level will be changed to a level of  $\frac{2}{5}$  instead of  $\frac{1}{5}$ . Assuming that placing two coils oppositely of each other does not influence the torque created by each coil, this will provide even greater torque at  $\frac{4}{5}$  of the test level. This will however also increase the power consumption further, and the powerbudget should be evaluated to check if any of these changes are allowable. However as figure 12.1 illustrates, where a simulation of these changes are shown, it would actually create a system with a response almost equal to the test setup.

## 12.2 Magnetorquer Coil Design

As it was found that circular coils would produce the same amount of torque, it is suggested to produce circular coils. The tools are already provided to do this. The circular coils will have the advantage of equal distribution of heat. Another design improvement could be to wound the coils around a circuit board. This will glue it directly on to a structure and would improve the strength of the mechanical design. And provide a large circuit board which could be utilized for mounting the camera lens, the sensors, or other circuits not currently in the centered stack. It has been determined from beacon data that the subsystems in the stack in AAUSAT-II is being heated up by the sun, most of them are designed with a thermal coupling and never reaches temperatures above 60 °Celsius. However a circuit board at the sides would absorb much of the sunlight, and thus keep the stack better temperated.

## 12.3 Three-dimensional Orientation

It does still apply in 3D that the angle which defines the torques direction, is placed between the created magnetic fields vector, and the current outer B-field vector. If the magnetorquer abstraction layer can handle the secondary angle geometrically, the linkage between an attitude error, and the applied torque strength remains one-dimensional. This is for system without motion simply a matter of solving a set of equations similar to the one used in this project,

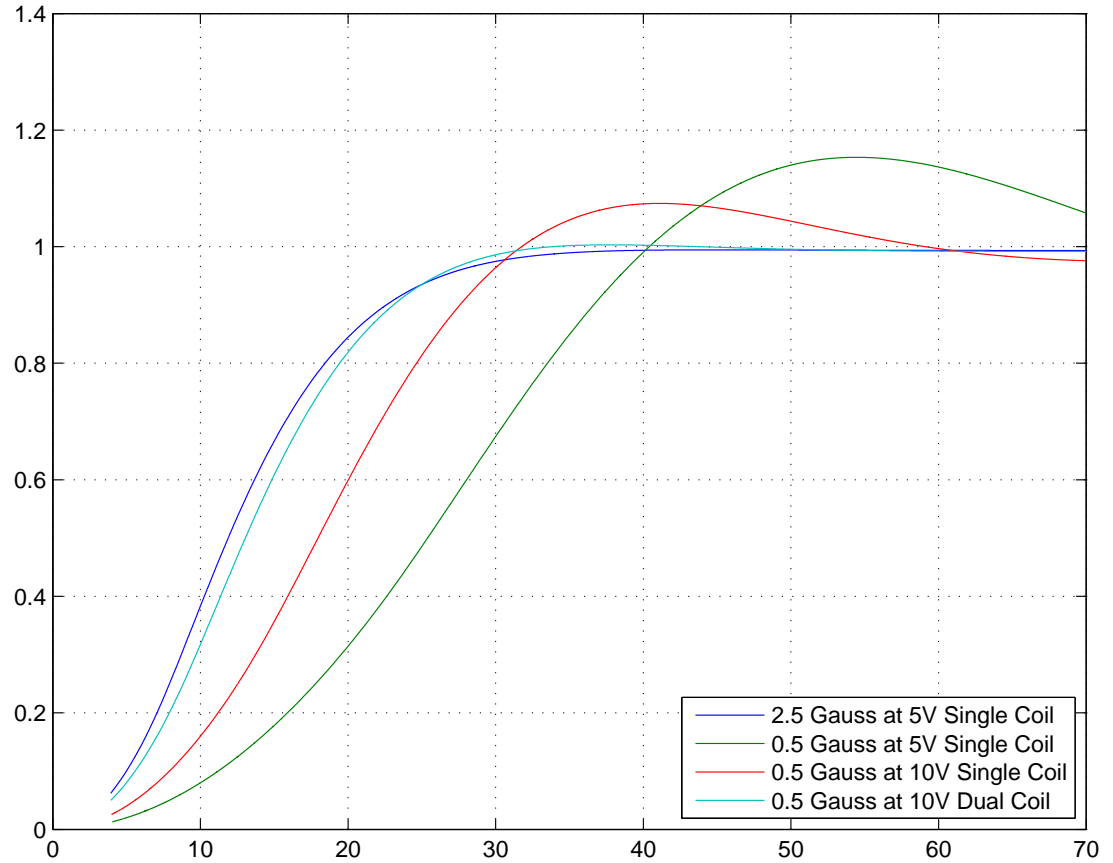


Figure 12.1: PID controller in a realistic magnetic field strength, if improvements are done to the coils.

for both an x-component and a z-component in respect to the y-axis. It can be thought of as rotating the z-axis appropriately, and then redo the calculations for a single-axis system. The influence from motions should be investigated before this can be verified, but it is assumed that as the abstraction layer works perfectly in 1D, a 2D abstraction layer would be able to achieve a performance that is equally good. Should this be the case, the torque controller implemented could very well be a simple PID controller. However it is not investigated how such a system will perform in 3D tumbling. This will also have to be investigated further, and perhaps a completely different scheme should be used for detumbling. It is suggested to implement a detumbling algorithm known as  $\dot{B}$ , which already is implemented on AAUSAT-II.

# CHAPTER 13

ICD internal communication

## 13.1 ADCS

### 13.1.1 Command list

- Set Reference Attitude
- Stop Controller
- Set PWM

#### Set Reference Attitude

Purpose: To set the reference attitude relative to zenith Aalborg.

Command: ACS\_SET

Arguments: uint16  $\theta_x$ , uint16  $\theta_y$ , uint16  $\theta_z$

Response: ACS\_ACTIVATED, ACS\_RANGE\_ERROR( $\theta_x, \theta_y, \theta_z$ )

, ACS\_FAILURE

Comment: Acceptable  $\theta$  values are in the range 0 - 360

#### Stop Controller

Purpose: To stop the controller from actuating, but continue measuring sensor outputs.

Command: ACS\_OFF

Arguments: None

Response: ACS\_DEACTIVATED

Comment: Changes state to IDLE where no calculations are done, except from gathering sensor data for housekeeping.

#### Set PWM

Purpose: To manually set PWM output to an actuator.

Command: PWM\_SET

Arguments: uint8 actuator\_no, int8 duty\_cycle

Response: PWM\_SET\_OK(actuator\_no), PWM\_SET\_ERROR(actuator\_no), PWM\_ACSError

Comment: Can be used for debug purposes when ADCS subsystem is in IDLE state. Acceptable range for actuator\_no is 1 - 3, duty\_cycle is in the range  $\pm 100$ .

## BIBLIOGRAPHY

- [ARIANESPACE, 2006] ARIANESPACE (2006). Vega User's Manual. On the web. <http://www.arianespace.com/site/documents/VEGAUsersManual.pdf>.
- [California Polytechnic State University, 2007] California Polytechnic State University (2007). Cubesat design specification. On the web. [http://cubesat.atl.calpoly.edu/media/CDS\\_rev10A.pdf](http://cubesat.atl.calpoly.edu/media/CDS_rev10A.pdf).
- [DSRI and NASA, 2007] DSRI, N. O. and NASA, T. J. S. (2007). Comprehensive modeling of the geomagnetic field. On the web. <http://denali.gsfc.nasa.gov/cm/>.
- [Engineering Group, 2007] Engineering Group (2007). Mission description document. On the web. AAUSAT3 trac On the CD mission purpose.odt.
- [ESA Education Office, 2008] ESA Education Office (2008). Call for cubesat proposals. On the web. [http://esamultimedia.esa.int/docs/LEX-EC/CubeSat\\_CFP\\_issue\\_1\\_rev\\_1.pdf](http://esamultimedia.esa.int/docs/LEX-EC/CubeSat_CFP_issue_1_rev_1.pdf).
- [Feedback control of dynamic systems, 2006] Feedback control of dynamic systems (2006). *Gene F. Franklin & J. David Powell & Abbas Emami-Naeini*. Upper Saddle River, New Jersey, 5th edition edition.
- [Pedersen et al., 2004] Pedersen, D., Grunnet, J., Larsen, J., Laursen, K., Kolakowska, E., and Amo, I. (2004). Attitude Control System for AAUSAT-II. On the web. <http://www.control.aau.dk/~jal/aausatii/acs-report.pdf>.
- [Philips, 2003] Philips, D. T. (2003). Earth's inconstant magnetic field. On the web. [http://science.nasa.gov/headlines/y2003/29dec\\_magneticfield.htm](http://science.nasa.gov/headlines/y2003/29dec_magneticfield.htm).
- [Physics for Scientists and Engineers, 2004] Physics for Scientists and Engineers (2004). *Raymond A. Serway & John W. Jewett, Jr.* California State Polytechnic University Pomona, 6th edition edition.
- [Wertz and Larson, 1999] Wertz, J. R. and Larson, W. J. (1999). *Space Mission Analysis and Design*. Kluwer Academic Publishers, 3rd edition.

## APPENDIX A

### Helmholtz coil

A Helmholtz coil is an apparatus with two coils of the same size placed with the radius of the coil between them. The apparatus gives a controllable homogenous magnetic field in a specific direction, between the coils.

To make it easier to verify the satellite behaviour in Earth environment a Helmholtz coil is used to compensate for magnetic disturbance from electronic measuring equipment and computers surrounding the experimental setup.

When the magnetic field is increased the magnetic sensors give a higher value in the direction of the B-field the Helmholtz coil produces. This gives a higher interval in each direction, which negates the magnetic field other equipment gives. Beside this the increased magnetic field also increases the torque the magnetorquers produce, which also can compensate for atmospheric drag and the nylon wire used.



Figure A.1: Picture taken of the produced Helmholtz coil.

The Helmholtz coil used in the experimental setup is designed with two coils with a radius of 25 cm and a spacing of 25 cm. The copper wire used is 0.8 mm thick and is wound 153 turns

## APPENDIX A. HELMHOLTZ COIL

---

on each coil. A diagram of the magnetic field produced can be seen at figure A.2, and a picture taken of the coil is shown in figure A.1

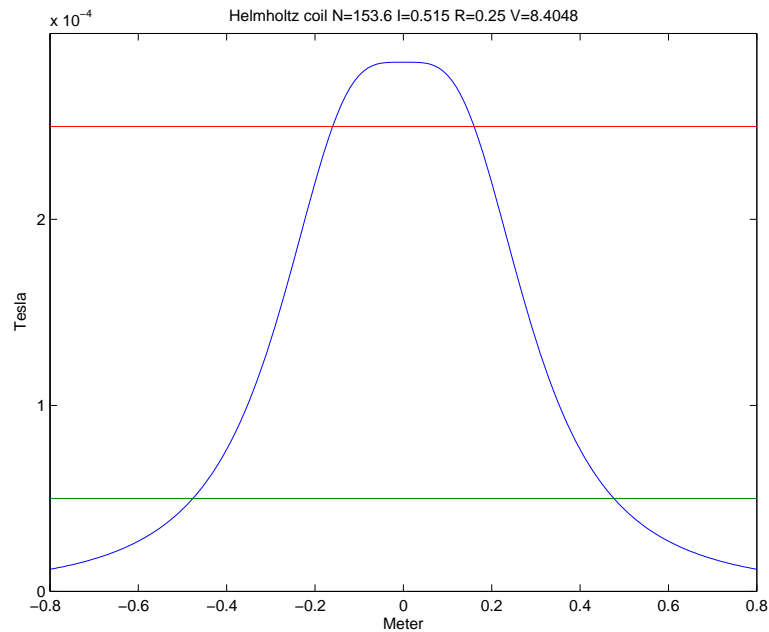


Figure A.2: Magnetic field diagram of the Helmholtz coil. Blue line represents the magnetic field produced. Green line represent Earth's magnetic field, and red is the desired field level 5 times higher than the Earth's.

## APPENDIX B

### Coil Machine

For producing magnetorquers for the AAUSAT3, the search begun after the originally designed coil machine used for AAUSAT-II. Eventually after some searching it was considered as disappeared. However, it is known that the coil machine were designed by mechanical engineering students, and coils were made by AAUSAT-II people.

After the search for the old coil machine had failed, it was decided to make a new simple one that would fulfill the needs. The coil machine is made of wood and Lego NXT for controlling the rotation. The coil form, that is made of wood, is shown in figure B.1. For gluing the wire together, polyester resin was used. The polyester resin does however not comply with the classification for space. However it combines the wire as expected and gives a consistency of the space classified glue at a lower price.

The final result of a coil is shown at figure B.2. The coil machine is shown at figure B.3.

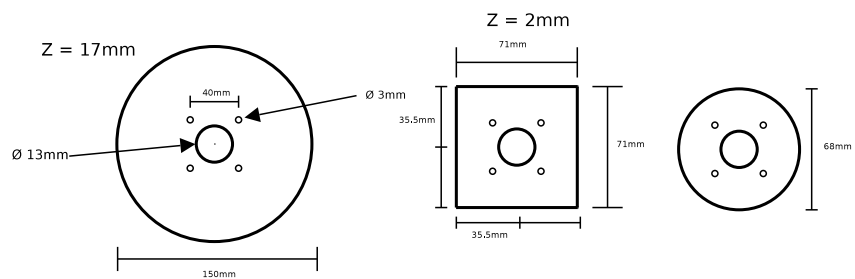


Figure B.1: Image of the coil form.

## APPENDIX B. COIL MACHINE

---



Figure B.2: A finished magnetorquer.

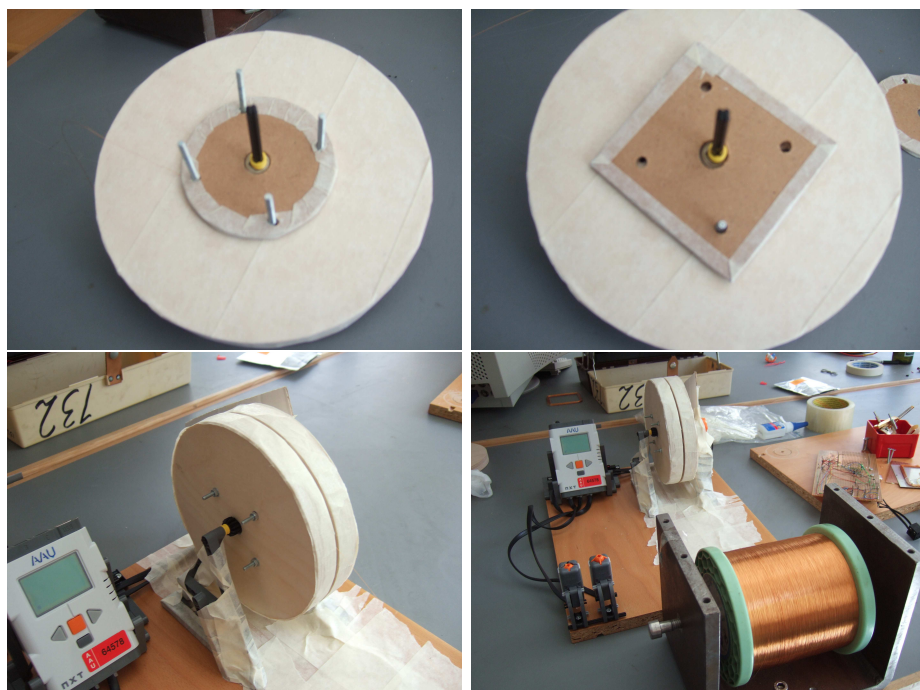


Figure B.3: Pictures of the coil machine.

## APPENDIX C

---

Source code

### C.1 PI controller

The source code for the PI Controller

---

```
#include "pid.h"
#include "debug.h"
#include "settings.h"

char pid_flag = PIDON;
int control_signal = 0;

void pid_init()
{
    set_theta_ref(0);
    pid_conf(&d1,DEFAULT_KP,DEFAULT_KI,50);          10
    pid_conf(&d2,DEFAULT_KD,0,50);
}

void set_pid_flag(char flag)
{
    pid_flag = flag;
}

char get_pid_flag(void)                                20
{
    return pid_flag;
}

int get_control_signal(void)
{
    return control_signal;
}

void set_control_signal(int ctrl_signal)               30
{
    control_signal = ctrl_signal;
}

void pid_conf(pid_opt* pid_opt, float kp, float ki, float T)
{
    pid_opt->xn0 = kp+((1/2)*T*ki);
    pid_opt->xn1 = -kp+((1/2)*T*ki);
}
```

40

```

float pid(pid_opt* pid_opt,float xin)
{
    pid_opt->yn[2] = pid_opt->yn[1];
    pid_opt->yn[1] = pid_opt->yn[0];

    pid_opt->xn[2] = pid_opt->xn[1];
    pid_opt->xn[1] = pid_opt->xn[0];
    pid_opt->xn[0] = xin;
    pid_opt->yn[0] = pid_opt->xn1 * pid_opt->xn[1] + pid_opt->xn0 * pid_opt->xn[0] + pid_opt->yn[1];
    return pid_opt->yn[0];
}

```

---

## C.2 Main loop

---

```

/**file main.c
 * brief program starts here.. and main loop is defined here
 *
 * the main loop contains the debug printout through print_house_keeping()
 * it also runs the code for handling inputs on the terminal.
 * interrupt A is also defined here, and is in charge of running the controller
 *
 * author 08gr633-ADCS
 * author AAUSAT3
 */

/*Includes*/
#include <io.h>
#include <math.h>
#include <signal.h>
#include "msp430.h"
#include <stdio.h>
#include "ascii.h"
#include "settings.h"
#include "pwm.h"
#include "adc.h"
#include "debug.h"
#include "commands.h"
#include "spi.h"
#include "uart.h"
#include "gyro.h"
#include "magnetorquer.h"
#include "errors.h"
#include "sensors.h"
#include "pid.h"
#include "matematik.h"

/* The threshold level for the speed, if the speed is more than this,
 * only D2 which controls the speed is used.
 * This introduces a detumbling mode, which is enabled whenever the speed is
 * higher than the PID controller was designed for
 */
float max_speed = DEFAULT_MAX_SPEED;

/* function to change the threshold, is runnable from terminal */
void set_max_speed(float mspeed)
{
    max_speed = mspeed;
}

/* Can be run from terminal, and is used to switch between the detumbling
 * and the angular control modes

```

```

/*
float get_max_speed(void)
{
    return max_speed;
}

/* The interrupt that samples the sensors and runs the PID controller,
 * thus it changes the level of the torque when PID is enabled
 */
interrupt (TIMERA0_VECTOR) TA_isr(void)
{
    /* Counter used as a software divider*/
    static count = 1;

    /* Sample the sensors */
    update_omega();
    update_theta();

    /* Check to see if the PID controller is enabled */
    if(get_pid_flag() == PIDON)
    {
        /* Initialise variables for the PID output*/
        int pid1 = 0;
        int pid2 = 0;

        /* when software divider allows for it..*/
        if(count >= 4)
        {
            /* Start the counter again */
            count = 1;

            /* If possible, go to angular control, but only if the speed is low enough
             * It is needed to run the D1 controller, otherwise it is not necessary.
             */
            if (abs(get_omega()) < max_speed)
            {
                /* if the coordinate system is rotated,
                 * the measured theta should be also,
                 * otherwise dont rotate them. Enables the satellite to be steered to
                 * point in more than +/- 90 degrees
                 */
                if(get_rotated_flag() == 0)
                {
                    pid1 = (int)(pid(&d1, get_theta_ref_rad() - get_theta()));
                }
                else
                {
                    pid1 = (int)(pid(&d1, get_theta_ref_rad() - rotate_coords_rad(get_theta())));
                }
            }

            /* max_speed exceeded. . detumbling */
            else
                pid1 = 0;

            /* calculate PID2 */
            pid2 = (int)(-pid(&d2, get_omega()));

            /* set a control signal level for debug print */
            set_control_signal(pid1+pid2);

            /* set the control signal level (torque)
             * using the two pid controllers signals
             */
            set_torque(pid1+pid2);
        }
    }
}

```

---

## APPENDIX C. SOURCE CODE

---

```

        /* use the magnetorquer abstraction layer to apply the calculated torque
         * as two currents,
         * The layer handles the torque variable, and retrieves it by itself,
         * but it needs to be supplied with the latest theta measurement.
         * The torque variable is saturated at +/- 100
         */
        magnetorquer(get_theta());                                         120
    }

    /* doing some software dividing */
    else
    {
        count++;
    }
    /* end of PID control routine */                                     130
}
/* nothing left to do, if the PID is disabled nothing was done
 * Interrupt routine ends here */
}

/* start the main software here */
int main (void)
{
    /* Initialize variables for regulating the print_housekeeping()
     * intervals. .
     */
    int counter = HKPRINTTIME - HKWAIT;
    flag = HKOFF;

    /* initialize the MSP clock*/
    clock_init();

    /* initialize the MSP analog to digital converters */
    adc_init();                                                       140

    /* preparing the uart for the debug terminal */
    uart_init();                                                       150

    /* send a init signal to the uart,
     * to alert that debugging is initialized,
     * and that the satellite has been reset
     */
    debug_init();

    /* prepare the appropriate output pins for PWM,
     * and set them to zero on the 4 output pins designated to the coils
     */
    pwm_init();                                                       160

    /* initialize the SPI interface for the gyro unit communication */
    spi_init();

    /* initialize the sensor handling part of the software*/
    sensor_init();                                                     170

    /* indicate on the hardware that you are alive,
     * by turning on the LED on the MSP board on top of the satellite
     */
    P1DIR = 0xFF;
    P1OUT = 0xFF;

    /* complete the initializing of the I/O pins */
    P3DIR |= 0x10;                                                     180

    /* start the control system with references set to zero*/
    pid_init();

```

```

/* prepare the software to output debug messages as house keeping data*/
hk_init();

/* initiate main loop */
while(1)
{
    /* Software divider, to make the output readable and avoid flickering
     * due to the continues clearing of the terminal screen
     */
    counter++;
    if (counter > HKPRINTTIME)
    {
        /* Output debugging data, and switch the LED state*/
        if(flag == HKON){
            /*clear screen*/
            putchar(FF);

            /*disable interrupts*/
            dint();

            /* update housekeeping variables*/
            update_house_keeping();
            /* print housekeeping to terminal */
            print_house_keeping();

            /*print bash input history before checking for new inputs */
            command_input(HISTORY_ON);
        }
        /* flick LED */
        P1OUT ^= 0x01;

        /* re-enable interrupts*/
        eint();
    }

    /* output only the measurement data instead of the vastly larger housekeeping data */
    if(flag == DATAOUTPUTMODE)
    {
        gyro_data();
    }

    /* divider */
    counter = 0;
}

/*check for inputs*/
else
{
    /*disable interrupts while checking for new inputs*/
    dint();
    /* check for new inputs from the terminal*/
    command_input(HISTORY_OFF);
    /* re-enable the interrupts */
    eint();
}
/*end of main loop*/
}

/*hopefully this never happens, as it corresponds to the software being killed*/
return(0);
}

```

---

## APPENDIX D

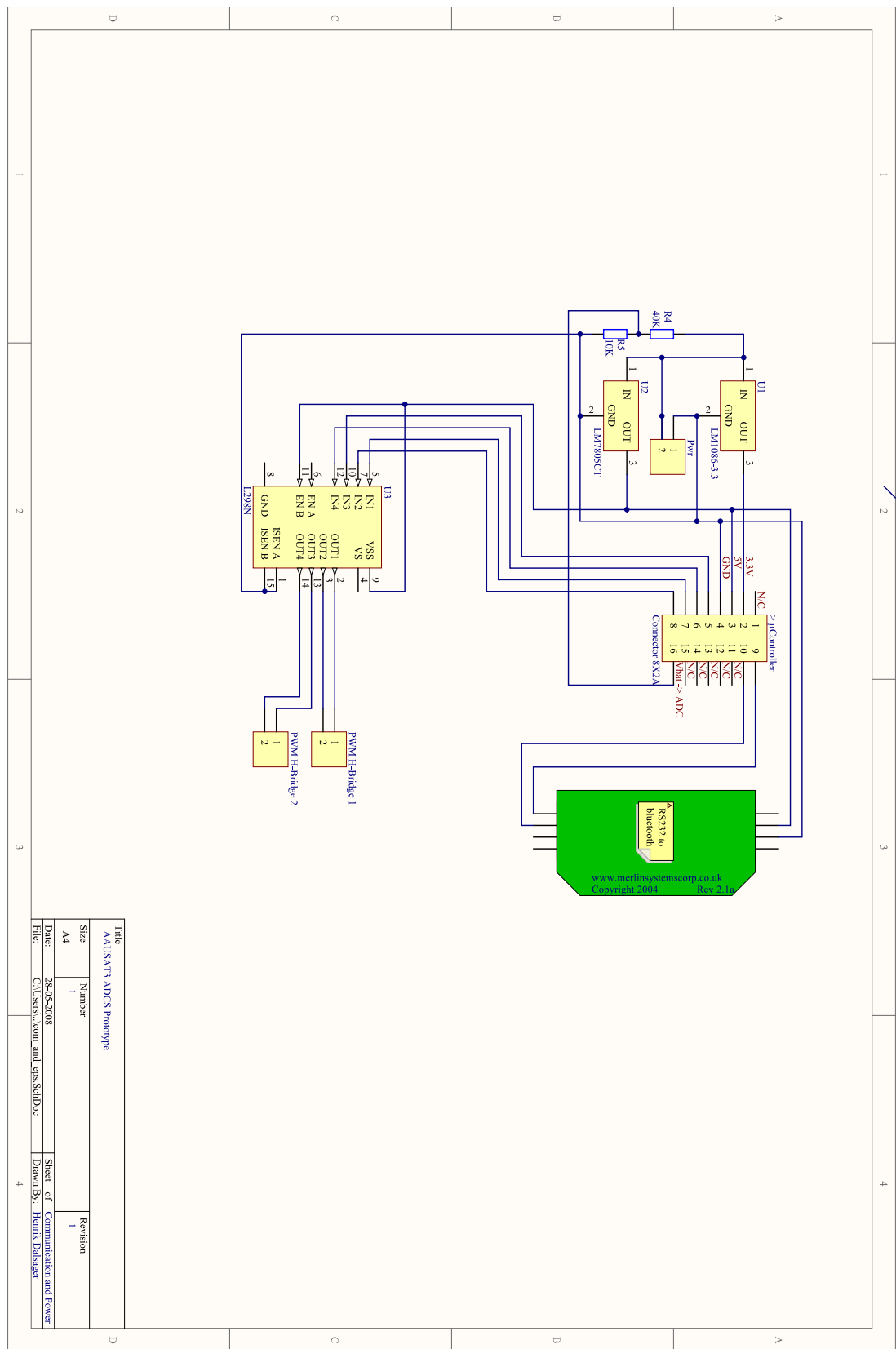
### Schematics

During the project a prototype model of the satellites ADCS system was developed. Some considerations was taken towards the further development. The considerations included a design where the analog magnetic sensors was sampled by the built in ADC in the gyro.

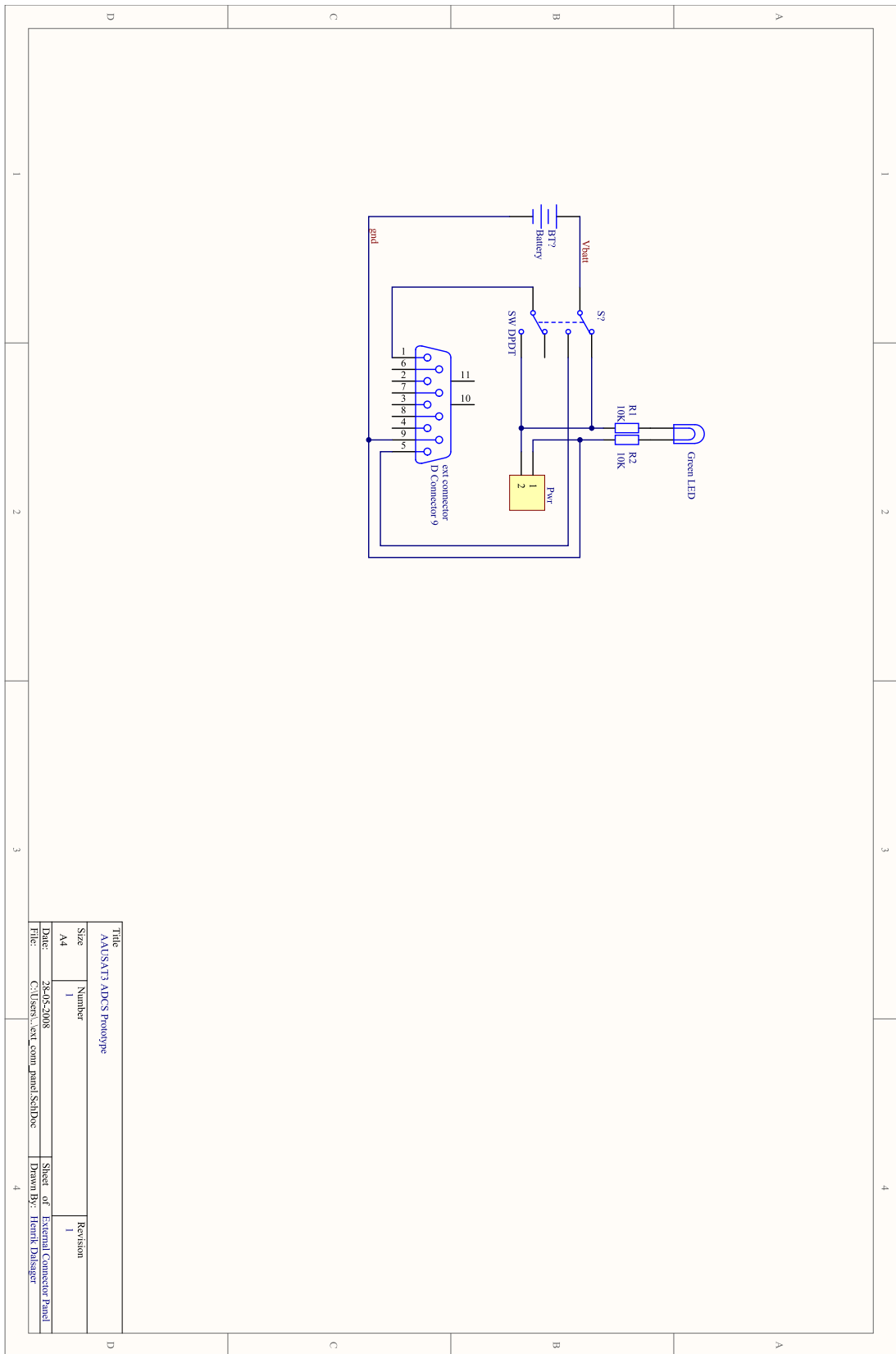
The advantage in this choice is that the micro controller can be reselected later on. In the further design it is considered an advantage to keep this feature, and equip the sidepanels with a set of the sensors, in a similar configuration. This should allow for redundant sensors, and if two types of gyros are used from this family, to gain a better resolution when at low speeds, the extra ADC channels can be used to sample the solarpanel voltage. The greatest advantage is however that the gyro family used has build in temperature sensors, which allows AAUSAT3 to measure the temperature at all the satellites surfaces.

The prototype also has a wireless bluetooth communication interface build in, this is implemented as an RS232 to bluetooth converter. And some voltage regulators for handling the power transfer from the battery. External connectors provide access to the circuits power line, and the battery. Which allows for charging the battery whithout disassembling the prototype. while charging the prototype can be powered from a powersupply to allow for debugging and testing.

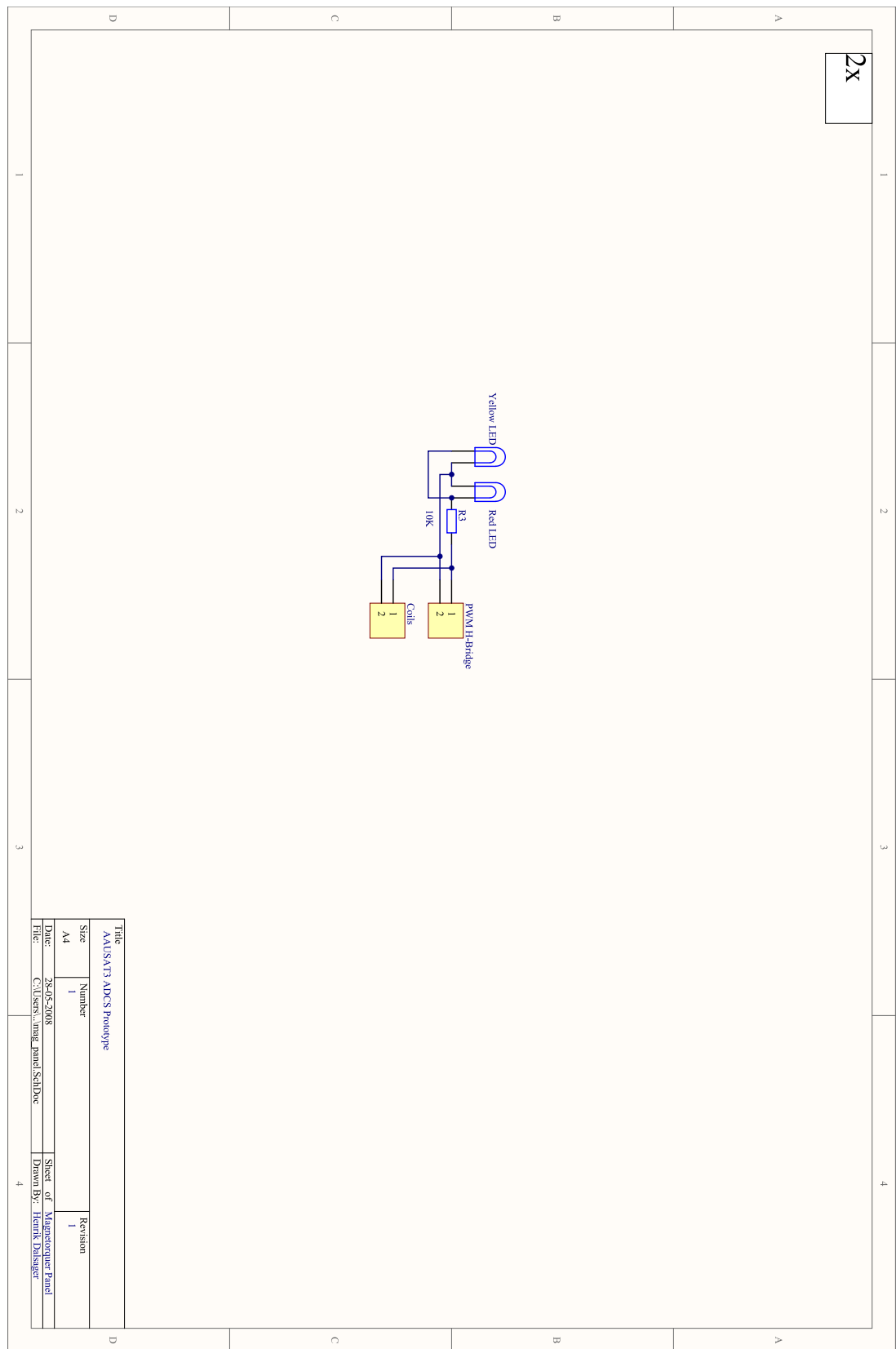
## APPENDIX D. SCHEMATICS



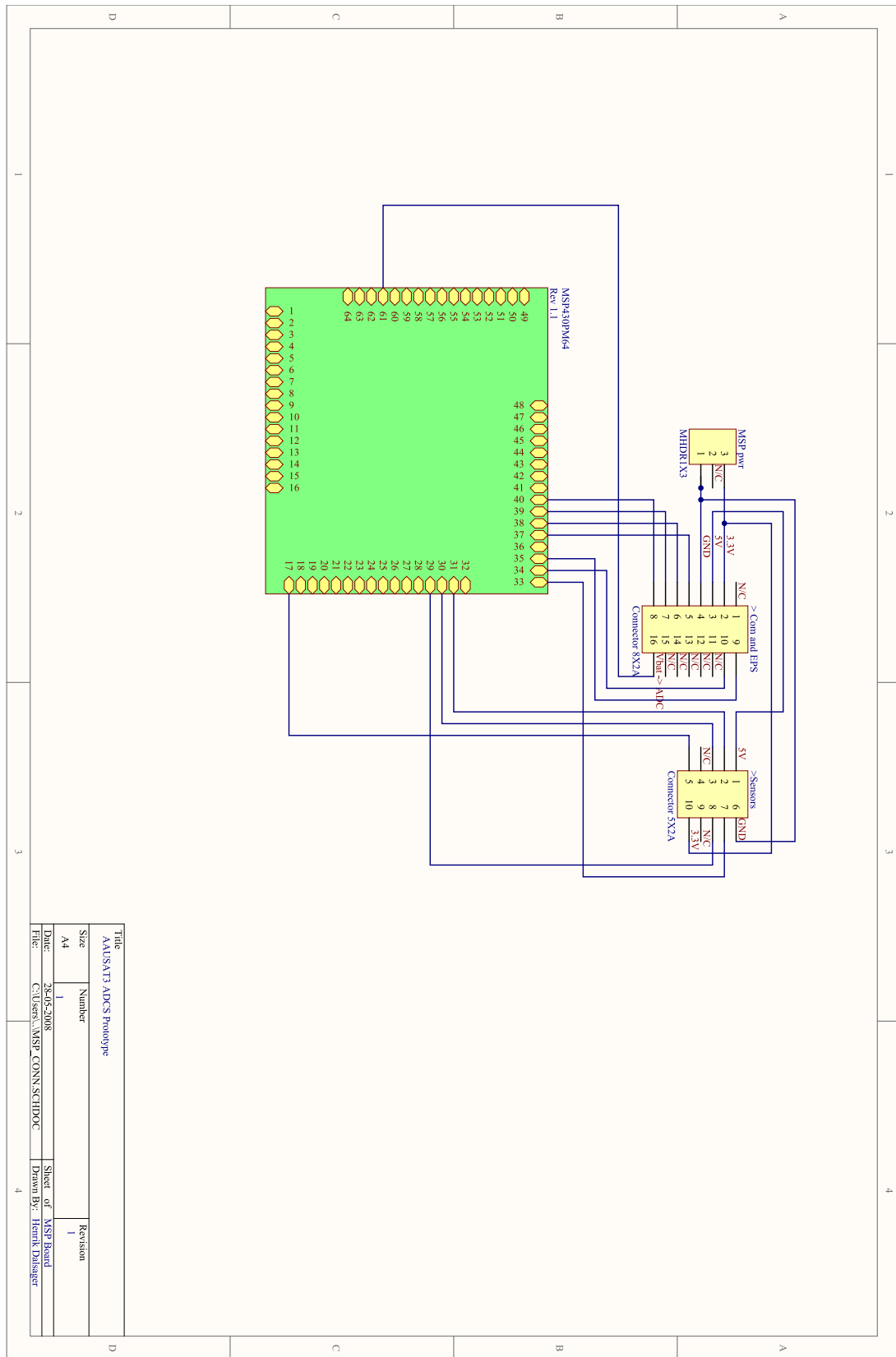
## APPENDIX D. SCHEMATICS



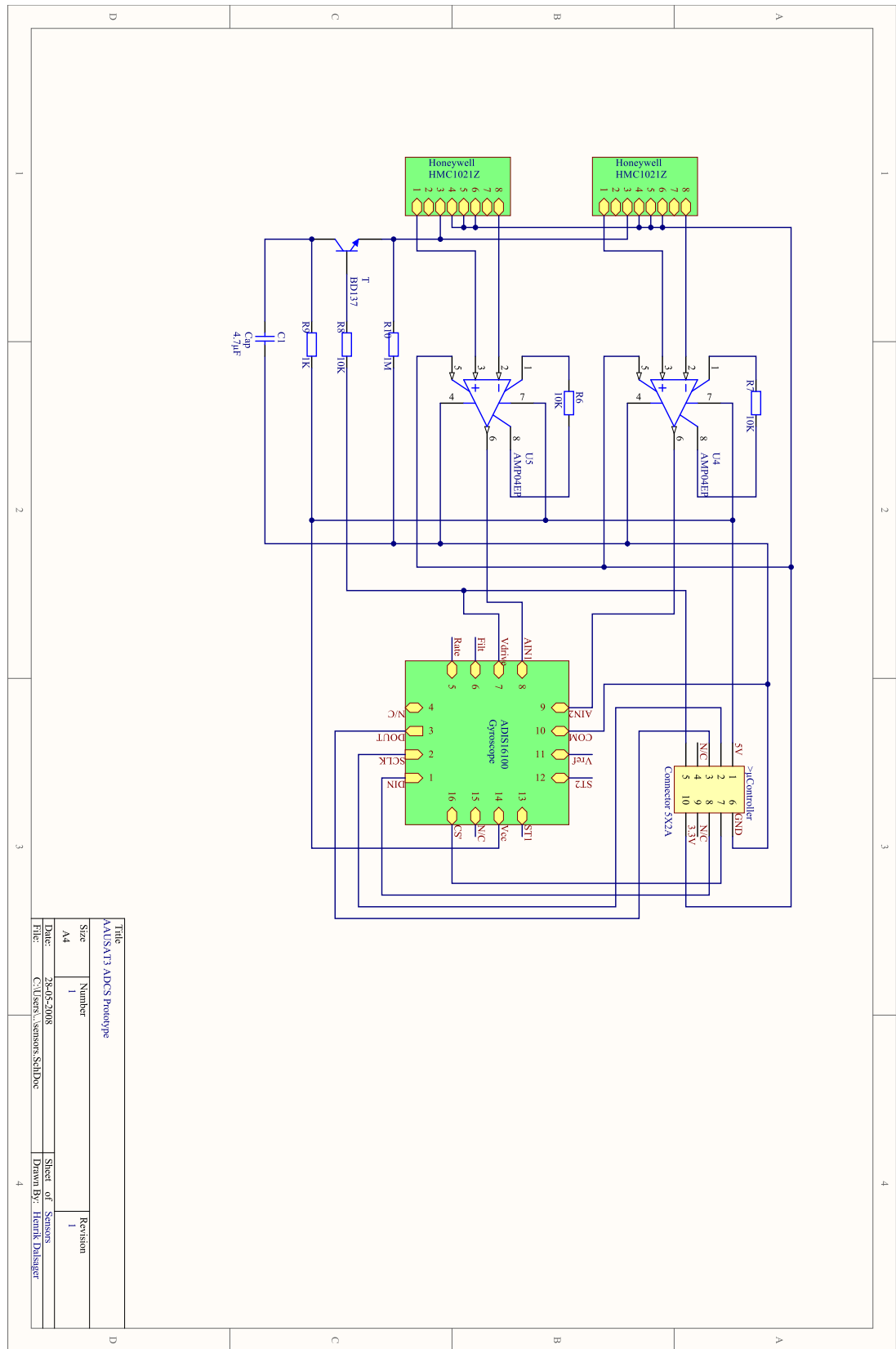
APPENDIX D. SCHEMATICS



## APPENDIX D. SCHEMATICS



## APPENDIX D. SCHEMATICS



## APPENDIX E

CD index

```
/  
├── Schematics  
├── Datasheets  
├── Drawings  
├── Pictures  
├── Sourcecode  
│   └── Doxygen  
│       ├── html  
│       └── latex  
└── Matlab files  
    └── rapport.pdf
```